

T151

49644

CENTRAL LIB
TEZPUR UNIV
Accession No. 49644
Date 14/9/11

REFERENCE BOOK
NOT TO BE ISSUED
TEZPUR UNIVERSITY LIBRARY

CENTRAL LIB
TEZPUR UNIVE
Accession No. T 151
Date 27/02/13

**STRUCTURAL AND ELECTRONIC PROPERTIES OF
BARE AND SUPPORTED PALLADIUM NANOCLUSTERS:
A DENSITY FUNCTIONAL APPROACH**

A THESIS SUBMITTED IN PARTIAL FULFILLMENT OF
THE REQUIREMENTS FOR THE DEGREE OF

DOCTOR OF PHILOSOPHY

By

BULUMONI KALITA

Registration No: 003 of 2009



**Department of Chemical Sciences
School of Science and Technology
Tezpur University
Napaam, Tezpur-784028
Assam, INDIA**

January 2010

Dedicated to

My Parents,

My Parents-In-Laws

&

My Husband

STRUCTURAL AND ELECTRONIC PROPERTIES OF BARE AND SUPPORTED PALLADIUM NANOCCLUSERS: A DENSITY FUNCTIONAL APPROACH

ABSTRACT

The aim of this thesis is to investigate the structure and energetics of small gas phase palladium (Pd) clusters. Density functional theory (DFT) calculations have been performed to optimize a large number of geometrical and spin isomers of bare neutral, cationic and anionic Pd_n (n=1–13) clusters. From these studies, different parameters namely bond length, binding energy, stability function, fragmentation energy, bond dissociation energy, ionization potential, electron affinity, HOMO-LUMO gap, global hardness and dipole moment have been calculated for the clusters. On the basis of these data, we have predicted the stability of small palladium clusters. Further, from the study of CO interaction with bare and oxidized Pd clusters, the intermediates of CO oxidation reaction catalyzed by small palladium clusters have been identified. The reaction energy profiles indicate the effect of charge state of Pd cluster on CO oxidation. We have also intended to study the effect of oxide support on the structural and electronic properties of small stable palladium clusters taking zeolite as a model support, with proper modelling of the support using hybrid quantum mechanics/molecular mechanics (QM/MM) methods. All the results are compared with the available experimental and theoretical values. The contents of the thesis have been distributed into seven chapters:

Chapter 1 gives brief introduction, importance and motivation of the present work along with the review of literatures on gas phase and supported palladium clusters. Metal nanoclusters exhibit significantly different physical properties from their bulk counterparts. Properties such as high electrical and thermal conductivity, high reflectivity and mechanical ductility in bulk metals may fully or partially be absent in metal nanoclusters, while new properties develop, which are strongly size

dependent. The change in relevant properties is due to the quantum confinement of electrons in metal nanoclusters compared to the delocalized electrons in bulk metals. In contrast to the simple metal clusters, transition metal clusters are extremely complicated. Because of the unfilled d orbitals, transition metal clusters possess a high density of states and exhibit interesting chemical, magnetic and electronic properties. When metal complexes and clusters are bonded to oxide or zeolite supports, they give rise to technologically advantageous solid catalysts having robustness for high temperature operation, lack of corrosiveness, ease of separation from products along with the selectivity of soluble molecular catalysts. Supported metal complexes have wide applications in heterogeneous catalysis.

Chapter 2 describes the electronic structure methods used in computational material science including density functional theory (DFT). We have also presented a detailed description of the basis sets and functionals used in DFT in this chapter. Moreover, we have discussed the usefulness of the hybrid quantum mechanics/molecular mechanics (QM/MM) method. The advantage of using QM/MM method lies in treating the active region (i.e., the site for chemical processes involving bond breaking and formation) accurately with a high level QM method and the remainder of the system with low level MM method.

Chapter 3 presents the results of structure and stability of neutral, cationic and anionic Pd_n ($n=1-13$) clusters on the basis of DFT calculations. We have used the DMol³ program for optimization of different structural and spin isomers of small palladium clusters. Double numerical polarization (DNP) basis set and exchange-correlation functional, BLYP, which is a combination of the exchange functional developed by Becke with the gradient corrected correlation functional of Lee, Yang and Parr, are adopted for geometry optimizations. Full geometry optimizations have been performed on different possible structural isomers of neutral Pd_n ($n=1-13$) clusters in their singlet ($M=1$), triplet ($M=3$) and quintet ($M=5$) states without imposing symmetry constraints. In the present work, cationic and anionic palladium clusters are formed by removing and adding one electron, respectively from the ground state neutral palladium clusters. Symmetry unrestricted geometry optimizations have been carried out for these ionized clusters in three different multiplicities ($M=2, 4, \text{ and } 6$). Frequency calculations have been performed on all

the structures and none of them is found to exhibit any imaginary frequency. Absence of imaginary frequency verifies the structures to be stable. In this study, we have calculated different parameters like bond length, binding energy, coordination number, stability function, fragmentation energy, bond dissociation energy, ionization potential, electron affinity, HOMO-LUMO gap, global hardness and dipole moment. Based on all these parameters, we have found Pd₄ to be the most stable cluster in the present study.

Chapter 4 discusses the interaction of carbon monoxide (CO) with the neutral, cationic and anionic Pd_n (n=1–7) clusters. Adsorption of CO on neutral clusters are examined with multiplicities M=1 and 3, while the calculations for cationic and anionic clusters have been performed with multiplicities M=2 and 4. Our results indicate that for both neutral and cationic complexes, all the 1-, 2- and 3-fold coordination are preferred by the CO molecule. But CO adsorption takes place mostly in single coordination in case of anionic clusters barring bridging adsorption in Pd₇⁻ cluster i.e., charge states of small palladium clusters have strong influence on adsorption configurations. The lowest value of CO binding energy is observed for neutral Pd₄ cluster, which implies higher stability of this cluster and its less reactivity towards CO.

Chapter 5 is focused on the study of adsorption sites of different forms of oxygen (O₂, 2O, O) as well as their co-adsorption with CO on neutral, cationic and anionic Pd₄ clusters. For all the clusters, the dissociative adsorption of oxygen (2O) sitting on Pd bridge sites is preferred. Pre-adsorption of O₂ is found to affect the adsorption geometry as well as the binding energy of CO in the co-adsorption complexes. Binding energies of both O₂ and CO are higher in anionic Pd₄ cluster followed by cationic and neutral clusters. However, binding energies of O₂ or CO in the co-adsorption complexes follow the trend: anionic > neutral > cationic Pd₄ clusters. Based on these observations, oxygen adsorbed anionic Pd₄ cluster is found to have strong binding towards CO followed by neutral and cationic clusters. DFT studies on the co-adsorbate combinations, including O₂+CO, 2O+CO and O+CO and O+CO₂ on neutral, cationic and anionic Pd₄ clusters revealed the possible intermediates of: (1) Pd₄+O₂+CO→Pd₄O+CO₂, (2) Pd₄+2O+CO→Pd₄O+CO₂ and

(3) $\text{Pd}_4 + \text{O} + \text{CO} \rightarrow \text{Pd}_4 + \text{CO}_2$ reactions. The energy profiles of these reactions indicate that Pd_4^+ and Pd_4 are more effective for catalyzing CO in comparison with Pd_4^- . It is further observed that dissociated oxygen is a superior oxidant for CO oxidation on Pd_4^q ($q=0, 1, -1$) than molecular and atomic oxygen.

Chapter 6 reports the investigation of metal-support interaction of a Pd atom with H-ZSM-5 zeolite by using cluster model and embedded cluster model. We have used two layer ONIOM (Our-own-N-layered Integrated molecular Orbital + molecular Mechanics) method, as implemented in the *Gaussian 03* program to perform the embedded cluster calculations. In our calculations, the 93T cluster has been divided into two regions: (i) inner core region consists of 7T sites including adsorbed Pd atom and adsorbates (CO, NO molecules) and (ii) outer region consists of the rest 86T sites. The high level (QM) region was treated with hybrid B3LYP functional using 6-31G (d,p) basis set for H, O, Al, Si and LANL2DZ relativistic pseudo potential for Pd atom. The outer region has been modelled by molecular mechanics using the universal force field (UFF). From the calculations, it is found that the Pd atom interacts with a Brønsted proton as well as a nearby oxygen atom of the zeolite framework. Interaction with the framework oxygen causes excess electron density on the Pd atom via charge transfer from the zeolite to the Pd atom, which is concurrently withdrawn by a Brønsted proton. Embedded cluster study has resulted in stronger interaction of Pd atom with H-ZSM-5 zeolite ($E_{\text{ads}} = -5.18$ kcal/mol) than that from the cluster model study ($E_{\text{ads}} = -1.83$ kcal/mol). Adsorption energy values as well as thermodynamic analyses have shown preferable adsorption of CO over NO on Pd-HZSM-5.

To determine the favourable chemical state of zeolite-supported Pd_4 clusters, we have modelled the support with 60T (T=tetrahedral atoms) clusters of faujasite (FAU) zeolites, including the super-cage, where the metal species and adsorbates can be trapped inside. The high level (QM) region of the system consists of 6T ring of FAU zeolite, in which, one, two and three Si atoms have been isomorphously substituted by Al atoms to generate three different QM clusters. Our results suggest that the lowest energy structures of Pd_4 in gas phase as well as on zeolite support are in triplet states. The calculations show that reverse hydrogen spillover from bridging OH groups of zeolite support onto Pd_4 results in hydrogenated $\text{Pd}_4\text{H}/\text{FAU}((m-1)\text{H})$, $m=1-3$ species, which are energetically preferable over bare zeolite-supported form

of Pd₄/FAU(mH). The process of single hydrogen transfer from zeolite support to Pd₄ cluster is found to be exothermic and more favourable than two and three proton transfer processes.

Chapter 7 summarizes the salient observations of the entire work and the future scopes of the present investigation. From the DFT study on a large number of structural and spin isomers of gas phase neutral and charged Pd_n (n=1–13) clusters, neutral Pd₄ cluster has been found to be the most stable cluster. Lowest value of CO binding energy with neutral Pd₄ cluster also signifies higher stability of the cluster. Therefore, we have chosen Pd₄ cluster for investigating adsorption of O₂, CO and their co-adsorption. This study reveals superior catalytic activity of neutral and cationic Pd₄ clusters for CO oxidation than anionic Pd₄ cluster. Binding of CO with Pd atom supported on H-ZSM-5 zeolite is preferred over NO. The lowest energy structures of Pd₄ in gas phase as well as on zeolite support are found to be in triplet states. Adsorption complex Pd₄H/FAU, formed by reverse spillover of single proton from faujasite zeolite to the Pd₄ cluster is more stable than the Pd₄/FAU complex.

In the **appendices A and B**, relative stability of different structural and spin isomers of gas phase palladium clusters and their interaction with different adsorbates are presented.

Declaration

I hereby declare that the thesis entitled "*Structural and Electronic Properties of Bare and Supported Palladium Nanoclusters: A Density Functional Approach*" being submitted to the Department of Chemical Sciences, Tezpur University, is a record of original research work carried out by me. Any text, figures, results or designs that are not of own devising are appropriately referenced in order to give credit to the original author(s). All sources of assistance have been assigned due acknowledgement. I also declare that neither this work as a whole nor a part of it has been submitted to any other university or institute for any other degree, diploma or award.

Date: 20.01.2010

Place: Tezpur

Bulumoni Kalita
(Bulumoni Kalita)



TEZPUR UNIVERSITY

(A Central University established by an Act of Parliament)

NAPAAM, TEZPUR – 784028

DISTRICT: SONITPUR :: ASSAM:: INDIA

Ph: 03712 – 267008

03712 –267009

Fax: 03712 –267005

03712 –267006

e-mail: ramesh@tezu.ernet.in

Dr. Ramesh Ch. Deka
Associate Professor
Department of Chemical Sciences
Tezpur University

This is to certify that the thesis entitled “*Structural and Electronic Properties of Bare and Supported Palladium Nanoclusters: A Density Functional Approach*” submitted by Ms. Bulumoni Kalita for the degree of Doctor of Philosophy of Tezpur University, embodies the record of original investigation carried out by her under my supervision. She has been duly registered and the thesis presented is worthy of being considered for the Ph. D. Degree. This work has not been submitted for any degree of any other University.

Date: 20.01.2010

Place: Tezpur

Signature of the Supervisor

ACKNOWLEDGEMENTS

I have my M. Sc. degree in Physics and never thought of pursuing my research in Chemistry. First and foremost, I, therefore, sincerely thank my research supervisor, Dr. Ramesh Ch. Deḡa, Associate Professor, Department of Chemical Sciences, Tezpur University, for selecting me as a Junior Research Fellow in a project under him. I gratefully acknowledge his support during the course of my research.

I heartily thank the Department of Chemical Sciences, Tezpur University for giving me the opportunity to carry out research for completion of a Ph. D. degree in a warm and highly scientific environment. It was accomplished during November, 2005 to December 2009 and was a turning point in my academic career. In this period, I got introduced with the field of clusters and nanoscience, which acts as a bridge between Physics and Chemistry. With the passage of time, I enjoyed my research work more and more.

I would like to thank all the faculty members and staff of the Department of Chemical Sciences, Tezpur University for their valuable suggestions and help in various ways during my research period.

I am thankful to the Council of Scientific and Industrial Research, New Delhi and the Department of Science and Technology, New Delhi for their financial support.

I sincerely express my deep sense of gratitude and respect to all my teachers, starting from my primary school to university and also those persons who instead of not being my formal teachers certainly contributed directly or indirectly to the realization of the present thesis.

I thank the entire team of computer centre, Tezpur University for giving the opportunity to carry out my research calculations and also for their instant supports regarding any short computer related problems.

I am thankful to the help and supports of my labmates. I also thank all the research scholars of the department of Chemical Sciences, Tezpur University, for their support in making my stay in the department a pleasant one.

I thank the faculty members and research scholars of various other departments of Tezpur University for their help and encouraging words.

I am pleased to acknowledge the help of my friend Anto (IITG), Parashaba (NEIST, Jorhat), Sucismita (Germany) and many others for providing me valuable research literature time to time.

Special thanks to Prof. Ödön Farkas (Hungary), developer of Gaussian and Dr. Alessandro Damin (Italy) for the fruitful discussions.

I am grateful to the support and encouragement of Dr. Anil Dutta and Dr. Juri Bhattacharjee of Tezpur, who stood beside me like my guardians.

Baba, Maa, Baideu, Bhaiti, Maina and Munuda, I must thank your moral support and belief in me; without your love, inspiration, blessings and scolds it would not have been possible to obtain the Ph. D. degree.

I would like to express my thanks and respect to my in-laws who have so much love and faith in me. I am sure that my father-in-law, whom I never met, would have been very happy this day if he were alive.

No words of appreciation can fulfill the status of my dear husband, Sumanta. I should not belittle you by thanking as you are the indispensable of my life. You are always there to take me away from any unpleasant situation and keep my spirits alive. I could not have completed my Ph. D. without you.

Department of Chemical Sciences

Tezpur University

Date: 20. 01, 2010

Bulumoni Kalita
Bulumoni Kalita

TABLE OF CONTENTS

ABSTRACT	i
ACKNOWLEDGEMENTS	viii
LIST OF ABBREVIATIONS	xiv
LIST OF TABLES	xv
LIST OF FIGURES	xvii

CHAPTER 1: INTRODUCTION AND MOTIVATION

GAS PHASE NANOCCLUSERS

1.1 Definition	1
1.2 Types of clusters and cluster bonding	2
1.3 Cluster generation and detection in gas phase	4
1.3.1 Cluster generation in gas phase	4
1.3.2 Cluster detection in gas phase	5
1.4 Size effects in clusters	5
1.4.1 High fraction of surface atoms	5
1.4.2 Electronic structure	7
1.5 Variation of cluster properties with size	8
1.6 Why clusters are interesting	11
1.7 Supported metal clusters	11
1.8 Importance of palladium clusters	13
1.8.1 Bare palladium clusters	14
1.8.2 Chemisorptions on small gas phase palladium clusters	15
1.8.3 Zeolite supported small palladium clusters	17
1.9 Objectives of the present work	19

CHAPTER 2: ELECTRONIC STRUCTURE METHODS

2.1 Introduction	20
2.2 Overview of computational methods	20
2.2.1 Molecular mechanical methods	21
2.2.2 Quantum mechanical methods	22
2.2.2.1 Hartree-Fock theory	22
2.2.2.2 Semiempirical methods	24
2.3 Density Functional Theory (DFT)	25
2.3.1 Hohenberg-Kohn theorem	26
2.3.2 Kohn-Sham equations and energy functional	27
2.3.2.1 The Local Density Approximation (LDA)	28
2.3.2.2 The Generalized Gradient Approximation (GGA)	29
2.3.2.3 Hybrid functional	29
2.3.3 Basis sets	31
2.3.3.1 Slater Type Orbitals (STO)	31
2.3.3.2 Gaussian Type Orbitals (GTO)	31
2.3.3.3 Double-zeta, Triple-zeta and Quadruple-zeta basis sets	31
2.3.3.4 Split-valence basis sets	32
2.3.3.5 Polarization functions	32
2.3.3.6 Diffuse functions	32
2.3.3.7 Numerical basis sets	32
2.3.3.8 Effective Core Potentials (ECP)	33
2.3.4 Basis Set Superposition Error (BSSE)	33
2.4 Quantum Mechanics-Molecular Mechanics (QM/MM) methods	34

CHAPTER 3: GAS PHASE SMALL PALLADIUM CLUSTERS

3.1 Introduction	36
3.2 Computational details	37
3.3 Results and discussion	39
3.3.1 Geometries and energetics	39

3.3.2	Relative stability	51
3.3.3	Electronic properties	54
3.3.3.1	Ionization potential and electron affinity	54
3.3.3.2	HOMO-LUMO gap, global hardness and dipole moment	56
3.4	Salient observations	58

CHAPTER 4: ADSORPTION OF CO ON GAS PHASE SMALL PALLADIUM CLUSTERS

4.1	Introduction	60
4.2	Computational details	61
4.3	Results and discussion	61
4.3.1	Geometries and energetics	61
4.3.2	Variation in bond lengths and adsorption properties	70
4.3.3	Vibrational properties	71
4.4	Salient observations	73

CHAPTER 5: CO-ADSORPTION OF CO, O₂ AND OXIDATION OF CO ON GAS PHASE Pd₄ CLUSTERS

5.1	Introduction	74
5.2	Computational details	75
5.3	Results and discussion	76
5.3.1	Adsorption of oxygen on Pd ₄ clusters	76
5.3.2	Adsorption of CO ₂ on Pd ₄ clusters	82
5.3.3	Co-adsorption of O ₂ , 2O, O, CO and CO ₂ on Pd ₄ clusters	83
5.3.4	CO oxidation reaction energy profiles	88
5.4	Salient observations	89

CHAPTER 6: SMALL PALLADIUM CLUSTERS ON ZEOLITE SUPPORT

6.1 Introduction	92
6.2 Computational details	93
6.3 Results and discussion	95
6.3.1 Pd atom supported on H-ZSM-5 zeolite	95
6.3.1.1 Structure and energetics	95
6.3.1.2 Interaction of CO and NO with Pd-H-ZSM-5	97
6.3.1.3 Charge analysis	99
6.3.1.4 Vibrational and thermodynamic analysis	102
6.3.2 Pd ₄ clusters supported on Faujasite zeolite	104
6.3.2.1 Structure and energetics of zeolite supported bare Pd ₄ clusters	104
6.3.2.2 Hydrogenated Pd ₄ clusters on zeolite	110
6.3.2.3 Charge analysis	113
6.3.2.4 Energies of adsorption and reverse hydrogen spillover	114
6.4 Salient observations	116

CHAPTER 7: CONCLUSIONS AND FUTURE SCOPES 118

BIBLIOGRAPHY	122
--------------	-----

APPENDIX A	136
------------	-----

APPENDIX B	148
------------	-----

LIST OF PUBLICATIONS	170
----------------------	-----

LIST OF ABBREVIATIONS

AMBER	Assisted Model Building and Energy Refinement
BDE	Bond Dissociation Energy
BE	Binding Energy
BLYP	Combination of Becke exchange functional and Lee-Yang-Parr correlation functional
BSSE	Basis Set Superposition Error
CHARMM	Chemistry at HARvard Molecular Mechanics
DFT	Density Functional Theory
DNP	Double Numerical with Polarization basis set
EA	Electron Affinity
E_{ads}	Adsorption energy
ECP	Effective Core Potential
FAU	Faujasite zeolite
GROMOS	GRoningen MOlecular Simulation package
HOMO	Highest Occupied Molecular Orbital
IP	Ionization Potential
LUMO	Lowest Occupied Molecular Orbital
MM1, MM2, MM3, MM4	Molecular Mechanics force field
ONIOM	Our-own-N-layered Integrated Molecular Orbital + Molecular Mechanics
QM	Quantum Mechanics
QM/MM	Quantum Mechanics/Molecular Mechanics
UFF	Universal Force Field
ZSM-5	Zeolite Socony Mobil – five
η	Global hardness

LIST OF TABLES

TABLE		Page No.
1.1	Classification of clusters according to the nature of bonding.	8
1.2	Variation of fraction of surface atoms (F_s) with number of atoms (N) of a Na cluster of diameter D (nm).	11
3.1	Average bond lengths ($\langle \text{Pd-Pd} \rangle$) in Å and binding energy per atom (BE/atom) in eV for the most stable palladium clusters as a function of cluster size.	46
3.2	Average coordination numbers (γ) of the ground state palladium clusters as a function of cluster size.	56
3.3	Fragmentation energies (eV) of the lowest energy neutral palladium clusters.	57
3.4	Fragmentation energies (eV) of the lowest energy cationic palladium clusters.	58
3.5	Fragmentation energies (eV) of the lowest energy anionic palladium clusters.	58
3.6	Ionization potentials (IP) and electron affinities (EA) in eV for the lowest energy palladium clusters.	60
3.7	Dipole moments μ_e (in debyes) of the ground state palladium clusters as a function of cluster size.	63
4.1	Calculated parameters of the most stable neutral Pd_nCO ($n=1-7$) complexes.	71

4.2	Calculated parameters of the most stable cationic Pd _n CO (n=1-7) complexes.	72
4.3	Calculated parameters of the most stable anionic Pd _n CO (n=1-7) complexes.	73
5.1	Spin multiplicity (M), bond distances (d) of the adsorbates in Å, binding energy (BE) and activation energy (E _a) and in eV, vibrational frequency in cm ⁻¹ and Mulliken charge (q) of the adsorbates for the lowest energy isomers of oxygen adsorbed neutral, cationic and anionic Pd ₄ clusters.	84
5.2	Bond distances (Å), binding energies BE (eV), vibrational frequencies (cm ⁻¹) and Mulliken charges (q) of the adsorbates for the co-adsorption complexes of Pd ₄ q (q=0, 1, -1) clusters.	90
6.1	Important geometrical parameters: bond distances R (Å), bond angles <Pd-C/N-O (deg) and calculated adsorption energies E _{ads} (kcal/mol) of the optimized Pd-HZSM-5 complexes.	103
6.2	Partial charges (au) and the electronic configurations based on NPA from NBO analysis of the optimized Pd-HZSM-5 complexes.	106
6.3	Vibrational and thermodynamic property analysis of CO and NO adsorbed Pd-HZSM-5 complexes at 298.15 K.	108
6.4	Important structural parameters, Mulliken charges and energetics of gas phase Pd ₄ , Zeo1 and Pd ₄ /Zeo1 complexes.	111
6.5	Important structural parameters, Mulliken charges and energetics of Zeo2 and Pd ₄ /Zeo2 complexes.	114
6.6	Important structural parameters, Mulliken charges and energetics of Zeo3 and Pd ₄ /Zeo3 complexes.	117

LIST OF FIGURES

FIGURE		Page No.
1.1	Schematic representation of cluster placed in between atom, molecule and bulk material.	7
1.2	Few examples of various cluster types.	7
1.3	Energy band structure in bulk metal turns to discrete energy levels in large and small metal clusters.	12
1.4	Schematic representation of variation of cluster properties with cluster size or number of atoms in the cluster.	13
1.5	Variation of ionization potential of potassium clusters with cluster size.	14
1.6	Experimental electron affinities of silver anionic clusters with cluster size.	14
1.7	Binding energy per atom versus $N^{1/3}$ for the cluster series of palladium (Pd_N , $N=2-23$, 55 and 147) clusters.	15
1.8	Variation of melting temperature of gold clusters with cluster size.	15
2.1	Number of publications where the phrase “density functional theory” appears in the title or abstract (taken from ISI Web of Science).	30
2.2	Comparison of accuracy of different computational methods.	35

2.3	Use of various basis sets with different computational methods leading to the exact solution of Schrödinger equation.	38
3.1	Lowest energy optimized structures of neutral Pd ₂ –Pd ₁₃ clusters.	45
3.2	Variation of average bond lengths (Å) with cluster size for the most stable palladium clusters.	54
3.3	Binding energies per atom in eV for the most stable palladium clusters as a function of cluster size.	54
3.4	Binding energies per atom versus $n^{-1/3}$ for the neutral, cationic, and anionic clusters.	55
3.5	The stability function of the most stable palladium clusters as a function of cluster size.	57
3.6	Bond dissociation energies in eV as a function of clusters size for most stable palladium clusters.	59
3.7	Variation of ionization potential (IP) and electron affinity (EA) of lowest energy palladium clusters with cluster size.	61
3.8	Variation of HOMO-LUMO gap with cluster size of most stable palladium clusters.	62
3.9	Global hardness of most stable palladium clusters with cluster size.	62
4.1	Optimized structures for the most stable geometries of Pd _n ^q CO (q=0, 1 and -1, n=1–4) clusters.	70
4.2	Optimized structures for the most stable geometries of Pd _n ^q CO (q=0, 1 and -1, n=5–7) clusters.	74

- 4.3** Linear correlation between change in the C-O bond length and shift in the C-O stretching frequency for adsorbed CO molecule in neutral (upper panel), cationic (middle panel), and anionic (lower panel) Pd_nCO clusters. 77
- 5.1** Reaction energy profile for dissociation of oxygen on gas phase neutral Pd₄ cluster for singlet and triplet states. 82
- 5.2** Reaction energy profile for dissociation of oxygen on gas phase cationic Pd₄ cluster. 83
- 5.3** Reaction energy profile for dissociation of oxygen on gas phase anionic Pd₄ cluster. 85
- 5.4** Lowest energy structures of: (a) neutral, (b) cationic and (c) anionic Pd₄O complexes. 86
- 5.5** Lowest energy structures of: (a) neutral, (b) cationic and (c) anionic Pd₄CO₂ complexes. 87
- 5.6** The lowest energy structures corresponding to the co-adsorption of O₂+CO, 2O+CO, O+CO and O+CO₂ on gas phase neutral (first row), cationic (second row) and anionic (third row) Pd₄ clusters. 89
- 5.7** Frontier molecular orbitals of lowest energy gas phase and oxygen adsorbed Pd₄^{0,±} clusters. 92
- 5.8** The energetic profiles of complete reaction cycles for CO oxidation on Pd₄^{0,±} clusters: (a) molecular O₂, (b) dissociated O₂ and (c) a single atomic O reacting with CO. 95
- 6.1** Optimized structures of H-ZSM-5; Pd on H-ZSM-5; CO and NO adsorption on Pd-H-ZSM-5: (a)-(d) 7T cluster model and (e)-(h) 93T embedded cluster model. 101

- 6.2** The interaction of Pd-HZSM-5 with: a CO molecule through (a) σ donation and (b) π back-donation; an NO molecule through (c) forming a covalent σ bond via sharing NO $2\pi^*$ and Pd d_σ electrons. 107
- 6.3** Lowest energy structures of (a) gas phase Pd₄ cluster; ONIOM2 model clusters of: (b) top and (c) side view of Zeo1(1H); (d) top and (e) side view of Pd₄/Zeo1(1H); (f) Pd₄H/Zeo1. 110
- 6.4** ONIOM2 optimized lowest energy structures of: (a) top and (b) side view Zeo2(2H); (c) Pd₄/Zeo2(2H); (d) Pd₄H/Zeo2(1H); (e) Pd₄H₂/Zeo2. 113
- 6.5** ONIOM2 optimized lowest energy structures of: (a) top and (b) side view Zeo3(3H); (c) Pd₄/Zeo3(3H); (d) Pd₄H/Zeo3(2H); (e) Pd₄H₂/Zeo3(1H); (f) Pd₄H₃/Zeo3. 116

CHAPTER

1

INTRODUCTION AND MOTIVATION

There's plenty of room at the bottom

(Richard Feynman on nanoscience)

GAS PHASE NANOCCLUSERS

1.1 Definition

Nanoclusters are defined as aggregates of atoms or molecules of nanometric size, containing a number of constituent particles ranging from ~ 10 to 10^6 [1,2]. The origin of the word cluster comes from the German word "*Klustro*" which represents a pile of material or nonmaterials [3]. The importance of clusters was first proposed by Robert Boyle in his book, *The Sceptical Chymist* (1661) [4], where he spoke of "*minute masses or clusters that were not easily dissipable into such particles that composed them*". "*Small is different*", was postulated a few years ago by U. Landman, referring to the physical and chemical properties of clusters, which can differ completely from those of the corresponding bulk materials [5]. Every cluster has its own intrinsic discrete electronic structure. Due to this, by adding or removing a single atom from a cluster of a certain size, drastic changes in the physical and chemical properties can be obtained. Bulk metallic properties such as delocalization of electrons, which imbue them with high electrical and thermal conductivity, light reflectivity and mechanical ductility may be wholly or partially absent in metal nanoclusters, while new properties develop in them [6]. Figure 1.1 depicts clusters as a state between isolated atoms or bulk solid [7]. It also implies that it is possible to get them either from atoms or molecules or from bulk material.

Clusters serve as a bridge among different disciplines of atomic, molecular, condensed matter and nuclear physics as well as physical, organic and analytical chemistry [8,9]. Improvements in experimental techniques and advancement in computational methods have increased the interest in cluster science.

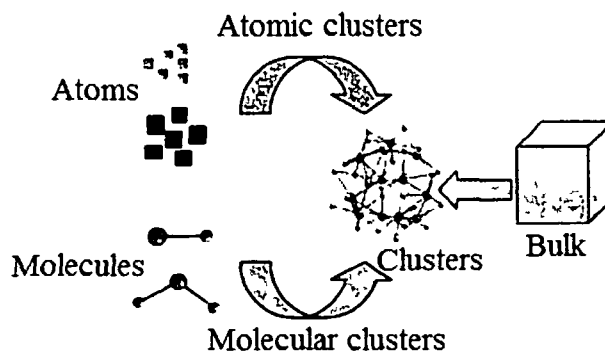


Figure 1.1: Schematic representation of cluster placed in between atom, molecule and bulk material. The dimension increases from left to right in the figure.

1.2 TYPES OF CLUSTERS AND CLUSTER BONDING

Clusters can be formed either from similar constituents or form the combination of different types of constituents. According to the nature of constituents clusters may be classified in the following way [2]:

Homo-atomic (or *homo-molecular*) clusters, A_n , are defined as clusters with identical constituent particles. Examples: rare gases (e.g. Ar_n), metals (e.g. Au_n), carbon (C_{60}), small molecules (e.g. $(H_2O)_n$).

Hetero-atomic (or *hetero-molecular*) clusters, A_nB_m , result from two or more different species. Examples: Cd_nSe_m , Pd_nPt_m etc.

Some of the cluster types are shown in Figure 1.2.

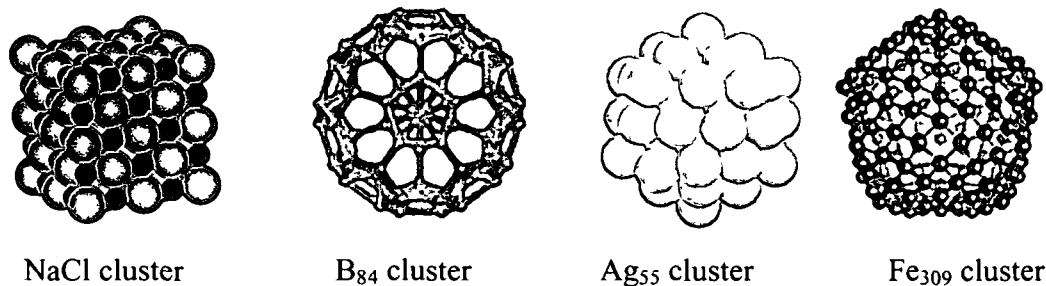


Figure 1.2: Few examples of various cluster types.

There are, of course, various types of clusters depending on the nature of chemical bonding among the constituents forming the aggregate, which may be of ionic, covalent, metallic, hydrogen bond and van der Waals in character. Table 1.1 shows a summary of the various cluster types according to the nature of bonding [7].

Table 1.1: Classification of clusters according to the nature of bonding.

Cluster type	Examples	Nature of bonding	Binding energy/mol (kcal)
<i>Ionic clusters</i>	$(\text{NaCl})_n$	Strong ionic bonding	~ 50 – 100
<i>Covalent clusters</i>	$\text{C}_{60}, \text{B}_n, \text{Si}_n$	Strong covalent bonding	~ 20 – 100
<i>Metal clusters</i>	<i>Simple and noble metal clusters</i> $(\text{Al}_n, \text{Ag}_n, \text{Au}_n)$	Moderately strong metallic bonding	~ 10 – 50
	<i>Transition metal clusters</i> $(\text{Fe}_n, \text{Pd}_n)$	Moderate to strong metallo-covalent bonding	
<i>Molecular clusters</i>	$(\text{H}_2\text{O})_n$	Molecular interactions, hydrogen bonding, van der Waals, etc.	< 10
<i>van der Waals clusters</i>	Rare gas clusters $(\text{Ar}_n, \text{Xe}_n)$	Weak bonding due to polarization	< 5

1.3 CLUSTER GENERATION AND DETECTION IN GAS PHASE

1.3.1 Cluster generation in gas phase

The formation of clusters in gas phase normally involves condensation of the vapour of the constituents. Vapours from non-volatile materials can be produced in one of the several ways including laser vaporization, thermal evaporation and sputtering [10].

(a) Supersonic expansion source

It is an indispensable tool in modern chemical physics and physical chemistry for effective production of weakly bonded clusters from gaseous species. A number of parameters (nozzle size, shape and backing pressure) can be varied to produce cold clusters and to tune cluster size distributions. A small amount of condensing gas is seeded in a helium beam to promote cluster formation and cooling. Clusters of rare gases and other molecules are produced and studied using the supersonic beam technique.

(b) Laser vaporization supersonic cluster source

It is one of the most popular and powerful techniques to produce metal and semiconductor clusters in the gas phase. In this technique, the target material is heated up to $\sim 10,000$ K with an intense pulsed laser beam, producing plasma with both neutral and charged atomic species. The cluster growth is initiated due to rapid cooling by introducing a pulsed high pressure carrier gas (usually helium). Mixed clusters can be produced using this technique either by using an alloy target or adding a reactive gas in the carrier gas. A two-laser vaporization source has also been used to produce alloy clusters [11,12].

(c) Thermal evaporation source

This is the earliest method used to produce mostly alkali and other low melting point metal clusters in the gas phase [13,14]. In this technique, a bulk sample is simply heated in an oven to produce the atomic vapour, which is entrained in a low-pressure gas flow for nucleation and cluster growth. Clusters of sodium atoms with more than 20,000 atoms have been made with this source [15].

(d) Sputtering source

In this method, sputtering of target surface is made with ion beams of the rare gases or cesium. Cluster sizes produced in this technique are generally limited and the cluster temperatures are high. A related technique is a cold cathode discharge in

flowing rare gas. The discharge ionizes the rare gas, which then sputter metal atoms off the cathode target. Cluster ions are formed through aggregation in the flowing gas stream.

1.3.2 Cluster detection in gas phase

The development of cluster research is driven by new techniques to generate clusters and by new experimental tools to probe them. *Mass spectrometry* is the most useful tool in gas phase cluster research because it gives the information about cluster's mass and size. Since more stable clusters tend to be more abundant, a mass distribution of clusters contains valuable information about cluster stabilities, revealing magic number clusters with significantly higher abundance than their neighbours. Some of the most important discoveries of cluster science viz., the shell structure of free electron metal clusters [16] and C₆₀ [17] are based on the mass distribution of clusters.

The most popular mass spectrometric technique is the *time of flight* (TOF) method [18], in which cluster mass information is obtained by measuring the flight times of a cluster ion beam in a given distance. This method is particularly suitable with pulsed laser vaporization cluster sources. *Ion cyclotron resonance* (ICR) is another powerful mass spectrometric technique used in cluster research [19], in which, highly accurate masses (m/q) can be obtained by measuring cyclotron frequencies, $\omega_c = qB/m$ for ion beam of charge q moving in a strong magnetic field B . There are other mass separation techniques such as the *quadrapole mass filter* (QMF) and *Wien filter*. *Ion chromatography* is one more mass spectrometry technique, which is also capable of gathering the information about cluster isomers of significantly different shapes, such as carbon and silicon clusters [20].

1.4 SIZE EFFECTS IN CLUSTERS

1.4.1 High fraction of surface atoms

One important difference of cluster properties from the corresponding material in macroscopic bulk phase is the high percentage of their atoms on the surface [2]. These under-coordinated surface atoms have tendency to form additional bonds with ligands to give stability to the clusters. The reactivity of surface atoms makes clusters interesting in heterogeneous catalysis.

In the Spherical Cluster Approximation (SCA), an N atom cluster is modelled by a sphere of cluster volume (V_c), radius (R_c) and surface area (S_c), which can be related to the volume (V_a), radius (R_a) and surface area (S_a) of the constituent atoms, as follows [2]:

$$V_c = NV_a \quad (1.1)$$

(Oversimplified equation without considering the fact that hard sphere cannot pack to fill up space exactly)

OR
$$\frac{4}{3}\pi R_c^3 = N \frac{4}{3}\pi R_a^3 \quad (1.2)$$

$$R_c = N^{1/3} R_a \quad (1.3)$$

$$S_c = 4\pi R_c^2 = 4\pi (N^{1/3} R_a)^2 = 4\pi N^{2/3} R_a^2 \quad (1.4)$$

In the limit of a large cluster, the number of surface atoms (N_s) in a cluster is given by dividing the surface area of the cluster by the cross sectional area of an atom (A_a):

$$N_s = \frac{4\pi N^{2/3} R_a^2}{\pi R_a^2} = 4N^{2/3} \quad (1.5)$$

For pseudo-spherical clusters, fraction of surface atoms (F_s) can be defined as

$$F_s = \frac{N_s}{N} = 4N^{-1/3} \quad (1.6)$$

Equation (1.6) indicates that the percentage of atoms becomes an appreciable fraction of the total number of atoms as the cluster size decreases. The variation of fraction of of surface atoms with different cluster sizes is shown in Table 1.2.

Table 1.2: Variation of fraction of surface atoms (F_s) with number of atoms (N) of a Na cluster of diameter D (nm).

Parameters	Small	Medium	Large
N	$\leq 10^2$	$10^2 - 10^4$	$> 10^4$
D	≤ 1.9	1.9 – 8.6	> 8.6
F_s	≥ 0.86	0.86 – 0.19	≤ 0.19

1.4.2 Electronic structure

Energy bands in a lattice arise from the discrete energy levels of the individual atoms forming the lattice. For a metal, the top occupied band, called the *conduction band* (CB) and the next higher unfilled band, called the *valence band* (VB) overlap with each other. The number of energy levels in a given interval of energy is termed as *density of states* (DOS). In reducing the size of a bulk metal to a few hundreds of atoms, there occurs a dramatic change in the DOS of the conduction band. The continuous DOS in the band is replaced by a set of discrete energy levels with spacings larger than the thermal energy $k_B T$ and a gap opens up. The changes in electronic structure during the transition of a bulk metal to a large cluster of 100 atoms and then down to a small cluster of less than 15 atoms, which is analogous to a molecule with bonding and antibonding orbitals are illustrated in Figure 1.3 [21].

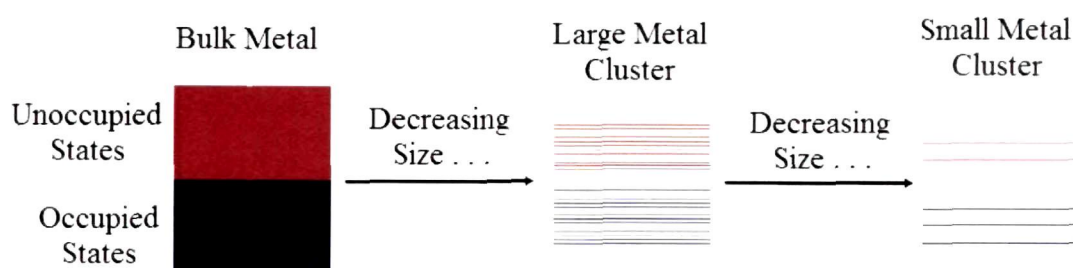


Figure 1.3: Energy band structure in bulk metal turns to discrete energy levels in large and small metal clusters.

Continuously decreasing cluster size leads to an extreme case, in which, particle diameters are in the order of wavelengths of electrons. In this situation, the energy levels can be modelled by the quantum mechanical treatment of a particle in a box. This phenomenon is referred to as the *quantum size effect* (QSE). The QSE leads to new electronic properties in metal nanoclusters, which can be understood in terms of Heisenberg uncertainty principle stating more an electron is spatially confined the broader will be its range of momentum [21].

1.5 VARIATION OF CLUSTER PROPERTIES WITH SIZE

Scaling laws

Considering spherical cluster model, the variation of cluster properties with size can be described by simple scaling laws (interpolation formulae) [2], either in powers of the cluster radius:

$$G(R) = G(\infty) + aR^{-\alpha} \quad (1.7)$$

or the number of atoms:

$$G(N) = G(\infty) + aN^{-\beta} \quad (1.8)$$

where $G(\infty)$ is the value of property G in the bulk limit.

Since many properties depend on the fraction of surface atoms in a cluster (F_s) and $F_s (\propto 1/R) \propto N^{-1/3}$, the exponents α in equation (1.7) and β in equation (1.8) are generally 1 and 1/3.

The variation in properties of elements from atoms to bulk is shown in Figure 1.4.

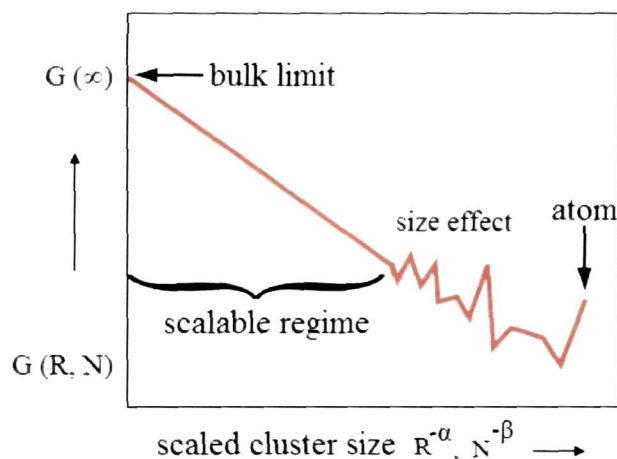


Figure 1.4: Schematic representation of variation of cluster properties with cluster size or number of atoms in the cluster.

It is seen from the figure that materials starting from a single atom to its bulk phase can be divided into two regions: (i) a scalable regime where properties vary smoothly until they reach the bulk limit and (ii) a non-scalable regime, characterized by clusters, where the variation is highly non-monotonic [22].

Variation of some cluster properties like ionization potential, electron affinity, melting temperature and binding energy with cluster size are shown in Figures 1.5 – 1.8.

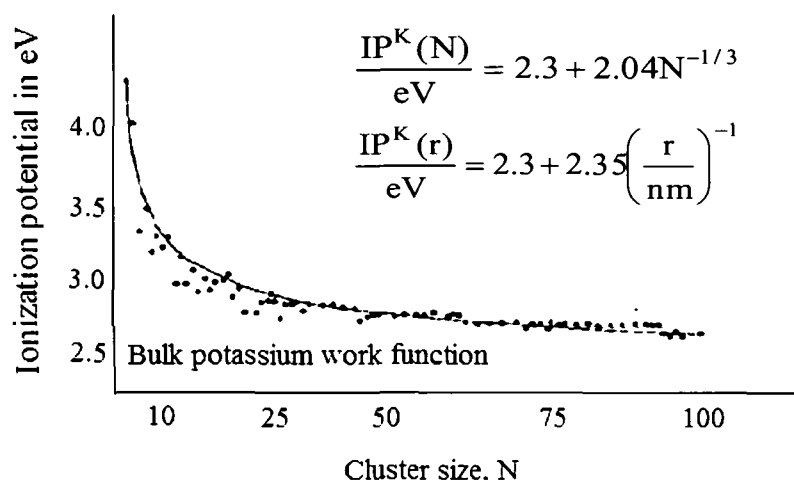
Ionization potential

Figure 1.5: Variation of ionization potential of potassium clusters with cluster size [2].

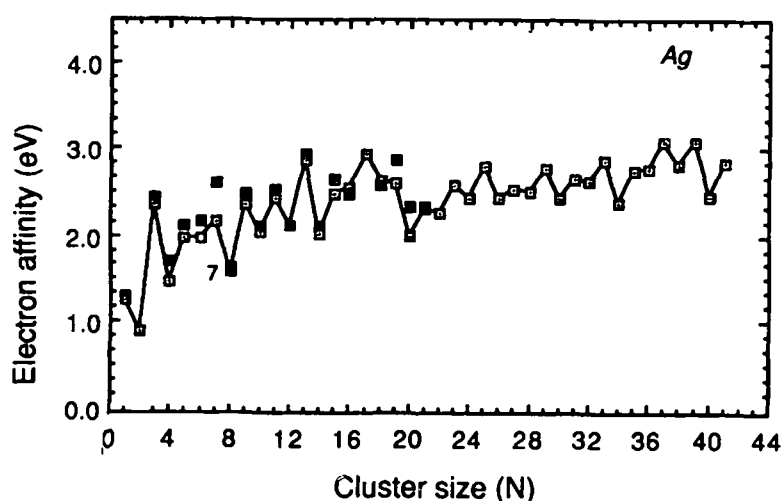
Electron affinity

Figure 1.6: Experimental electron affinities of silver anionic clusters with cluster size [23].

Binding energy

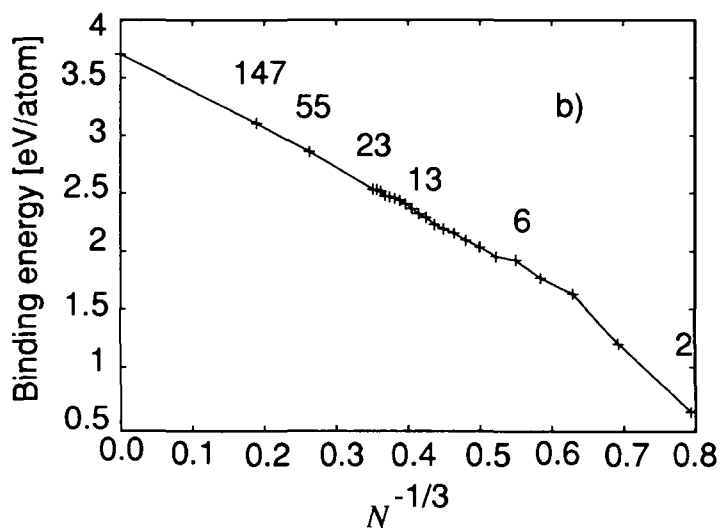


Figure 1.7: Binding energy per atom versus $N^{-1/3}$ for the cluster series of palladium (Pd_N , $N=2-23$, 55 and 147) clusters. [24].

Melting temperature

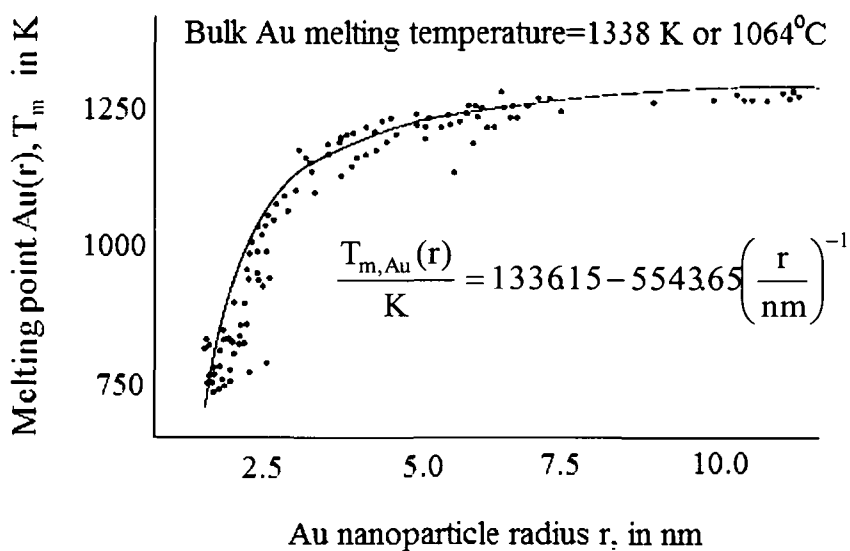


Figure 1.8: Variation of melting temperature of gold clusters with cluster size [2].

1.6 WHY CLUSTERS ARE INTERESTING?

Clusters possess properties significantly different from molecules and bulk material. These differences result from the fact that the number of surface atoms is a substantial fraction of the number of atoms forming the clusters of smaller sizes. The confinement of electrons in the potential well of small volume in clusters also gives rise to the differences from their bulk counterpart. Moreover, clusters containing not more than a few hundred particles have strongly size-dependent properties, viz., geometric and electronic structure, binding energy, melting temperature etc. These peculiar properties make nanoclusters well suited for several applications. Besides the traditional interest in applications as catalysts [25], nanoclusters have a much older history of their applications in the decoration of majolicas with lustre of Ag and Cu clusters by Renaissance masters in Umbria, Italy [26,27] to the more recent biological uses [28,29] of Au clusters.

Determination of geometric structure is the starting point for understanding the properties of nanoclusters. With this goal in mind, the first question to answer is: *what is the most stable structure of a cluster from an energetic point of view?* To answer this question we need to find the global minimum on the *potential-energy surface* (PES) of the cluster [30]. The focus of this thesis is to find the lowest energy structures of small palladium clusters based on density functional theory study. We remark that cluster science is an interdisciplinary field [9,9], in which, the interplay among experiments, theory and simulations is very active. In fact, the analysis of an experiment is very often carried out by some kind of simulation. In the words of Marks [31], *“small particle structures cannot be understood purely from experimental data and it is necessary to simultaneously use theoretical or other modeling”*. Due to these facts, theoretical approaches towards the study of metal nanoclusters have become a subject of many investigations during the last few decades.

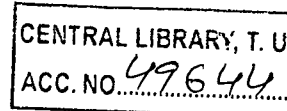
1.7 SUPPORTED METAL CLUSTERS

Supported metal cluster catalysis plays an enormous role in modern chemical industry and much effort is devoted in understanding this phenomenon at molecular level to design catalysts with high efficiency and selectivity [32-35]. High-area porous oxides and zeolites, normally used as supports have potential application in

heterogeneous catalysis [36-40]. With the recent emphasis on environmental protection, the need for solid catalysts to replace liquids has grown and this field is burgeoning from laboratory preparative chemistry to industrial applications. Metal clusters bonded to oxide or zeolite supports combine the technological advantages of solid catalysts (robustness for high temperature reaction, lack of corrosiveness, ease of separation from products) with the selectivity of soluble molecular catalysts. Uniform supported catalytic species are regarded as molecular analogues, with structures that may be determined far more precisely than those of conventional supported metal catalysts consisting of particles (or crystallites) of metal on supports [35]. The first step in understanding the properties of supported metal catalysts is to clarify how the interaction with the support can modify the structural and electronic properties of supported metal clusters. Charge transfer between support and cluster and diffusion of reactant molecules from support, a process known as reverse spillover [41], are some of the important and complex roles of the support materials in these catalytic systems.

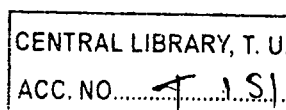
Researchers have dedicated substantial effort to the development of methods for synthesis and characterization of supported molecular metal complexes and clusters. These important classes of catalysts are typically prepared by the reaction of a metal complex incorporating reactive ligands (such as alkyls, allyls or carbonyls) with oxygen atoms or OH groups of oxide or zeolite supports [33]. The metal atoms in these complexes are normally bonded to the oxygen atoms of the support. Characterization of supported metal-clusters consisting of only one or a few atoms is challenging because of their small sizes, dispersed states and non uniformity. Therefore a large number of techniques are required to characterize their structures [35]. The intrinsic non uniformity of the sites on support surfaces also gives variations in structure and bonding of the supported species. Due to this, the anchored materials are generally not characterizable by crystallographic methods such as X-ray diffraction. Instead, the most appropriate methods for characterizing local surface structure and bonding include (i) transmission electron microscopy (TEM); (ii) a set of spectroscopic methods viz., X-ray absorption (comprising extended X-ray absorption fine structure (EXAFS) and X-ray absorption near edge structure (XANES)), NMR, infrared (IR), Raman, Mössbauer, UV-visible and others; (iii) temperature-programmed methods such as reduction, oxidation and decomposition and (iv) theoretical techniques. These methods are developing

rapidly and the results emerging from different investigations provide important segment for their improvement at fundamental level.



1.8 IMPORTANCE OF PALLADIUM CLUSTERS

Most of the properties of transition metal (TM) clusters are entirely different from simple metal clusters due to the significant contribution from localized and unfilled *d* electrons. The unusual electronic and magnetic properties have made TM clusters a subject of many investigations [42,43]. These properties depend on the geometric and electronic structures of the lowest energy isomers and that is why the search for the global minimum becomes very important. The possibility of coexisting various low energy isomers with different spin states adds a lot of difficulties to the study of the geometric [44] and electronic properties of 4*d* TM clusters [45,46]. Palladium (Pd) is one of the best studied 4*d* TM element due to its wide application in catalytic reactions. Small clusters of Pd are used in automotive exhaust systems to reduce toxic pollutants such as CO, NO and hydrocarbons. Ultra-dispersed Pd clusters supported on alumina are found to be more active than Pd (111) single crystals for oxidation of CO [47]. In exhaust gas treatment, catalytic reduction of nitrogen monoxide with propane takes place on zeolite supported Pd clusters [48,49] and CO reduces the extremely reactive NO in presence of highly dispersed Pd clusters supported on γ -alumina [50]. Moreover, ultra-dispersed Pd clusters up to 2 nm (150 atoms) in size act as highly active catalysts in hydrogenation processes [51], having much higher selectivity in the conversion of triple to double bonds than that of bulk Pd [52]. Due to this remarkable property, Pd nanoclusters replace Rh in automobile catalytic converters [53,54]. In addition, recent observation of ferromagnetism in Pd nanoparticles makes the possibility of their potential use in magnetic storage materials [55-57]. Extensive experimental investigations [58-68] have been performed to study the geometric and electronic structures of small palladium clusters, which allow one to understand the size-dependencies of their chemisorptive and catalytic properties in a better way. In the following sections, we have presented a brief review of the research work made on palladium nanoclusters in gas phase as well as in support.



1.8.1 Bare palladium clusters

One important feature of Pd metal is that in bulk form, it exhibits high paramagnetic susceptibility and only 6% lattice expansion induces ferromagnetism in it [69]. However, small clusters of Pd are found to possess magnetic moments [70-80]. In contrast, the Pd atom is nonmagnetic with a closed-shell electronic configuration of $4d^{10}5s^0$. In gas-phase palladium clusters, the interaction between the Pd atoms involves *s-d* hybridization, which leads to the depletion of *4d* levels giving rise to the local magnetic moments and magnetism in small Pd clusters [74] and enhances their reactivity. Although many theoretical and experimental studies have been performed to study the magnetic moment of small palladium clusters, some of them are found to contradict each other. The Stern-Gerlach experiments [81-83] showed the absence of magnetic moments in Pd clusters, while photoemission experiments [84] suggested a Ni-like spin-distribution in Pd_N clusters with $N \leq 6$, and non-magnetic behavior for $N \geq 15$. In contrast, dc susceptibility measurements [57] resulted in magnetic moments of $(0.23 \pm 0.19) \mu_B$ per atom in Pd clusters with diameters in the range of 50 to 70 Å.

However, experimental determination of ground state structure for small TM clusters is difficult due to their extremely small sizes that make experimental methods based on diffraction techniques not useful to elucidate the structures. Therefore, a large number of theoretical approaches [24,85-100] have been used to study the electronic structures and geometries of ultra dispersed Pd clusters. Theoretical studies become highly efficient because direct calculations of small sized clusters is possible with complete minimization of their total energy with respect to all the atomic positions. The theoretical studies are based on a wide variety of different approaches, ranging from multi-configuration self consistent field calculations for smallest clusters [88,89,89] over density functional theory (DFT) calculations for small and medium clusters [91-100] to extended Hückel [86,86] and tight-binding methods [90] applied to large clusters.

Different studies [72,93] have confirmed the non-zero spin of the lowest lying isomers of small Pd clusters, being thus magnetic. Zhang *et al.* [100] have performed an extensive study of the structural, energetic, electronic, and magnetic properties of Pd_N clusters ($N \leq 13$ and selected structures at $N=19$ and 55) with DFT method. Their results indicate that binding energy of these clusters increases from

linear to planar, and further to three-dimensional conformations and that icosahedral structures are favoured over both decahedral and cuboctahedral structures for $N=13$ and 55. These results are in good agreement with previous calculations of Kumar and Kawazoe [24]. Rogan *et al.* [99] reported increment of bond lengths and binding energies with increasing cluster size of small Pd_N clusters ($2 \leq N \leq 13$) and predicted Pd_{13} as a magic-number cluster. From a recent study on Pd_N clusters ($14 \leq N \leq 21$) [101], they have found that the minimal energy configurations are not necessarily associated with high symmetry of the atomic arrangement. Luo *et al.* [102] observed variation of magnetic moments with cluster size and shape for Pd_N , $N=2-15$ clusters. Nava *et al.* [103] investigated neutral ligand-free Pd_n clusters, $n=2-309$, using density functional calculations. They treated numerous clusters and optimized them within a given symmetry and investigated Jahn-Teller distortions for n up to about 100. Rösch and co-workers [90] observed increment of average bond lengths with cluster size from an all-electron DFT study on a series of gas-phase Pd_N ($N= 4-309$) clusters. This study also revealed accuracy of LDA over GGA calculations in determining bond distances. Recently, Zhang *et al.* [75] showed that fcc-like structures generated from Pd_{19} octahedron dominate the growth pathway of Pd_N clusters ($N=15-23$) based on spin-polarized density functional calculations. Molecular dynamics study on size dependent analysis of structural stabilities and energetics of Pd_N ($N \leq 40$) clusters [104] resulted preferable three-dimensional structures. A very recent DFT study [105] showed relative stability of Pd_4 , Pd_6 and Pd_9 clusters among a series of Pd_N ($N=1-9$) clusters. Special attention has been put forward to study 13-atom palladium clusters [106-111] because it is the first magic number according to geometric shell model to form high symmetric icosahedral and cuboctahedral structures. Recent first-principles calculations showed that the ground state structures of Pd_{13} cluster do not favour high-symmetry compact structures. Instead, there are less symmetric structures such as cubic [112] and buckled biplanar (BBP) [108,113] structures lying significantly lower in energy than the icosahedral isomers [24,72,100].

1.8.2 Chemisorptions on small gas phase palladium clusters

Studies of chemisorption and oxidation reactions of transition metal clusters can provide information about the properties of the clusters in comparison to those of the

bulk metals. The interaction between CO and a metal atom was first described by Blyholder, in a model based on Hückel molecular orbitals (MOs) [114]. According to this model, the nature of CO interaction with transition metal surfaces is determined by two main components: a σ bond formed between the CO carbon atom and metal surface mainly due to the electron transfer from the adsorbent to the surface and the partial filling of the π^* orbitals of CO due to back-donation from the metal d orbitals. CO is one of the most studied molecules to probe metal surfaces [115] due its simplicity and importance in the field of heterogeneous catalysis. Its vibrational properties reflect the metal-CO bond strength at various possible sites and also the influence of direct environment. Previous theoretical studies of CO chemisorption on palladium clusters include extended Hückel [116], X_α [117], local spin density [118] and Hartree-Fock [119] methods. A pseudopotential CI investigation [120] on CO adsorbed Pd_n ($n=2-4$) clusters provided some insights into the nature of Pd-CO bonding, confirming the repulsive nature of the σ interaction and the essential role of the π -back-donation mechanism for the formation of Pd-CO bond. Ab initio studies of PdCO and Pd_nCO ($n=1-4$) clusters, with or without relativistic corrections and correlation effects, have led to a predominant π bonding, coherent with d^{10} or d^9 metal atomic configurations for Pd system [120-123]. A series of all-electron CCSD(T), QCISD(T) and MP4(SDQ) methods were applied to study details of molecular structure, bonding and vibrational spectrum of PdCO [124]. Hartree-Fock study [125] showed that besides the classical π back-donation from transition metal to CO, the CO σ donation to the partially occupied $4d\sigma-5sp$ metal hybrid orbitals significantly contributes to the chemisorption energy of CO. DFT calculations based on LCGTO-MCP-DF [126] gave different binding energy values of CO bonded to top, bridge, and 3-fold sites of small Pd_2 and Pd_4 clusters, having largest value corresponding to the 3-fold adsorption site. Calculations performed with LCGTO-DF method [127] observed non-negligible relativistic effects for palladium monocarbonyls. Adsorption of CO on nanosize Pd particles of about 140 atoms was studied theoretically (DFT method) and spectroscopically (IRAS and SFG method) by Freund and co-workers [128]. Bertin *et al.* [129] studied chemisorption of CO on some active sites of Pd, Pd_2 and Pd_4 clusters. CO adsorption on large palladium clusters were investigated by Yudanov *et al.* [130] using LCGTO-FF-DF method. Recently, Zanti and Peeters [105] have used DFT method to study the interaction of a CO molecule with Pd_n

($n=1-9$) clusters, which shows that the favoured co-ordination mode of CO is one that promotes the back-bonding interaction. Moreover, the interaction is found to affect the metal-metal bond along with the singlet state of the cluster in the ground state. Experimentally, bond dissociation energies of palladium trimer anion, Pd_3^- , and its carbonyls, $\text{Pd}_3(\text{CO})_n^-$ ($n=1-6$), were measured in gas phase by the energy-resolved collision-induced dissociation method [131]. Gruene *et al.* [132] applied infrared multiple photon dissociation (IR-MPD) spectroscopy to study the adsorption of CO on singly charged palladium clusters containing 3–25 metal atoms. From this study, they have concluded that palladium clusters exhibit a variety of binding sites for CO including a-top, bridge and hollow positions. Catalytic oxidation of CO to CO_2 on palladium is of great practical importance and it is used in commercial three-way catalysts to reduce automotive emission [133,134]. In the real oxidation process, dissociation of O_2 and diffusion of adsorbates on the surface also play important roles. Thus knowledge of co-adsorption properties of CO and O is essential in studying catalytic CO oxidation. Due to this fact, interaction between adsorbed CO and oxygen on palladium has been a subject of large number of experimental [135-142] and theoretical [143-146] studies over the years. Engel and Ertl [136,137] proposed that CO oxidation on Pd occurs via Langmuir-Hinshelwood mechanism, where CO molecules adsorb on the surface and react with chemisorbed oxygen. They found that adsorbed CO inhibits oxygen adsorption, but the reverse is not true. Experimental study of Gabasch *et al.* [141] showed that the reactivity of several Pd–O species towards CO oxidation decreases with increasing oxidation state. Oxidation of CO by supported Pd clusters has also been reported using various experimental and theoretical techniques [142,144-146].

1.8.3 Zeolite supported small palladium clusters

Zeolite supported transition metals have been found to show catalytic activities for many reactions [147-150]. Zeolites are crystalline microporous materials and are being used widely as industrial catalysts. Zeolites ZSM-5 (MFI) and Faujasite (FAU) are the two most important members of the zeolite family, possessing medium and large pores in their respective frameworks.

Since the pioneering work of Li and Armor [151] on the catalytic activity of Co-ZSM-5, metal exchanged ZSM-5 have appeared to be promising catalysts for

catalytic reduction of NO_x by methane in presence of excess O_2 . Recently, zeolite supported Pd catalysts; especially, Pd-ZSM-5 and Pd-H-ZSM-5 have drawn a lot of attention worldwide [152-157] due to their excellent catalytic activity in methane combustion [158-160], NO reduction by CH_4 [161] and many organic reactions [162]. The findings of Nishizaka and Misono [163] suggest that Brønsted acid sites may play important role in stabilizing Pd in a highly dispersed state and this form of Pd is required to achieve high activity and selectivity for NO reduction by CH_4 in the presence of O_2 . Okumura and Niwa [156] used X-ray photoelectron spectroscopy and EXAFS spectra to study Pd loaded on various kinds of metal oxide and zeolites. This study revealed that the metal-support interaction is an important factor affecting profoundly the structure, oxidation state, mobility and catalysis of Pd. Quantum chemical investigations have been widely and successfully applied to study the properties of metal particles within zeolites [164-169]. Rice *et al.* [154] studied the co-ordination and stability of Pd^{2+} in ZSM-5 using gradient corrected density functional theory. Bell and his co-workers [170,171] investigated the state of Pd in Pd-H-ZSM-5 by means of infrared and mass spectroscopies, using CO and NO as probe molecules. Recently, Barone *et al.* [165] have shown that the lowest energy state of a single Pd atom on H-ZSM-5 support is singlet with finite modelling of the support framework.

A large number of experimental studies have been put forward to study the incorporation of small palladium clusters inside pores of FAU zeolites [172-184]. The transmission electron microscopy (TEM) and extended X-ray adsorption fine structure (EXAFS) techniques have confirmed the existence of small Pd_n clusters ($n=1-4, 6, 13$) inside sodalite cages and supercages of FAU zeolites [172-184]. There is also evidence for pure silica-supported palladium clusters [185]. To understand the protonation of zeolite-supported small palladium clusters and the effect of protonation on interaction of these clusters with CO probe molecules, Yakovlev *et al.* [186] carried out density functional based investigation on free and protonated Pd_4 and Pd_6 clusters. From this study, they showed that electron-deficient $[\text{Pd}_n\text{H}]^+$ species can be formed in faujasites (e.g., Pd/NaY) as a result of interaction of guest metal particles with zeolitic protons. It was also found that protonation reduces the CO adsorption energy and increases the vibrational frequency of adsorbed CO. Harmsen *et al.* [187] reported a model describing the interaction of a palladium atom with the Brønsted acidic site of zeolite. They found

that the reduction of Pd^{2+} to Pd^0 and 2H^+ is strongly exothermic. Recently, Morokuma and co-workers [188] have studied the reactivity of zeolite-supported palladium tetramers towards hydrogen molecules. They found that embedding of Pd_4 on a zeolite reduces the barrier for H_2 addition by 7.53 kJ/mol from that in the gas-phase Pd_4 cluster. During the last few years, Rösch and co-workers [189-193] have developed a systematic study of reverse hydrogen spillover from the hydroxyl groups of zeolite support onto four atom and six atom metal clusters. In an extended study [190] on zeolite-supported transition metal clusters (M_6) of platinum and gold groups (Fe, Co, Ni, Cu, Ru, Rh, Pd, Ag, Os, Ir, Pt, Au), resulted energetically favorable reverse hydrogen spillover process for all the metals.

In spite of these experimental and theoretical studies, there are several issues to be addressed on the structure and reactivity of gas phase and supported palladium clusters. Some of these points will be covered in the present thesis.

1.9 OBJECTIVES OF THE PRESENT WORK

The present Ph. D. work was undertaken with the following objectives:

1. Systematic investigation of structural and electronic properties of small gas phase neutral, cationic and anionic palladium clusters and to find their stability and reactivity based on Density Functional Theory (DFT).
2. Theoretical studies of the nature of chemisorption of carbon monoxide and oxygen on small stable gas phase palladium clusters.
3. DFT studies of adsorption and coadsorption of oxygen and carbon monoxide on lowest energy palladium clusters.
4. DFT studies on the effect of zeolite support on the geometry and adsorption properties of small stable palladium clusters using hybrid QM/MM method.

CHAPTER

2

ELECTRONIC STRUCTURE METHODS

*I don't like it, and I'm sorry
I ever had anything to do with it
(Erwin Schrödinger on quantum mechanics)*

2.1 INTRODUCTION

Quantum mechanics, formulated over 100 years ago, is one of the most successful scientific theories ever created. The exact determination of the electronic structure of atoms, molecules and solids is a difficult problem, as the electrons must be treated using the laws of quantum mechanics and not those of classical physics. Among the different quantum mechanics based methods, Density Functional Theory (DFT) has long been the mainstay of electronic structure calculations in all areas of modern computational science including chemistry, physics, material science, biochemistry and geophysics. With its early developments in the late 1920's by Thomas and Fermi, DFT is the first successful method avoiding the most fundamental difficulty in condensed matter theory- the many body problems. It is until now one of the most popular quantum mechanical approaches to electronic structure calculations of molecular and condensed matter systems. In this chapter, we will give a short insight into the most important concepts of the computational methods used to investigate structural and electronic properties of materials.

2.2 OVERVIEW OF COMPUTATIONAL METHODS

Computational methods act as a bridge connecting theory and experiment. It is an interdisciplinary subject implying the synergy of quantum, classical and statistical physics, chemistry and even biochemistry. Computational methods combine all numerical methods based on molecular mechanics, molecular dynamics, Monte Carlo and quantum mechanics employed for qualitative and quantitative

informations like the atomic structure of the material, viz., bond lengths and angles, crystal lattice parameters, surface reconstructions, structural phase transitions; its electronic, optical and magnetic properties; reactivity of surfaces; chemical reactions and catalytic behaviour.

In the present thesis, we have used density functional theory (DFT) based quantum mechanics (QM) and quantum mechanics/molecular mechanics (QM/MM) methods to perform all the calculations. A brief discussion on these methods has been given in the following sections.

2.2.1 Molecular mechanical methods

These methods apply classical laws of physics to predict the structures and properties of molecules. Molecular mechanics view a molecule as spheres of different masses (atoms) connected together by a variety of springs (chemical bonds). The coordinates of all the atoms at the equilibrium length of all the springs correspond to the lowest energy state of the molecule. Molecular mechanics represent the interactions between the atomic species by *force field* method. All the energy terms to define the different types of interactions in a molecule is called the “steric” energy or the total potential energy of the molecule, which is given by

$$E_{total} = E_{stretch} + E_{bend} + E_{torsion} + E_{vdW} + E_{HB} + E_{electro} \quad (2.1)$$

where $E_{stretch}$ in equation (2.1) is the bond stretching, E_{bend} is the bond angle bending, $E_{torsion}$ is the dihedral angle rotation, E_{vdW} is the van der Waals forces, E_{HB} is the hydrogen bonding and $E_{electro}$ is the electrostatic interaction term.

E_{total} is the basis of a *force field*, which allows calculation of all the forces on a system giving its energy. Molecular mechanics calculations are performed based on nuclei interactions and do not treat the electrons in a molecular system explicitly. However, electronic effects are included implicitly in force fields through parameterizations.

Advantages: They

- rely on *force-field* with embedded empirical parameters.
- are computationally least intensive - fast and useful with limited computer resources.

- can be used for bio-molecules as large as enzymes (thousands of atoms).

Disadvantages: They

- are applicable only for a limited class of molecules.
- do not calculate electronic properties.
- require experimental data (or data from *ab-initio*) for parameters.
- calculate systems or processes with no breaking or forming of bonds.

Models: MM1, MM2, MM3, MM4, AMBER, CHARMM, GROMOS, UFF

2.2.2 Quantum mechanical methods

Quantum mechanical methods can be divided into two categories: *ab initio* and *semi-empirical* models. *Ab initio* methods include Hartree-Fock (HF), Möller-Plesset perturbation theory (MP), Configuration Interaction (CI), Coupled Cluster (CC) method and density functional theory (DFT). A drawback of *ab initio* calculations is the extremely demanding computer resources, especially for large molecular systems. Semi-empirical quantum chemical methods lie between *ab initio* and molecular mechanics (MM). Like MM, they use experimentally derived parameters to strive for accuracy; like *ab initio* methods, they are quantum mechanical in nature. Semi-empirical methods are computationally fast because many of the difficult integrals are neglected. The error thus introduced is compensated through the use of parameters. The following subsections briefly discuss about some important quantum mechanical methods.

2.2.2.1 Hartree-Fock theory

The electronic structure and total electronic energy of atoms, molecules and crystals can be obtained by solving the time-independent, non-relativistic Schrödinger equation:

$$\hat{H}\psi = E\psi \quad (2.2)$$

The Born-Oppenheimer approximation allows us to calculate the wave function for electrons moving in the potential field of positively charged fixed nuclei.

Within this approximation, the Hamiltonian, \hat{H} , is expressed as

$$\hat{H} = \frac{1}{2} \sum_i \nabla_{r_i}^2 - \sum_i \sum_A \frac{Z_A}{R_{Ai}} + \sum_{i < j} \frac{1}{r_{ij}} + \sum_{A < B} \frac{Z_A Z_B}{R_{AB}} \quad (2.3)$$

The first term on right hand side of equation (2.3) represents the kinetic energy of electrons i , the other terms represent the potential energies, including attractions between electron i and nuclei A separated by a distance of R_{Ai} ; repulsions among electrons i and j ; repulsions among nuclei A and B of atomic numbers Z_A and Z_B separated by a distance of R_{AB}

The many electron wave function Ψ is approximated as a product of one electron wave functions or molecular orbitals ϕ_i , which can be expanded as a linear combination of atomic orbitals or basis functions, χ_μ :

$$\phi_i = \sum_\mu \chi_\mu c_{\mu i} = X C_i \quad (2.4)$$

Utilization of variational principle $\langle \psi | H | \psi \rangle / \langle \psi | \psi \rangle \geq E(\text{exp})$ yields an eigenvalue equation that gives molecular orbitals and energies:

$$f_i \phi_i = \varepsilon_i \phi_i \quad (2.5)$$

where f is an effective one-electron Fock operator with matrix elements given by

$$F_{uv} = \langle \chi_u | f | \chi_v \rangle = H_{uv} + \sum_{st} P_{st} [\langle uv | st \rangle - \langle us | vt \rangle / 2] \quad (2.6)$$

The one-electron matrix elements are given by

$$H_{uv} = \left\langle u \left| -\frac{1}{2} \nabla^2 \right| v \right\rangle - \sum_B Z_B \left\langle u \left| \frac{1}{R_B} \right| v \right\rangle \quad (2.7)$$

and two-electron integrals by

$$\langle uv | st \rangle = \iint d\tau(1) d\tau(2) \chi_u(1) \chi_v(1) \left(\frac{1}{r_{12}} \right) \chi_s(2) \chi_t(2) \quad (2.8)$$

P is the first-order Fock-Dirac (or one-particle) density matrix

$$P_{uv} = \sum_i n_i c_{ui} c_{vi} \quad (2.9)$$

where n_i occupation number, 0, 1 or 2.

The Fock equations can be solved by matrix diagonalization of the matrix equations

$$FC = SCE \quad (2.10)$$

where S is the overlap matrix and C is a square matrix with the i th column being the MO coefficients of the i th molecular orbital.

The real cost of computation of HF methods is due to the two-electron integrals in the Hamiltonian that has been simplified in semiempirical methods.

2.2.2.2 Semiempirical methods

Semiempirical methods are simplified versions of Hartree-Fock theory using empirical (derived from experimental data) corrections in order to improve performance. These methods are based on three approximation schemes:

(a) *The elimination of the core electrons from the calculation*, (b) *The use of the minimum number of basis sets* and (c) *The reduction of the number of two-electron integrals*. The hierarchy of integral approximation and their effect on the Fock matrix formation are given below.

Zero Differential Overlap (ZDO) method

In this method, the integral containing the product $\chi_u \chi_v$ in equation (2.8) is neglected when u is not equal to v . This leads to:

$$\langle uv|st\rangle = \delta_{uv} \delta_{st} \langle uu|ss\rangle$$

$$\text{where } \delta_{uv} = \begin{cases} 0 & u \neq v \\ 1 & u = v \end{cases}$$

Methods such as the *Pariser-Parr-Pople method* (PPP) and *Complete Neglect of Differential Overlap method* (CNDO) use the ZDO approximation completely.

Intermediate Neglect of Differential Overlap (INDO) method

In contrast to PPP and CNDO methods, in INDO, the ZDO approximation is not applied to the one-center two-electron integrals, $\langle uv|st\rangle$, with ϕ_u, ϕ_v, ϕ_s and ϕ_t all on the same atom. Models such as *Modified Intermediate Neglect of Differential Overlap* (MINDO) and parameterized versions of INDO, such as INDO/S and ZINDO/S are based on INDO methods.

Neglect of Diatomic Differential Overlap (NDDO) method

NDDO goes beyond INDO in that the ZDO approximation is not applied to orbitals on the same atom, i.e., ZDO is used only for atomic orbitals on different atoms. NDDO is the basis of the currently popular semiempirical methods: *Modified*

Neglect of Differential Overlap (MNDO), Austin Model 1 (AM1) and Parametric Method 3 (PM3).

Ab initio methods include all the difficult integrals neglected in semiempirical techniques. Moreover, ab initio methods such as DFT include electron correlation, which provide accuracy comparable with experiment in predicting structure and energy of a molecule. The basic idea of density functional theory has been discussed in the following section.

2.3 DENSITY FUNCTIONAL THEORY (DFT)

Starting from the late eighties and early nineties density functional theory (DFT) gained an enormous popularity due to its high computational efficiency and very good accuracy for determining the structure of molecules, crystals, surfaces [194] and since then it has enjoyed a meteoric rise from a peripheral position in quantum chemistry to centre stage. In Figure 2.1 we have shown the increasing number of publications where the phrases 'DFT' or 'density functional theory' appear in the title or abstract covering the years from 1980 to 2000.

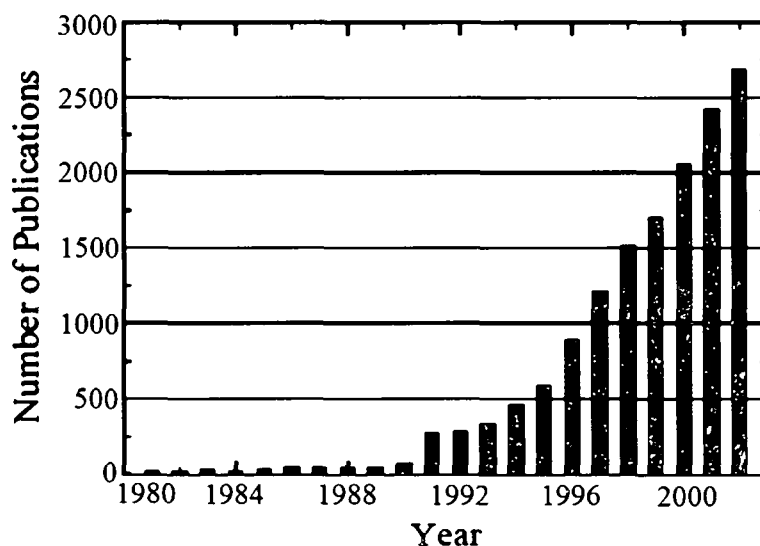


Figure 2.1: Number of publications where the phrase “density functional theory” appears in the title or abstract (taken from ISI Web of Science).

DFT is based on the proof of Hohenberg and Kohn [195] that ground-state electronic energy is determined completely by the electron density ρ in the system of non-interacting electrons.

$$\rho(\vec{r}) = N \int \dots \int |\psi(x_1, x_2, \dots, x_N)|^2 ds_1 d\vec{x}_2 \dots d\vec{x}_N \quad (2.11)$$

where $\rho(\vec{r})$ determines the probability of finding any of the N electrons within the volume element $d\vec{r}_1$, but with arbitrary spin while the other $N-1$ electrons have arbitrary positions and spin in the state presented by ψ . Clearly $\rho(\vec{r})$ is a non-negative function of only three spatial variables in contrast to wave function (ψ), which is a function of $4N$ variables (3 spatial variables and 1 spin variable for each electron) for an N electron system. Moreover, unlike the wave-function, the electron density is an observable and can be measured experimentally, e.g. by X-ray diffraction [196].

2.3.1 Hohenberg-Kohn theorem

The first Hohenberg-Kohn (H-K) theorem demonstrates that the electron density $\rho(\vec{r})$ uniquely determines the external potential $V_{ext}(\vec{r})$ in the Hamiltonian operator of the Schrödinger equation and hence all the properties of the ground state. The total energy can therefore be written as

$$E[\rho] = E_{Ne}[\rho] + T[\rho] + E_{ee}[\rho] = \int \rho(\vec{r}) V_{Ne}(\vec{r}) d\vec{r} + F_{HK}[\rho], \quad (2.12)$$

$$F_{HK}[\rho] = T[\rho] + E_{ee}[\rho] \quad (2.13)$$

where $E_{Ne}[\rho]$ is electron-nuclei interaction energy, $T[\rho]$ is the kinetic energy, $E_{ee}[\rho]$ is the electron-electron interaction energy, the explicit form of which is

$$E_{ee}[\rho] = \frac{1}{2} \iint \frac{\rho(\vec{r}_1)\rho(\vec{r}_2)}{r_{12}} d\vec{r}_1 d\vec{r}_2 + E_{Ncl}[\rho] = J[\rho] + E_{Ncl}[\rho] \quad (2.14)$$

$J[\rho]$ is the classical part and $E_{Ncl}[\rho]$ is the non-classical contribution to the electron-electron interaction: self-interaction correction, exchange and Coulomb correlation.

The second H-K theorem states that the functional $F_{HK}[\rho]$ delivers the ground state energy of a system, if and only if the input density is the ground state density. However, the exact form of $F_{HK}[\rho]$ is a major challenge in DFT and H-K theorem does not tell anything regarding the form of such functional. Moreover, the performance of $F_{HK}[\rho]$ is really bad with the poor approximation of kinetic energy

by Thomas and Fermi [197,198]. To solve this problem, Kohn and Sham proposed an approach, which is described below.

2.3.2 Kohn-Sham equations and energy functional

In 1965, Kohn and Sham [199] developed a formulation defining atomic orbitals, that yields a practical way to solve the Hohenberg-Kohn theorem for a set of interacting electrons. They introduced a universal functional $F[\rho]$, which contains the contributions of the kinetic energy, the classical Coulomb interaction and the non-classical portion:

$$E[\rho] = T_S[\rho] + J[\rho] + E_{xc}[\rho] \quad (2.15)$$

where $E_{xc}[\rho]$ is the so-called *exchange-correlation energy* defined as

$$E_{xc}[\rho] \equiv (T[\rho] - T_S[\rho]) + (E_{ee}[\rho] - J[\rho]) \quad (2.16)$$

E_{xc} is the functional that contains all the unknown terms.

The subscript S in $T_S[\rho]$ of equations (2.15) and (2.16) denotes that it is the kinetic energy calculated from a Slater determinant as

$$T_S = \sum_{i=1}^n \left\langle \phi_i \left| -\frac{1}{2} \nabla^2 \right| \phi_i \right\rangle \quad (2.17)$$

where ϕ_i is the Kohn-Sham (KS) orbitals that satisfies the Kohn-Sham (KS) equation

$$h_{KS} \phi_i = \varepsilon_i \phi_i \quad (2.18)$$

where

$$h_{KS} = -\frac{1}{2} \nabla^2 + V_{eff}, \quad V_{eff} = V_{Ne}(r) + \int \frac{\rho(r')}{|r-r'|} dr' + V_{xc}(r) \quad (2.19)$$

where V_{xc} is the functional derivative of the exchange-correlation energy, given by

$$V_{xc}[\rho] = \frac{dE_{xc}[\rho]}{d\rho} \quad (2.20)$$

The Kohn-Sham (KS) orbitals can be expressed as a linear combination of a set of functions known as basis functions $\{\eta_\mu\}$ as

$$\phi_i = \sum_{\mu} \eta_{\mu} c_{\mu i} \quad (2.21)$$

The electron density ρ is related to the KS orbital by

$$\rho(r) = \sum_{i=1}^n |\phi_i(r)|^2 \quad (2.22)$$

The importance of the KS orbitals is that they allow density to be calculated. The solution of the KS equation proceeds via a self-consistent fashion, starting from a crude charge density, which could be simply the superposition of the atomic densities of the constituent atoms. An approximate form for the functional that describes the dependence of the E_{xc} on the electron density is then used to calculate V_{xc} . This allows the KS equation to be solved, yielding initial set of KS orbitals. This set of orbitals is then used to calculate an improved density from equation (2.22). This procedure is repeated until the density and the exchange-correlation energy satisfies a convergence criterion.

The exact form of exchange-correlation functional is currently unknown. Approximate $E_{xc}[\rho]$ are however available in various forms. Most existing exchange-correlation functionals are split into a pure exchange and correlation contribution, i.e.,

$$E_{xc}[\rho] = E_x[\rho] + E_c[\rho] \quad (2.23)$$

2.3.2.1 The local density approximation (LDA)

The *LDA* is the basis of all approximate exchange-correlation energy functionals. The central idea of this model is a uniform electron gas, in which, the electrons move in a positive background of charge distribution so that the total ensemble is neutral. With this assumption, the E_{xc} takes the form

$$E_{xc}^{LDA}[\rho] = \int \rho(\vec{r}) \varepsilon_{xc}(\rho(\vec{r})) d\vec{r} \quad (2.24)$$

Here, $\varepsilon_{xc}(\rho(\vec{r}))$ is the exchange-correlation energy per particle of a uniform electron gas of density $\rho(\vec{r})$.

$\varepsilon_{xc}(\rho(\vec{r}))$ can be further split into exchange and correlation contributions,

$$\varepsilon_{xc}(\rho(\vec{r})) = \varepsilon_x(\rho(\vec{r})) + \varepsilon_c(\rho(\vec{r})) \quad (2.25)$$

The exchange part, $\varepsilon_{xc}(\rho(\vec{r}))$, which represents the exchange energy of an electron in a uniform electron gas of a particular density, was originally derived by Bloch and Dirac [200] in the late 1920's.

$$\varepsilon_x = -\frac{3}{4} \left(\frac{3\rho(\vec{r})}{\pi} \right)^{1/3} \quad (2.26)$$

No such explicit expression is known for the correlation part, $\varepsilon_c(\rho(\vec{r}))$. However, highly accurate numerical quantum Monte-Carlo simulations of the homogeneous electron gas are available [201].

Example: LSD (Exchange functional of Dirac and Slater 1951) [202,203], VWN (Correlation functional of Vosko, Wilk and Nusair 1980) [204].

In LDA, the paired electrons with opposite spin have (or occupy) the same KS orbital. The *local spin density approximation (LSDA)*, on the other hand, allow the electrons (with opposite spins α and β) to have different KS orbitals, in analogy with unrestricted Hartree-Fock (UHF) method.

2.3.2.2 The generalized gradient approximation (GGA)

The first logical step to go beyond LDA is to consider the non-homogeneity of the true electron density, which is taken into account in the GGA method by making the exchange and correlation energies dependent not only on the density but also on the gradient of the density $\Delta\rho(r)$. In this model, the exchange-correlation energy takes the form

$$E_{xc}^{GGA}[\rho] = \int \rho(\vec{r}) \varepsilon_{xc}(\rho, \nabla\rho) d\vec{r} \quad (2.27)$$

Examples: B88 (Exchange functional of Becke, 1988) [205], PW91 (Perdew-Wang correlation functional, 1991) [206], LYP (Lee-Yang-Parr correlation functional, 1988) [207], PBE (Perdew-Bourke-Ernzerhof exchange-correlation functional, 1996) [208] and BLYP (Combination of B88 with LYP functional).

2.3.2.3 Hybrid functional

It is to be noted that the exchange contributions are usually significantly larger in absolute numbers than the corresponding correlation effects [196]. Therefore, an accurate expression for the exchange functional in particular is a prerequisite for

obtaining meaningful results from density functional theory. This suggests a combination of the Hartree-Fock exchange with the DFT functionals,

$$E_{xc} = E_x^{HF} + E_{xc}^{KS} \quad (2.28)$$

Examples: B3LYP:

$$E_{xc}^{B3LYP} = (1-a)E_x^{LSD} + aE_x^{HF} + bE_x^{B88} + cE_c^{LYP} + (1-c)E_c^{VWN} \quad (2.29)$$

The values of the three parameters are

$$a=0.20, b=0.72 \text{ and } c=0.81$$

Figure 2.2 shows the comparison of density functional theory (DFT) with other available computational methods. It is seen that the accuracy of DFT is close to the computationally more expensive CCSD(T) method and higher than that of HF, MP2, AM1 and PM3 methods. A great advantage of the DFT method over the wave function-based methods is in its computational costs or economy. For this reason, DFT is applicable to fairly large molecular systems. The computational effort is similar to a SCF calculation, but since DFT implicitly includes electron correlation, the accuracy of DFT is often similar to that obtained with other ab initio methods or even better.

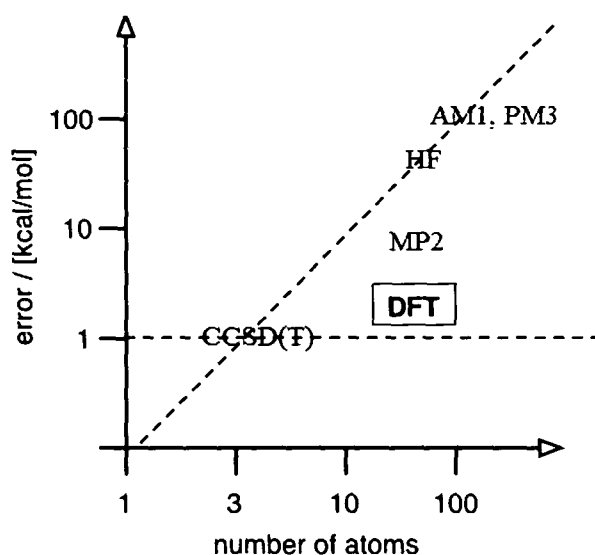


Figure 2.2: Comparison of accuracy of different computational methods (taken from <http://www.chm.bris.ac.uk/pt/manby/l1>).

The next important point to discuss is the kind of basis functions $\{\eta_\mu\}$ used to express the Kohn-Sham orbitals ϕ_i using equation (2.21). The following section provides an overview of the basis sets generally used in DFT calculations.

2.3.3 Basis sets

A basis set is a mathematical description of orbitals of a system, which is used to approximate theoretical calculation or modelling. Basis sets can be broadly classified into the following types:

2.3.3.1 Slater Type Orbitals (STO)

J. C. Slater first introduced the idea of basis sets in computation, known as Slater Type Orbitals (STOs). STOs use a function that correctly models the form of the variation of the electron density with distance from the nucleus.

$$f^{STO}(r) = \left(\frac{\xi^3}{\pi} \right)^{0.5} \exp(-\xi r) \quad (2.30)$$

However, STOs is a very tedious calculation. To overcome this problem, S. F. Boys developed Gaussian Type Orbitals (GTOs) as an alternative.

2.3.3.2 Gaussian Type Orbitals (GTO)

GTOs have the advantage that the two electron integrals may be quickly and easily evaluated. The form of a GTO is

$$f^{GTO}(r) = \left(\frac{2\alpha}{\pi} \right)^{0.5} \exp(-\alpha r^2) \quad (2.31)$$

In order to achieve comparable accuracy for GTOs to that of STOs, GTOs are generally grouped together as linear combinations to provide a best fit to an STO. All basis set equations in the form STO-NG (where N represents the number of GTOs combined to approximate the STO) are called *minimal basis sets*.

Minimal basis sets approximate all orbitals to be of the same shape. For more accurate representation of orbitals, the following basis sets have been defined.

2.3.3.3 Double-zeta, Triple-zeta and Quadruple-zeta basis sets

The double-zeta (DZ) basis set treats each orbital separately as the sum of two STOs with different zeta (ξ) values in equation (2.30). The different ξ values represent different sizes of the orbitals, the linear combination of which gives the atomic orbital. The triple-zeta (TZ) and quadruple-zeta (QZ) basis sets are similar to that of DZ, except they use three and four STOs instead of two as in DZ.

2.3.3.4 Split-valence basis sets

In order to avoid the rigorous calculations involved in DZ basis set for each orbital of an atom, inner-shell electrons can be described by a single STO and only the valence electrons can be treated with DZ basis sets. These types of basis sets are called *split-valence basis sets*. A few examples of common split valence basis sets are 3-21G, 4-31G and 6-31G. In 3-21G, three GTOs are summed to describe the single STO of inner-shell electrons. The first and second STO of the DZ of outer electrons is comprised of two and one GTOs, respectively.

2.3.3.5 Polarization functions

As atoms are brought close together, their charge distribution causes a polarization effect which distorts the shape of the atomic orbitals. In this case, *s* orbitals begin to have a little of the *p* flavour and *p* orbitals begin to have a little of the *d* flavour. One asterisk (*) at the end of a basis set denotes that polarization has been taken into account in *p* orbitals. Examples: 3-21G* and 6-31G*. Two asterisks (**) means that polarization has taken into account in *s* orbitals in addition to *p* orbitals. Examples: 3-21G** and 6-31G**.

2.3.3.6 Diffuse functions

Diffuse functions are basis functions with a larger spatial extent than the normal ones, which are particularly important in the modelling of anions or excited states of an atom. Diffuse basis sets are represented by the '+' signs. One '+' means that we are accounting for the *p* orbitals, while '++' signals that we are looking at both *p* and *s* orbitals.

2.3.3.7 Numerical basis sets

Another kind of basis function is realized within the program DMol³ [209,210], which does not use analytical but *numerical basis functions*. Here, the orbitals are represented numerically on atomic centered grids with cubic spline interpolations between mesh points [196]. These basis functions are generated by numerically solving the atomic KS equations with the corresponding approximate exchange-correlation functional. Thus numerical basis sets provide exact energies (within the given functional) for a molecule.

2.3.3.8 Effective Core Potentials (ECP)

These basis functions are useful for heavy elements (4th period onwards) to include *relativistic effects*. The electrons near the very positive nucleus of a heavy element experience a larger relative attraction than for lighter elements, which accelerates the electrons close to the speed of light. In this situation, Einstein's theory of special relativity starts to have an effect on the shape of the atomic orbitals. The net effect is that the inner core orbitals of a heavy element are contracted relative to the corresponding orbitals in a lighter element. Moreover, the core orbitals are in most cases not affected significantly by changes in chemical bonding. This prompted the development of ECP approach, which allows treatment of inner shell electrons as some average potential. ECP's are not orbitals but modifications to a hamiltonian, and as such are very efficient computationally.

Figure 2.3 represents the tradeoff/relationship between basis sets and accuracy. Moving across from left to right in the figure, the calculations account for the electron correlation. Similarly moving from bottom to top indicates more complex and more accurate basis set calculations. Therefore it is important to choose a basis set that will run a molecule fast without compromising the desired level of accuracy.

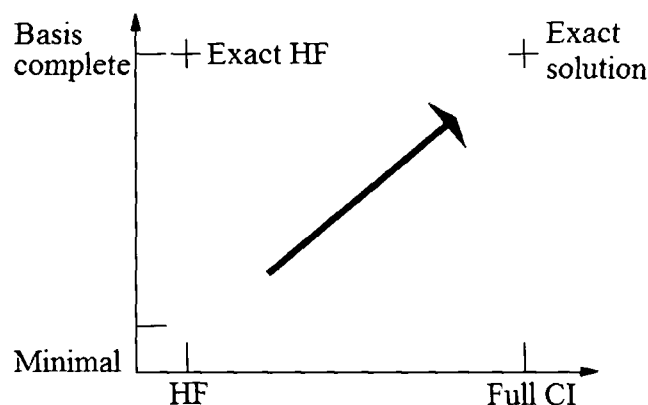


Figure 2.3: Use of various basis sets with different computational methods leading to the exact solution of Schrödinger equation.

2.3.4 Basis Set Superposition Error (BSSE)

As the atoms of interacting molecules (or of different parts of the same molecule) or two molecules approach one another, their basis functions overlap. Hence the basic function of each component is influenced by functions of the nearby components, giving rise to an effective increase in its basis sets. It can lead to a spurious result

known as *basis set superposition error*. This is rapidly grasped in the context of the binding of two molecules A and B, to form a complex AB

$$E_{binding} = E_{AB}^{ab} - (E_A^a + E_B^b) \quad (2.32)$$

where *a* refers to the basis set on *A*, *b* refers to the basis set on *B* and *ab* indicates the union of these two basis sets. Now in the complex *AB*, the basis set *a* will be used to describe (i) the electrons on *A*, (ii) in part, the electrons involved in the binding of *A* and *B* and (iii) aid in the electrons on *B*. The same is true for the basis set *b*. The result is that the complex *AB*, by having a larger basis set than available to describe either *A* or *B* individually, is treated more completely and its energy will consequently be lowered, relative to the energy of *A* or *B*. The binding energy will therefore be larger (more negative) due to this basis set superposition error.

The counterpoise method proposed by Boys and Bernardi [211] attempts to remove some of the effects of BSSE. The counterpoise correction is defined as

$$E_{CP} = E_{A^*}^{ab} + E_{B^*}^{ab} - (E_{A^*}^a + E_{B^*}^b) \quad (2.33)$$

$E_{A^*}^{ab}$ is the energy of molecule *A* in its geometry of the complex *AB* computed with the basis set *a* and the basis set of *B* placed at the position of the nuclei of *B*, but in the absence of the nuclei and electrons of *B*. These basis functions are called *ghost orbitals*. $E_{B^*}^{ab}$ is the energy of *B* in its geometry of the complex *AB* computed with its basis functions and the ghost orbitals of *A*. $E_{A^*}^a$ and $E_{B^*}^b$ are the energies of *A* and *B* respectively in their isolated structures with their individual basis functions. The counterpoise corrected binding energy is then

$$E_{binding}^{CP} = E_{binding} - E_{CP} \quad (2.34)$$

2.4 QUANTUM MECHANICS-MOLECULAR MECHANICS (QM/MM) METHODS

Although molecular mechanical (MM) methods are widely used to treat large and complex molecules, they are unable to describe the changes in the electronic structure of a system undergoing a chemical reaction. Such changes require quantum mechanics (QM) for a proper treatment. However, due to the very demanding computational cost, the application of QM is still limited to relatively small systems consisting of up to tens or several hundreds of atoms, or even to smaller systems when the highest levels of theory are employed. Algorithms that

combine quantum mechanics and molecular mechanics can provide a solution to this problem. These algorithms in principle combine the accuracy of a quantum mechanical description with the low computational cost of molecular mechanics, which leads to the combined quantum mechanics/molecular mechanics (QM/MM) methodology. The advantage of using QM/MM method lies in treating the active region (i.e., the site for chemical processes involving bond breaking and formation) accurately with a high level QM method and the remainder of the system with low level MM method. ONIOM (Our-own-N-layered Integrated molecular Orbital + molecular Mechanics) is a hybrid QM/MM method developed by Morokuma and co-workers [212-215] and this method has been implemented in Gaussian03 program. The simplified expression of total energy of the whole system within the framework of ONIOM methodology can be given as,

$$E_{ONIOM2} = E_{Low}^{Real} + (E_{High}^{Cluster} - E_{Low}^{Cluster}) \quad (2.35)$$

where the superscript “Real” means the whole system and the superscript “Cluster” means the active region. Subscripts “High” and “Low” mean high- and low-level of calculations used in the ONIOM method. The scheme can be extended to three or multiple layers. This method has been successfully applied to deal with problems in bond energies in large molecular systems, organometallic reactions and homogeneous catalysis, structure, reactivity and bond energies of large organic molecules including fullerenes, nanotubes and biomolecular structure and enzymatic reaction mechanisms [216].

In the present thesis, we have performed DFT based QM and QM/MM calculations on small gas phase and zeolite supported palladium clusters using DMol³ and Gaussian 03 program, respectively. The results of these investigations are summarized in the following chapters.

CHAPTER

3

GAS PHASE SMALL PALLADIUM CLUSTERS

Palladium—Metal of the 21st Century
(www.palladiumcoins.com)

In this chapter, we present a comprehensive investigation of gas phase palladium (Pd_n , $n=1-13$) clusters using density functional theory. The novel aspects of our study are the symmetry unrestricted geometry optimization of small palladium clusters in different spin multiplicities and in different charge states. In several cases, very small energy differences among various structural and spin isomers give the idea of their coexistence at room temperature. We have calculated electronic properties such as binding energy, fragmentation energy, bond dissociation energy, ionization potential, electron affinity, chemical hardness and dipole moment of the optimized clusters. From comparison of these parameters, we have predicted the four-atom palladium cluster (Pd_4) to be a magic number cluster [Kalita and Deka, *J. Chem. Phys.* **127**, 244306 (2007)].

3.1 INTRODUCTION

In the recent years, transition metal clusters like palladium have been widely studied experimentally [70-80] and theoretically [85-100] primarily because of their unique catalytic properties. In spite of these, a detail study on Pd clusters is still missing to correlate different cluster properties such as bond length, coordination number, binding energy, fragmentation energy, bond dissociation energy, ionization potential, electron affinity, HOMO-LUMO gap and global hardness with cluster size and stability. In the present work, we have carried out density functional theory studies of small Pd clusters to obtain their accurate geometric and electronic structures as well as to find the most stable and/or reactive cluster on the basis of the

various cluster properties mentioned above. Moreover, for the first time, we have performed a systematic investigation of the structural and electronic properties of small cationic and anionic palladium clusters. The results from this study will be helpful in providing basic understanding of the catalytic activities of these clusters.

3.2 COMPUTATIONAL DETAILS

All the density functional calculations reported here have been carried out using the DMol³ package [209,210]. Relativistic calculations are performed with scalar relativistic corrections to valence orbitals (referred to as VPSR) [217]. This method uses a local pseudopotential [217] acting on all electrons, for the correction of the atomic properties due to relativistic affect, which arises mainly from the mass-velocity, Darwin terms and higher-order kinematics. However, the spin-orbit coupling term appearing in Dirac's equation is eliminated in this approximation. In our calculations, self consistent field procedures are performed with a convergence criterion of 2×10^{-5} a.u. on the total energy and 10^{-6} a.u. on electron density. DMol³ realizes the use of numerically tabulated basis functions [Section 2.3.3.7 in Chapter 2]. Generation of an entire second set of functions results in doubling the basis set size; this is referred to as a double-numerical (DN) set. We have used the DNP basis set [209] for our calculations. These basis sets are significantly improved from DN basis by adding higher angular momentum valence polarization functions and also by core polarization functions. Adding a function on each atom with one angular momentum unit higher than that of its highest occupied orbital leads to a double numerical with polarization (DNP) basis set. These basis sets are generally more complete than a comparable set of linearly independent Gaussian functions and have been demonstrated to have small basis set superposition errors [218,219]. The DNP basis set is comparable to Gaussian 6-31G** basis set [220-222]. We have used the generalized gradient approximation (GGA) implemented in the exchange-correlation functional, BLYP, which is a combination of the exchange functional developed by Becke [205] with the gradient corrected correlation functional of Lee, Yang and Parr [207].

Full geometry optimizations have been performed for different possible structural isomers of neutral Pd_n (n=1–13) clusters in their singlet states (M=1) without imposing symmetry constraints. The corresponding calculations for the large sized palladium clusters have been carried out on a large number of initial geometries that have been modelled by considering all possible orientations of the palladium atoms. Some of the optimized structures resulted in negative frequency values, which were removed by re-optimizing the structures with re-ordered xyz coordinates (CCL January 21, 2002 [003]). However, some of the optimized structures gave large values of negative frequencies even after the re-optimizations, which were not taken for consideration. The optimized structures have been considered as the initial geometries for the optimization in higher multiplicities and we followed the same procedure as

before to get rid of the negative frequencies. The energy landscapes of the different sized clusters have been obtained by comparing their respective energies in different multiplicities. In extending the calculations to higher multiplicities ($M=3, 5$), most of the clusters are found to retain the symmetries of their singlet states. However, some clusters change symmetry while changing multiplicity. In order to compare energy values of these clusters we have performed symmetry-restricted calculations at higher multiplicities. We have also carried out symmetry unrestricted geometry optimizations for single charged clusters in three different multiplicities ($M=2, 4$ and 6). In the present work, the cationic and anionic Pd_n ($n=1-13$) clusters have been formed by removing and adding one electron, respectively from the ground state of neutral Pd_n , $n=1-13$ clusters. Frequency calculations have been performed for all the isomers and none of them is found to exhibit any imaginary frequency. Absence of imaginary frequency in the ground-states verifies them to be the true minima on the potential energy surfaces. The zero-point vibrational energy corrections have been included in all calculations.

In the results to follow, the binding energy per atom of optimized neutral clusters are computed as

$$BE = -E_{\text{tot}} / n \quad (3.1)$$

where E_{tot} is the total energy of a cluster defined as $E_{\text{tot}} = E_n - nE_1$ with E_1 and E_n are the energies of a neutral Pd atom and of the optimized cluster, respectively and n is the number of Pd atoms in the cluster.

For ionic clusters, the formula used for binding energy per atom calculation is

$$BE = -E_{\text{tot}}^{\pm} / n \quad (3.2)$$

where $E_{\text{tot}}^{\pm} = E_n^{\pm} - (n-1)E_1 - E_1^{\pm}$ is the total energy of an ionized cluster, in which E_1^{\pm} and E_n^{\pm} are the energies of the single charged Pd atom (Pd_1^{\pm}) and Pd_n^{\pm} clusters ($n=2-13$), respectively.

Several reactivity descriptors are used in density functional theory to define the reactivity of molecules. One such descriptor is global hardness (η), which is defined as the second derivative of energy (E) with respect to the number of electrons (N) at constant external potential, $v(\vec{r})$ [223]

$$\eta = \frac{1}{2} \left(\frac{\partial^2 E}{\partial N^2} \right)_{v(\vec{r})} = \frac{1}{2} \left(\frac{\partial \mu}{\partial N} \right)_{v(\vec{r})} \quad (3.3)$$

where μ is the chemical potential of the system.

Using the finite difference approximation, global hardness, η can be approximated as

$$\eta = \frac{IP - EA}{2} \quad (3.4)$$

where IP and EA are respectively the first vertical ionization potential and vertical electron affinity of the chemical system.

3.3 RESULTS AND DISCUSSION

3.3.1 Geometries and energetics

Pd^{0,±} atom

First we present the results obtained for single Pd atom. Our results show that for Pd atom, singlet state is the lowest energy state with 0.75 eV lower in energy than the triplet state. This value is in close agreement with the experimental value (0.82 eV) [224] and previous theoretical values of 0.87 eV by Valerio and Toulhoat [92] and Seminario *et al.* [97] using B3LYP functional. It is observed that the most stable structures of both the cation and the anion of Pd atom are doublets (M=2). For Pd⁺ and Pd⁻, the quartet-doublet energy separations are 3.31 and 4.78 eV, respectively.

Pd₂^{0,±} cluster

The lowest energy structures of neutral Pd_n (n=2–13) clusters are shown in Figure 3.1. Similar structures are possessed by the corresponding lowest energy cationic and anionic clusters. The average bond lengths and binding energies of all the lowest energy palladium clusters are given in Table 3.1. The lowest energy structure of neutral Pd₂ is a triplet with a symmetric point group of D_{∞h}, in agreement with other studies [92,97,98,99,126]. The bond length of this structure is found to be 2.54 Å, which agrees well with B3LYP/LANL2DZ result of Valerio and Toulhoat [92] (2.53 Å) and B3LYP/HUZINAGA result of Seminario *et al.* [97] (2.559 Å). The calculated value is slightly higher than the experimental value of 2.48 Å [66]. It is seen from Table 3.1 that the binding energy of the ground state Pd₂ is 1.11 eV, in agreement with the trustworthy value of (1.03±0.16 eV) [58,225]. The singlet and triplet states are very close in energy, the singlet state lies only 0.0018 eV higher in energy than the triplet state (Appendix A).

For both Pd₂⁺ and Pd₂⁻, the lowest energy structures are doublets with symmetric point group of D_{∞h}. It is seen from Table 3.1 that the bond lengths for Pd₂⁺ and Pd₂⁻ are 2.70 Å and 2.54 Å, respectively. For Pd₂⁺, this value is slightly higher and for Pd₂⁻, it is lower than the earlier results (2.661 Å for Pd₂⁺ and 2.675 Å for Pd₂⁻) of Efremenko and Sheintuch [86]. For Pd₂⁺ and Pd₂⁻, the quartet states are higher in energy by 0.57 eV and 0.98 eV, respectively compared to their doublet states. Binding energy per atom for Pd₂⁺ is 1.087 eV/atom, which is slightly higher than the value reported by Efremenko and Sheintuch [86] (1.059 eV/atom). Binding

energy per atom for Pd_2^- is 1.31 eV/atom (Table 3.1) and this is higher than the value 0.944 eV/atom, reported by Efremenko and Sheintuch [86].

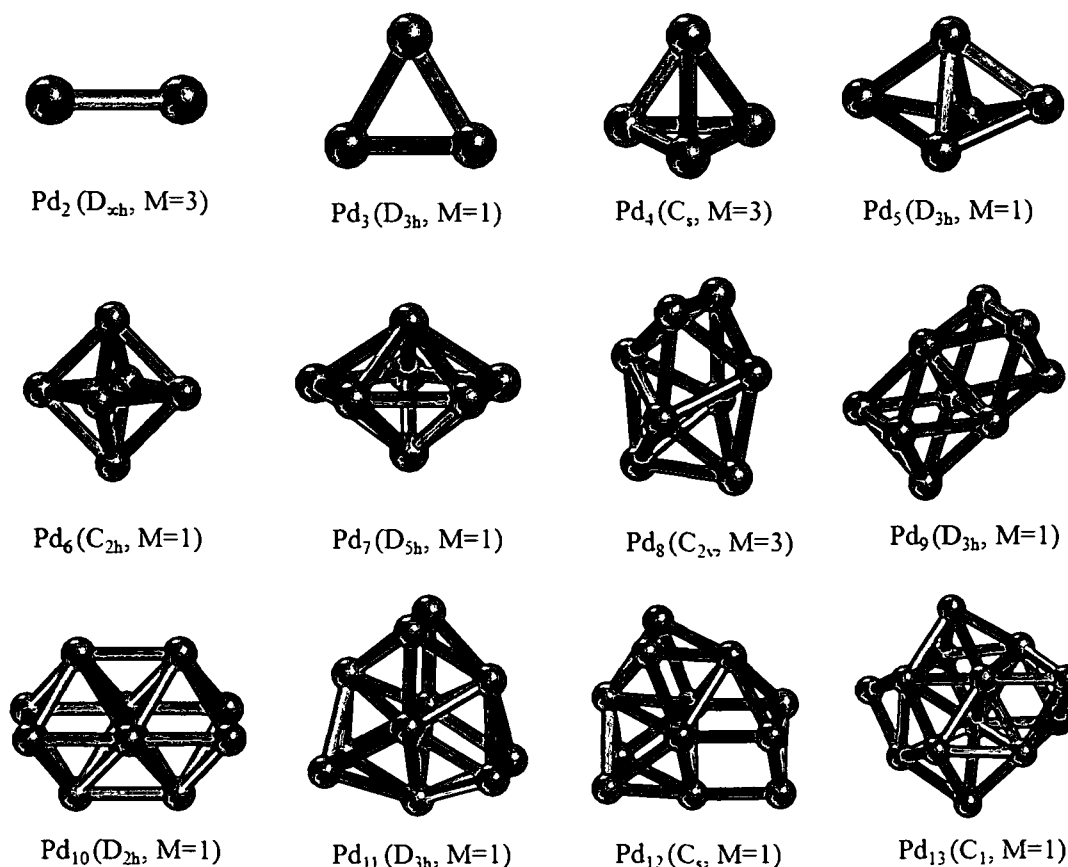


Figure 3.1: Lowest energy optimized structures of neutral Pd_2 – Pd_{13} clusters. The point group symmetry and spin multiplicity for each cluster are shown in parenthesis. Blue spheres represent the palladium atoms.

$\text{Pd}_3^{0,\pm}$ cluster

For neutral Pd_3 , the lowest energy isomer is a singlet with an equilateral triangular structure of bond length 2.52 Å in D_{3h} symmetry. The energy difference between the singlet and the triplet state is only 0.046 eV (Appendix A). This contradicts the results of Seminario *et al.* [97] and Nakao *et al.* [98] stating the lowest energy state of Pd_3 to be a triplet with D_{3h} symmetry. Valerio and Toulhoat [92] and Nava *et al.* [103] reported that the lowest energy state of Pd_3 is a triplet in C_{2v} symmetry. Our result is in agreement with that of Luo *et al.* [102] and Zacarias *et al.* [226]. The binding energy per atom for most stable Pd_3 cluster is 1.11 eV/atom. This value is

less than the reported value 1.203 eV/atom by Kumar and Kawazoe [24] (GGA) and 1.23 eV/atom by Zhang *et al.* [100] (PW91).

Table 3.1: Average bond lengths ($\langle \text{Pd-Pd} \rangle$) in Å and binding energy per atom (BE/atom) in eV for the most stable palladium clusters as a function of cluster size.

Cluster size (n)	Neutral clusters		Cationic clusters		Anionic clusters	
	$\langle \text{Pd-Pd} \rangle$ (Å)	BE/atom (eV)	$\langle \text{Pd-Pd} \rangle$ (Å)	BE/atom (eV)	$\langle \text{Pd-Pd} \rangle$ (Å)	BE/atom (eV)
2	2.54	0.56	2.70	1.09	2.54	1.08
3	2.52	1.11	2.52	1.48	2.52	1.44
4	2.67	1.41	2.64	1.87	2.72	1.60
5	2.71	1.48	2.69	1.90	2.73	1.69
6	2.72	1.60	2.71	1.99	2.73	1.76
7	2.75	1.61	2.74	1.95	2.75	1.81
8	2.74	1.70	2.74	1.98	2.74	1.87
9	2.73	1.75	2.72	2.02	2.73	1.93
10	2.75	1.77	2.75	2.02	2.76	1.94
11	2.74	1.81	2.75	2.02	2.74	1.99
12	2.72	1.84	2.72	2.05	2.73	2.00
13	2.74	1.86	2.74	2.06	2.74	2.02

For Pd_3^+ , the lowest energy structure is a quartet with triangular structure and D_{3h} symmetry. The doublet state of this triangular structure is 0.52 eV higher in energy. The binding energy per atom for the lowest energy state is 1.48 eV/atom. This value is higher than that reported by Efremenko and Sheintuch [86] (1.185 eV/atom). Lowest energy structure of Pd_3^- is a doublet with triangular structure (D_{3h} symmetry), which is not definitely known from spectroscopy [227]. However, from the calculations of Balasubramanian [89], it is indicated that the most stable structure of neutral Pd_3 has a triangular geometry. The additional electron in the anion can occupy moderately bonding or nonbonding molecular orbitals in the calculated configuration [89] of the lowest energy state. Therefore, it is likely that the lowest energy isomer of Pd_3^- is triangular [131]. The quartet state lies 0.72 eV higher in

energy. The binding energy per atom for the lowest energy state of Pd_3^- is 1.44 eV/atom, which is close to the value reported by Efremenko and Sheintuch [86] (1.503 eV/atom). From Table 3.1, both Pd_3^+ and Pd_3^- are found to have an average bond length of 2.52 Å. These values are less than the previous results (2.756 Å for Pd_3^+ and 2.604 Å for Pd_3^-) [86].

$\text{Pd}_4^{0,\pm}$ cluster

A triplet state with distorted tetrahedron and C_s symmetry is found to be the lowest energy structure for neutral Pd_4 (Figure 3.1). The average bond length of this structure is 2.67 Å (Table 3.1). Kumar and Kawazoe [24] reported a similar lowest energy state for Pd_4 with an average bond length of 2.61 Å. The energy difference between the triplet and the singlet state is 0.017 eV. A regular tetrahedron (T_d symmetry) in triplet state is found to be 0.0022 eV higher in energy than the lowest energy structure (Appendix A). The structure and relative stability of some other isomers are shown in Appendix A. Binding energy for the most stable structure of Pd_4 is 1.41 eV/atom (Table 3.1), which is lower than the earlier observations of 1.628 eV/atom by Kumar and Kawazoe [24] (GGA), 1.58 eV/atom by Goursot *et al.* [126] (VWN), and 1.63 eV/atom by Nava *et al.* [103] (BP86) but higher than the reported value of 1.245 eV/atom by Valerio and Toulhoat [92] (B3LYP).

For Pd_4^+ , the most stable structure is a quartet with a regular tetrahedron in T_d symmetry. The average bond length of this structure is 2.64 Å (Table 3.1). The doublet state lies 0.07 eV higher in energy. Binding energy per atom of the lowest energy structure is 1.87 eV/atom. For Pd_4^- , the lowest energy structure is a doublet with a regular tetrahedron and the average bond length is 2.72 Å. This structure is 0.38 eV lower in energy than the quartet state. Binding energy for Pd_4^- is 1.60 eV/atom.

$\text{Pd}_5^{0,\pm}$ cluster

The lowest energy structure of neutral Pd_5 is a singlet in D_{3h} symmetry as shown in Figure 3.1. The average bond length of this trigonal bipyramidal structure is 2.71 Å (Table 3.1). A similar lowest energy state was reported by Kumar and Kawazoe [24] with an average bond length of 2.65 Å (GGA) and by Rogan *et al.* [99] with an average bond length of 2.69 Å (LSDA result). Two tetragonal pyramid structures in

C_{2v} and C_{4v} symmetries in the singlet states are found to lie 0.0017 and 0.0038 eV higher in energy, respectively, than the lowest energy state. It is found that a trigonal bipyramid structure (D_{3h} symmetry) in the triplet state lies 0.024 eV higher in energy than the most stable one. The relative energies of all the structural and spin isomers with respect to the most stable cluster are given in Appendix A. The binding energy per atom for the lowest energy structure is 1.48 eV/atom (Table 3.1) and it is less than the results of Kumar and Kawazoe [24] (1.766 eV/atom) and Nava *et al.* [103] (1.744 eV/atom).

A quartet state with a trigonal bipyramid of an average bond length of 2.69 Å in D_{3h} symmetry is the lowest energy structure for Pd_5^+ . The doublet state lies only 0.0036 eV higher in energy. It is seen from Table 3.1 that the binding energy per atom for the most stable structure of Pd_5^+ is 1.90 eV/atom. Pd_5^- is a doublet with trigonal bipyramidal structure (D_{3h} symmetry) and average bond length of 2.73 Å in its lowest energy. The corresponding quartet state is 0.16 eV higher in energy. The binding energy per atom of the lowest energy structure is 1.69 eV/atom.

$Pd_6^{0,\pm}$ cluster

For neutral Pd_6 , the lowest energy structure is a distorted octahedron with C_{2h} symmetry (Figure 3.1) and its average bond length is 2.72 Å (Table 3.1). This structure is a singlet, in agreement with the earlier observation by Kumar and Kawazoe [24]. The triplet state of this structure lies 0.067 eV higher in energy compared to the singlet state. An octahedral structure (O_h symmetry) in singlet state lies 0.004 eV higher in energy than the lowest energy structure. Few other structural and spin isomers with their relative energies are given in Appendix A. The binding energy (1.60 eV/atom) for the lowest energy state is found to be less than those reported by Kumar and Kawazoe [24] (1.922 eV/atom) and Nava *et al.* [103] (1.878 eV/atom), but higher than the result of Valerio and Toulhoat [92] (1.411 eV/atom).

For Pd_6^+ , the lowest energy structure is a doublet with an octahedron in O_h symmetry. The average bond length is 2.71 Å. The corresponding quartet state lies 0.055 eV higher in energy. Binding energy for the lowest energy structure is 1.99 eV/atom. The most stable structure of Pd_6^- is also a doublet with an octahedron (O_h symmetry) of average bond length of 2.73 Å. The quartet state of this structure is

0.13 eV higher in energy. The binding energy for the most stable Pd_6^- is 1.76 eV/atom.

$\text{Pd}_7^{0,\pm}$ cluster

The most stable structure of neutral Pd_7 is a singlet with pentagonal bipyramid (PBP) structure (Figure 3.1), average bond length of 2.75 Å and D_{5h} symmetry. This result is in agreement with the suggestion [84] based on the photoemission data that Pd_7 may be a closed shell species with zero magnetic moment. The relative energies and structures of some other structural and spin isomers with respect to the lowest energy structure are given in Appendix A. It is seen from Table 3.1 that the binding energy for the PBP structure is 1.61 eV/atom, which is less in comparison to the earlier results of Kumar and Kawazoe [24] (1.917 eV/atom) and Nava *et al.* [103] (1.903 eV/atom).

The lowest energy structure of Pd_7^+ is a doublet with a pentagonal bipyramid structure in D_{5h} symmetry and the average bond length is 2.74 Å. The quartet state lies 0.049 eV higher in energy than the lowest energy structure. The binding energy for the lowest energy isomer is 1.95 eV/atom. The most stable structure of Pd_7^- is also a doublet with a pentagonal bipyramid structure (D_{5h} symmetry) of average bond length of 2.75 Å. The quartet state of this structure is 0.045 eV higher in energy compared to the lowest energy state. The binding energy per atom of the most stable Pd_7^- is 1.81 eV.

$\text{Pd}_8^{0,\pm}$ cluster

The lowest energy structure of neutral Pd_8 cluster is a bicapped octahedron as shown in Figure 3.1. The structure is a triplet with C_{2v} symmetry and its average bond length is 2.74 Å. This structure is similar to the earlier observations [24,102-104,228]. However, the lowest energy structure found by Zhang *et al.* [100] and Rogan *et al.* [101] are in the singlet and quintet states, respectively. In our study, the corresponding singlet state lies 0.223 eV higher in energy than the lowest energy structure. Binding energy of the most stable structure is found to be 1.70 eV/atom (Table 3.1), which is less than the earlier reported values [24,100,103]. It is found that an isomer having similar structure as that of the most stable one with D_{2d} symmetry in singlet, triplet and quintet states lie 0.226, 0.242 and 0.351 eV higher in

energy, respectively, than the ground state. The relative stabilities and structures of some other isomers with different spin multiplicities are presented in Appendix A.

The lowest energy structure of Pd_8^+ is a bicapped octahedron with D_{2d} symmetry in doublet state. The corresponding structures in quartet and sextet states lie 0.040 and 0.253 eV higher in energy, respectively, than the lowest energy structure. The average bond length and binding energy per atom values of the most stable structure are 2.74 Å and 1.98 eV/atom, respectively. The most stable structure of Pd_8^- is also a bicapped octahedron with D_{2d} symmetry in doublet state. This structure is found to have an average bond length of 2.74 Å and binding energy per atom of 1.87 eV/atom. The relative energies of this structure in quartet and sextet states are 0.049 and 0.235 eV, respectively, with respect to the lowest energy state.

$\text{Pd}_9^{0,\pm}$ cluster

For neutral Pd_9 cluster, the most stable structure is composed of double octahedrons fused with one facet (Figure 3.1). This structure is in singlet spin multiplicity and with D_{3h} point group symmetry. Büyükatana and Belchior [104] have also predicted this structure to be the most stable configuration using molecular dynamics. A similar ground state structure has been observed by Zanti and Peeters [105] and Luo *et al.* [102] in quintet and triplet states, respectively. The calculated average bond length and binding energy per atom of the most stable isomer are 2.73 Å and 1.75 eV/atom, respectively (Table 3.1). Our calculated triplet and quintet states of the lowest energy structures lie 0.022 and 0.131 eV, higher in energy, respectively, than the singlet state. Several other local minima structures have been predicted, which are shown with their relative energies in Appendix A.

The lowest energy structure of Pd_9^+ and Pd_9^- are similar to that of the ground state structure of neutral Pd_9 cluster. These structures have doublet spin states and D_{3h} symmetries. The average bond lengths and binding energies per atom of these structures are found to be 2.72, 2.73 Å and 2.02, 1.93 eV/atom, respectively (Table 3.1). The cationic Pd_9 cluster in quartet and sextet spin states lie only 0.003 and 0.109 eV higher in energy, respectively, than the lowest energy state. Similarly, the

relative energies of the quartet and sextet states with respect to the lowest energy state of anionic Pd₉ cluster are 0.073 and 0.259 eV, respectively.

Pd₁₀^{0,±} cluster

The configuration with edge sharing double octahedrons in singlet state with D_{2h} symmetry is found to be the lowest energy structure for Pd₁₀ in our calculations, which is shown in Figure 3.1. A similar structure in quintet state has been predicted to be the ground state by Nava *et al.* [103]. It has been observed that the lowest energy structure lies only 0.010 and 0.068 eV lower in energy than the triplet and quintet states, respectively. The calculated average bond length and binding energy per atom of the lowest energy structure are 2.75 Å and 1.77 eV/atom, respectively (Table 3.1). We have predicted a large number of low energy geometric and spin isomers, whose structures and relative energies from the lowest energy structures are summarized in Appendix A.

Pd₁₀⁺ and Pd₁₀⁻ clusters are found to have similar structures as that of the neutral Pd₁₀ cluster. These two structures have D_{2h} symmetry and they are in doublet states. The average bond lengths of these isomers are found to be 2.75 and 2.76 Å, respectively. Their respective binding energy values are 2.02 and 1.94 eV/atom. The corresponding structures in quartet and sextet states for cationic and anionic Pd₁₀ clusters lie 0.004, 0.033 and 0.069, 0.158 eV, respectively.

Pd₁₁^{0,±} cluster

The highest binding energy structure of Pd₁₁ cluster consists of three octahedrons, each of which fuses one facet with the other two (Figure 3.1). This structure is in singlet state with D_{3h} symmetry. A similar lowest energy structure in triplet state has been predicted by Luo *et al.* [102]. The average bond length of our calculated lowest energy structure is 2.74 Å with binding energy value of 1.81 eV/atom (Table 3.1). The triplet and quintet states of this structure are almost degenerate to the singlet state (0.004 and 0.032 eV higher in energy, respectively). A structure formed by two fused Pd₇ decahedra (structure 11(c) in Appendix A) was found to be the most stable structure by Nava *et al.* [103]. However, our study shows that this structure in singlet, triplet and quintet states lie 0.413, 0.424 and 0.481 eV higher in energy, respectively than that of the lowest energy structure. Several other spin

isomers with different structures have also been detected lying in varieties of energies relative to the ground state energy (Appendix A).

The lowest energy structures of Pd_{11}^+ and Pd_{11}^- are found to be similar to that of neutral Pd_{11} cluster. They are in quartet and doublet states, respectively, with D_{3h} symmetry. The average bond lengths of the two isomers are 2.75 and 2.74 Å, respectively. Their respective binding energies per atom are found to be 2.02 and 1.99 eV/atom (Table 3.1). The doublet and sextet states of anionic Pd_{11} cluster have small energy difference of 0.003 and 0.006 eV from the ground state. For cationic Pd_{11} , the quartet and sextet states lie 0.027 and 0.116 eV higher in energy, respectively, than the lowest energy state.

$\text{Pd}_{12}^{0,\pm}$ cluster

We have detected a structure consisting of two octahedrons, a square pyramid and a prism, each of which shares one facet with the two others to be the most stable structure of Pd_{12} . This structure is found to be in singlet state with C_s symmetry and it has not been reported earlier. An average bond length of 2.72 Å and binding energy of 1.84 eV/atom have been calculated for the most stable structure of Pd_{12} (Table 3.1). This structure in triplet and quintet states has small difference of energy (0.014 and 0.069 eV, respectively) from that of the ground state. A different structure with two octahedrons and a pentagonal bipyramid was predicted to be the lowest energy Pd_{12} structure by Luo *et al.* [102]. Similar to the observation of Luo *et al.* [102], our calculations reveal that an icosahedral structure in singlet state lie 0.694 eV higher in energy than the lowest energy isomer. Several other local minima structures have also been predicted with different relative energies with respect to the ground state as given in Appendix A.

Pd_{12}^+ and Pd_{12}^- clusters are found to have similar structure as that of neutral Pd_{12} cluster with C_s symmetry in doublet states. The average bond lengths and binding energies of these two isomers are calculated to be 2.72 Å, 2.05 eV/atom and 2.73 Å, 2.00 eV/atom, respectively (Table 3.1). For Pd_{12}^+ , the quartet and sextet states lie 0.016 and 0.062 eV higher in energy, respectively, than the lowest energy state. Similarly, the respective energies of quartet and sextet states of Pd_{12}^- are 0.042 and 0.155 eV higher than that of the ground state.

$Pd_{13}^{0,\pm}$ cluster

In contrast to the previously predicted icosahedral structures [24,74,103], we have found a less symmetric (C_1 point group) structure to be the most stable form of Pd_{13} . This structure is in singlet state and is composed of two octahedrons, a pentagonal bipyramid and a square pyramid sharing facets with one another. The corresponding triplet and quintet states are 0.014 and 0.073 eV higher in energy, respectively than the ground state. An icosahedral isomer in singlet state (structure 13(g) in Appendix A) has an energy difference of 0.124 eV relative to the lowest energy structure. Recent theoretical calculations [108,112] have also predicted non icosahedral low symmetry open structures to be the ground state of Pd_{13} . Our computed values of average bond length and binding energy for the most stable Pd_{13} cluster are 2.74 Å and 1.86 eV/atom, respectively. The relative energies of different geometric and spin isomers of Pd_{13} clusters are given in Table 3.1 and their structures are shown in Appendix A.

For Pd_{13}^+ and Pd_{13}^- , the lowest energy structures are similar to that of neutral Pd_{13} . These two structures lie in doublet states and with C_1 symmetry. Their average bond lengths (2.74 Å) are also similar to that of neutral Pd_{13} cluster. Binding energy values of these clusters are 2.06 and 2.02 eV/atom, respectively. The corresponding quartet and sextet states of cationic and anionic Pd_{13} lie 0.016, 0.041 eV and 0.076, 0.144 eV higher in energies, respectively.

The variations in the global minima structures as observed above depend on different exchange-correlation functional as well as basis functions used for calculations [111].

Trends

Variation of average bond lengths of the most stable clusters with cluster size is shown in Figure 3.2. It is quite visible from the figure that the average bond length decreases as we go from Pd_2^q to Pd_3^q ($q=0, 1, -1$) and then it increases very slowly with slight variation with cluster size. The increase in average bond length from $n=3$ may be due to the growing of three dimensional configurations at $n=4$.

In Figure 3.3, we have plotted the binding energies per atom of the most stable structures of all the clusters as a function of cluster size. It is observed that for neutral, cationic and anionic clusters, the binding energy per atom, in general, increases with the number of atoms in the cluster. It shows that the stability of the clusters increases with cluster size and this increment becomes very slow toward the

bigger sized clusters. This gives an idea that a very large number of atoms in the cluster are needed to reproduce the bulk cohesive behaviour, as the experimental value of bulk binding energy is 3.91 eV/atom [229].

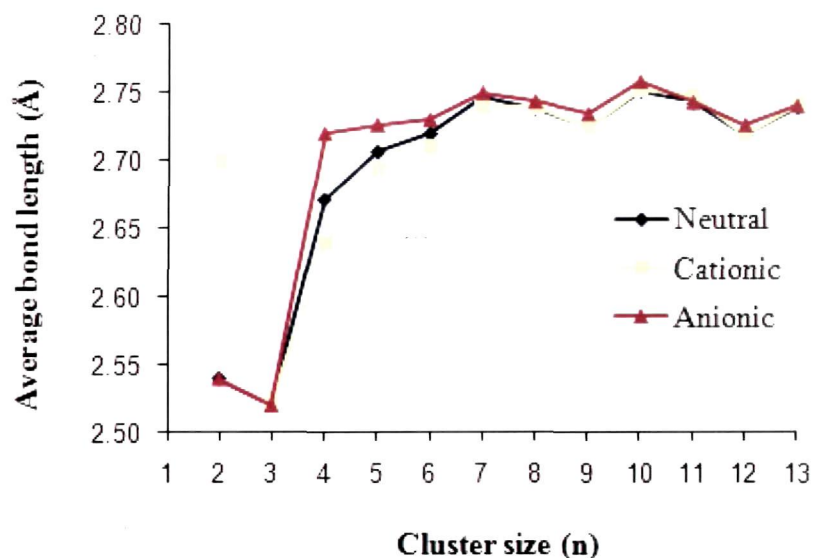


Figure 3.2: Variation of average bond lengths (Å) with cluster size for the most stable palladium clusters.

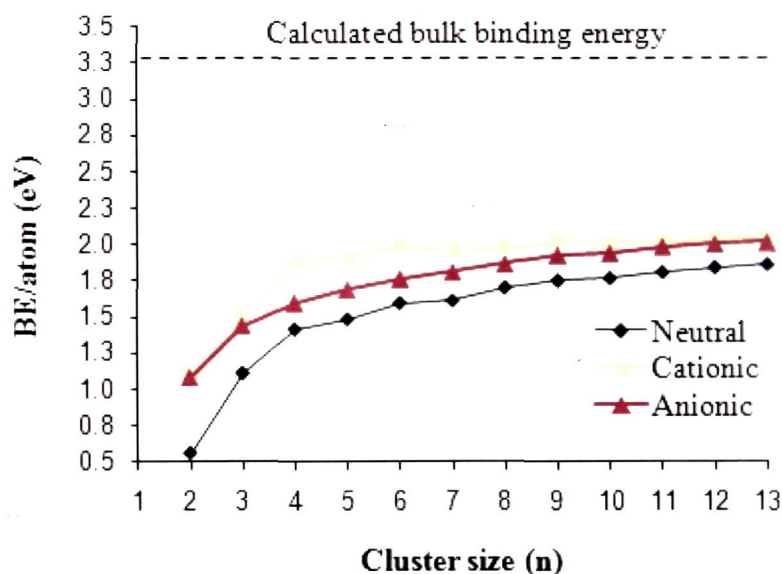


Figure 3.3: Binding energies per atom in eV for the most stable palladium clusters as a function of cluster size.

In accordance with the spherical drop model [230,231], we have also plotted the binding energy per atom for the lowest energy clusters as a function of the inverse of the cluster radius R , $R^{-1} \sim n^{-1/3}$ [232] (Figure 3.4).

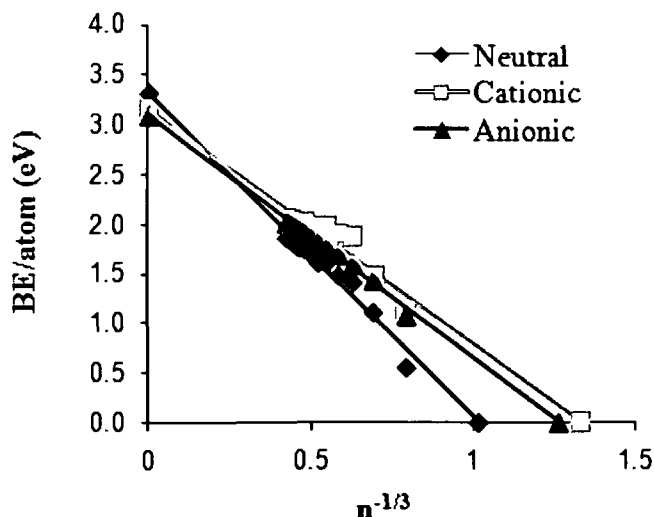


Figure 3.4: Binding energies per atom versus $n^{-1/3}$ for the neutral, cationic, and anionic clusters.

There is a linear correlation with correlation coefficients of 0.989, 0.977 and 0.998 for neutral, cationic and anionic clusters, respectively. Moreover, the plot indicates the charge distribution in anionic clusters is more “spherical” compared to that in neutral and cationic clusters. This is because of the large spatial extents of the electrons in anions due to the presence of extra electrons. If we extrapolate our data, we obtain a value of ~ 3.30 eV/atom for the bulk cohesive energy of neutral clusters, which is fairly close to the experimental value of 3.91 eV/atom [229].

We have also defined the coordination number γ , as the average number of bonds for each atom in a cluster. Values of γ for the lowest energy palladium clusters are tabulated in Table 3.2. This value is found to be equal for neutral, cationic, and anionic clusters of the same size. Naturally, the coordination numbers increase with the number of atoms in the cluster (except only for $\text{Pd}_{12}^{0,\pm}$). We have already seen that the binding energy of all the lowest energy isomers of palladium clusters increases with the cluster size (Figure 3.3). Therefore, we can say that the stabilities of the most stable neutral, cationic, and anionic clusters increase as the coordination number increases. This is in agreement with the principle proposed by Stave and DePristo [233] which states that transition metal clusters generally maximize the minimum coordination of any atom.

Table 3.2: Average coordination numbers (γ) of the ground state palladium clusters as a function of cluster size.

Cluster size	Average coordination number (γ)		
	Neutral	Cationic	Anionic
3	2.00	2.00	2.00
4	3.00	3.00	3.00
5	3.60	3.60	3.60
6	4.00	4.00	4.00
7	4.29	4.29	4.29
8	4.50	4.50	4.50
9	4.67	4.67	4.67
10	5.00	5.00	5.00
11	5.09	5.09	5.09
12	4.75	4.75	4.75
13	5.15	5.15	5.15

3.3.2 Relative stability

To examine the relative stability of the clusters, we have calculated the second finite difference of the total energies, i.e. the stability function as defined below:

$$S^{0;\pm}(n) = E_{n+1}^{0;\pm(\text{tot})} + E_{n-1}^{0;\pm(\text{tot})} - 2E_n^{0;\pm(\text{tot})} \quad (3.5)$$

for neutral and ionized clusters, respectively. Figure 3.5 displays the evolution of $S^{0;\pm}(n)$ as a function of cluster size. Noticeable peaks at $n = 4, 6$ and 9 for neutral clusters indicate that these clusters are more stable than the neighboring clusters.

We have also calculated the fragmentation energies of all the clusters into different binary channels from

$$E_{n \rightarrow (n-m)+m} = E_{n-m} + E_m - E_n, n > m \geq 1, \quad (3.6)$$

for the channel $Pd_n \rightarrow Pd_{n-m} + Pd_m$, where E_n is the energy of the corresponding stable structure. These values for neutral, cationic and anionic clusters are displayed in Tables 3.3, 3.4 and 3.5, respectively. The preferred decay channel for each of the neutral clusters involves a neutral atom. For the cationic as well as for the anionic clusters, the most favorable decay channel is that in which the larger fragment carries the charge and neutral palladium atom is one of the decay products.

As a subset of the fragmentation energy, the bond dissociation energy (BDE), defined as the energy required in fragmenting a cluster Pd_n to Pd_{n-1} and Pd, is plotted for all the ground state clusters as a function of cluster size in Figure 3.6.

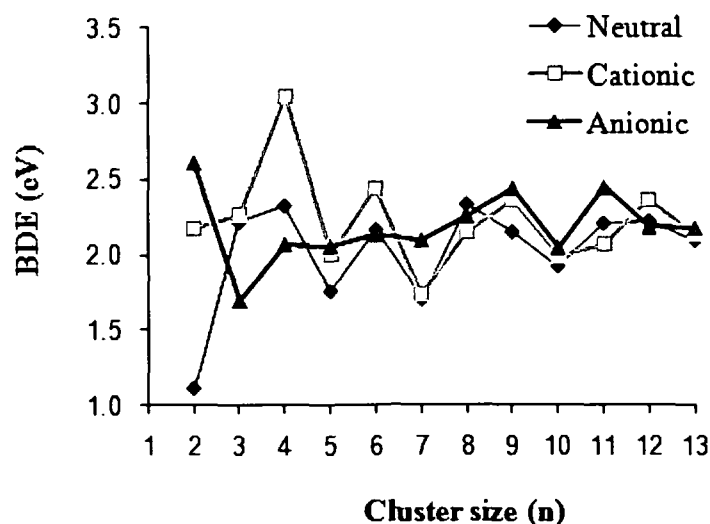


Figure 3.6: Bond dissociation energies in eV as a function of clusters size for most stable palladium clusters.

Bond dissociation energy for Pd_2 , is found to be 1.11 eV (first row of Table 3.3), which is very close to the experimental value of 1.03 ± 0.16 eV by Shim and Gingerich [225]. For Pd_2^- , the observed value is 2.15 eV and the experimental value is 2.15 ± 0.17 eV by Ho *et al.* [59]. For Pd_3 and Pd_3^- , bond dissociation energies are 2.21 eV and 2.16 eV, respectively. These are in agreement with the experimental values (2.49 ± 0.42 eV for Pd_3 and 2.28 ± 0.42 eV for Pd_3^-) reported by Spasov and Ervin [131]. Higher values of bond dissociation energies are observed for neutral Pd_3 , Pd_4 , Pd_6 , Pd_8 and Pd_{12} clusters, indicating them to be more stable than their neighbors and Pd_4 is found to have the highest among all the clusters.

3.3.3 Electronic properties

3.3.3.1 Ionization potential and electron affinity

We have computed the adiabatic and vertical ionization potentials (AIP and VIP respectively) of the clusters using the formula

$$IP = E_n^+ - E_n, \quad (3.7)$$

where E_n^+ is the energy of the cationic clusters at the optimized geometry of the cation (for AIP) and at the optimized geometry of neutral cluster (for VIP).

The adiabatic and vertical electron affinities (AEA and VEA, respectively) are calculated from

$$EA = E_n - E_n^-, \quad (3.8)$$

where E_n^- is the energy of the anionic clusters at the optimized geometry of anion (for AEA) and at the optimized geometry neutral cluster (for VEA).

Ionization potentials and electron affinities are compared with the experimental values in Table 3.6. It is seen from the table that adiabatic ionization potential for Pd atom is 8.69 eV. This is close to the experimental value of Ishikawa (8.3365±0.0001) [234] and Lide (8.3369±0.0001) [235]. The value of AIP for Pd₂ is 7.63 eV, which agrees well with the experimental result (7.7±0.3) of Gingerich *et al.* [236].

Table 3.6: Ionization potentials (IP) and electron affinities (EA) in eV for the lowest energy palladium clusters.

Cluster size (n)	AIP	VIP	IP (Expt.) ^a	AEA	VEA	EA (Expt.) ^b
1	8.6883	8.6883	8.3365±0.0001, 8.3369±0.0001	0.5402	0.5402	0.5620±0.0050, 0.5570 ± 0.0080
2	7.6280	7.6936	7.7 ± 0.3	1.5809	1.5809	1.6850±0.0080, 1.30 ± 0.15
3	7.5734	7.6084	—	1.5230	1.4860	1.35 ± 0.10, <1.50 ± 0.10
4	6.8492	6.8580	—	1.2695	1.2388	1.35 ± 0.10
5	6.6006	6.6046	—	1.5698	1.5575	1.45±0.10
6	6.3289	6.3268	—	1.5377	1.5307	1.65±0.10
7	6.2949	6.2992	—	1.9346	1.9224	1.70±0.15
8	6.4834	6.4910	—	1.8579	1.8569	1.85±0.25
9	6.2654	6.2646	—	2.1542	2.1456	1.95±0.25
10	6.2011	6.2004	—	2.2787	2.2772	2.00±0.25
11	6.3336	6.3377	—	2.5220	2.5139	1.95±0.25
12	6.1991	6.1975	—	2.4839	2.4753	2.00±0.30
13	6.1615	6.1621	—	2.5679	2.5595	2.25±0.30

^a References 234-236.

^b References 59, 65, 227, 238.

Variation of IP and EA with cluster size is plotted in Figure 3.7. Work function of Pd is 4.97 eV [237]. Therefore it is clear that convergence to the bulk limit is slow for small palladium clusters.

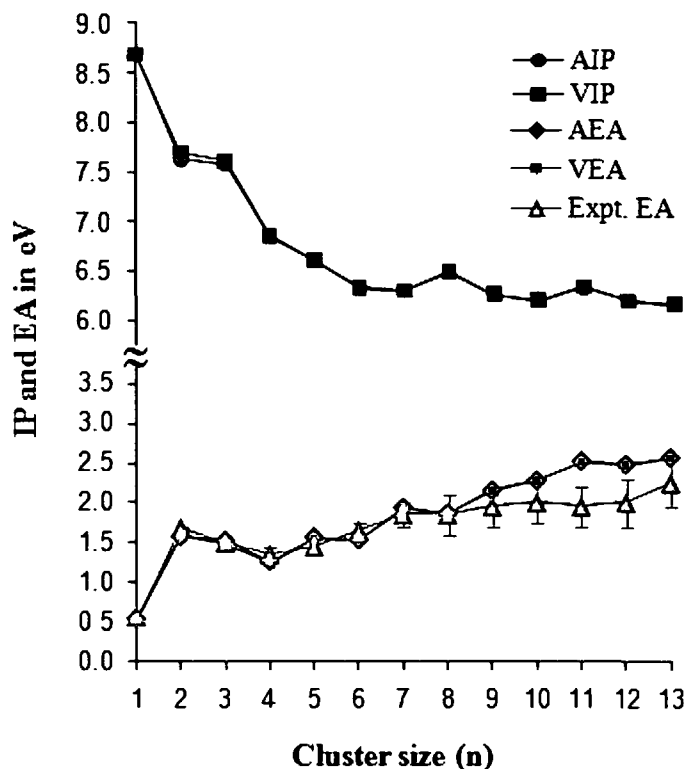


Figure 3.7: Variation of ionization potential (IP) and electron affinity (EA) of lowest energy palladium clusters with cluster size.

It is clear from Table 3.6 and Figure 3.7 that the calculated EA values agree well with the experimental values. We have obtained an EA value of 0.54 eV for single Pd atom, which agrees well with the experimental results of Ho *et al.* [59] (0.5620 ± 0.0050) eV and Hotop *et al.* [238] (0.5570 ± 0.0080) eV. EA values obtained for all other clusters are close to the experimental results of Ho *et al.* [59], Ervin *et al.* [227] and Ganteför *et al.* [65]. We note from the graph (Figure 3.7) that Pd₄, Pd₆, Pd₈ and Pd₁₂ have rather low EAs, which support the result of higher stability of these clusters predicted from stability function.

3.3.3.2 HOMO-LUMO gap, global hardness and dipole moment

We have plotted the HOMO-LUMO gaps of the lowest energy clusters in Figure 3.8. It has been observed that there is a kind of even-odd oscillation in the variation of the HOMO-LUMO gaps with respect to the cluster size. The HOMO-LUMO gaps

for cationic clusters are larger than those of neutral and anionic clusters. A gradual decrement in the magnitude of the gaps is evident. Among the neutral clusters, Pd₂ has the highest gap of 1.50 eV and Pd₄ has the next higher gap of 1.12 eV. For anionic clusters, except for smaller peaks at Pd₄ and Pd₉, the variation of the gap is almost smoother. It may be due to the presence of an extra electron in anions, which reduces the HOMO-LUMO gap and makes the variation smaller.

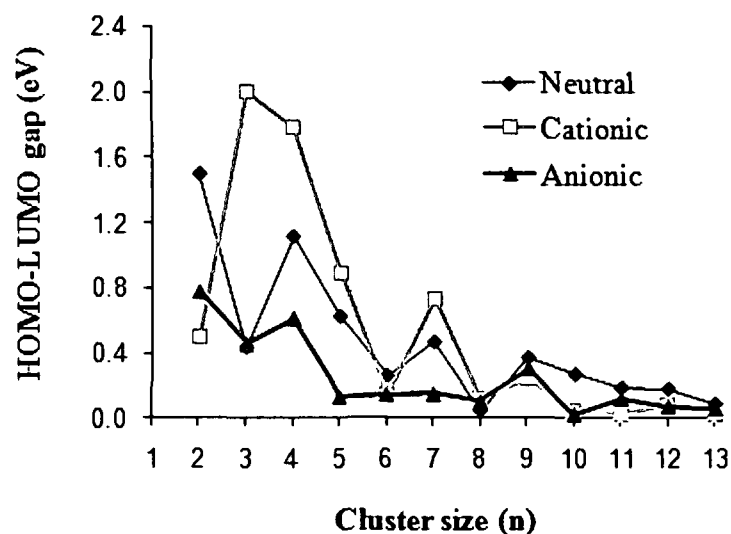


Figure 3.8: Variation of HOMO-LUMO gap with cluster size of most stable palladium clusters.

The results obtained for global hardness (η) are plotted in Figure 3.9.

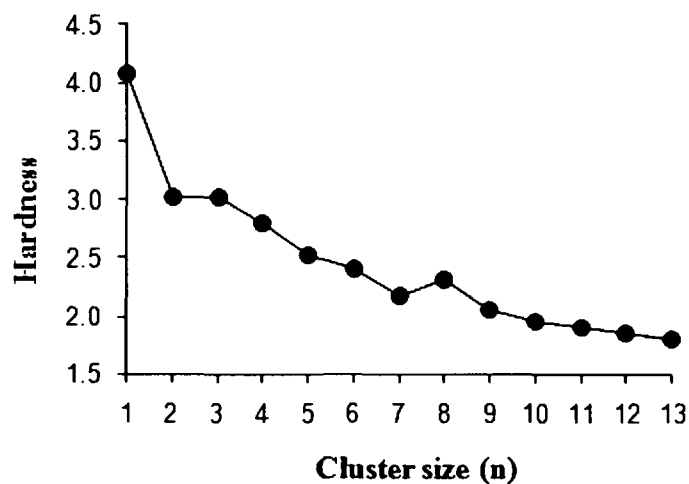


Figure 3.9: Global hardness of most stable palladium clusters with cluster size.

For single Pd atom, this value is found to be 4.07 eV, which is slightly higher than the experimental value of 3.89 eV [239]. Pd₂ and Pd₃ are observed to show almost the same hardness among the clusters followed by Pd₄. The value decreases continuously for larger sized clusters with a sudden increment in Pd₈.

Finally, we have shown the dipole moments μ_e (in debyes) of all the ground state clusters as a function of cluster size in Table 3.7. Almost zero values of μ_e indicate spherical charge distribution for most of the neutral, cationic and anionic clusters. However comparatively higher μ_e values represent the deviation from spherical charge distribution in Pd₁₂ and Pd₁₃ clusters.

Table 3.7: Dipole moments μ_e (in debyes) of the ground state palladium clusters as a function of cluster size.

Cluster size (n)	Neutral	Anionic	Cationic
2	0.0000	0.0127	0.0127
3	0.0000	0.0085	0.0085
4	0.0010	0.0069	0.0065
5	0.0019	0.0050	0.0001
6	0.0004	0.0066	0.0059
7	0.0038	0.0080	0.0012
8	0.0003	0.0004	0.0001
9	0.0001	0.0000	0.0000
10	0.0005	0.0005	0.0003
11	0.0000	0.0000	0.0004
12	0.0613	0.1135	0.0108
13	0.0935	0.0167	0.1884

3.4 SALIENT OBSERVATIONS

We have carried out systematic relativistic density functional calculations for a series of nanoscale bare palladium clusters with atoms from 1 to 13 for three different multiplicities M=1, 3, and 5. Cations and anions formed from the lowest energy states of neutral clusters are examined with multiplicities M=2, 4, and 6. In this study, we have calculated different parameters such as bond length, binding

energy, coordination number, stability function, fragmentation energy, bond dissociation energy, ionization potential, electron affinity, HOMO-LUMO gap, global hardness and dipole moment. Based on all the above-discussed data, we can draw an important conclusion on the magicity of the clusters. In light of the jellium model [231] clusters of simple metals exhibit electronic shell structure similar to the shell model of nucleus and this leads to magic behavior of clusters with 8, 20, 40; 58, 92,... valence electrons [24]. On this basis, Pd₄ can be claimed to exhibit shell closure as it has 40 valence electrons. However, photoelectron spectra of palladium cluster anions [65] reveal that the more localized *d* valence electrons in Pd clusters dominate the density of states near the Fermi level, which suppress possible shell structures. As mentioned before, it is found that Pd₄ has relatively high binding energy (1.41 eV/atom) and the stability function shows higher relative stability of Pd₄ than the neighbours. Again, Pd₄ is found to have considerably high (6.85 eV) adiabatic ionization potential and lowest adiabatic electron affinity (1.27 eV) among all the clusters. Moreover, Pd₄ possesses the highest value of bond dissociation energy (2.33 eV) in the cluster series and also a high HOMO-LUMO gap of 1.12 eV. Along with these, global hardness calculation and dipole moment value of Pd₄ showed higher chemical hardness and closed shell structure, respectively. Although binding energy values of Pd₅–Pd₁₃ are higher than that of Pd₄, their AIP values are lower and also they have higher AEAs. These clusters have lower HOMO-LUMO gaps, bond dissociation energies (except for Pd₆ and Pd₈) and global hardness values. Similarly, though Pd₂ has higher AIP, HOMO-LUMO gap and global hardness than Pd₄, the values of the other parameters do not support it as a magic cluster. Low electron affinity, high ionization potential (i.e., large HOMO-LUMO gap) and enhanced stability are hallmarks of magic clusters [240]. So, we can accept Pd₄ as the electronically most stable cluster or a magic-number cluster among the clusters studied here.

CHAPTER

4

ADSORPTION OF CO ON GAS PHASE SMALL PALLADIUM CLUSTERS

In the present chapter, we have presented the results of the DFT investigation of carbon monoxide adsorption on neutral, cationic and anionic Pd_n ($n=1-7$) clusters. In this study, we have checked all possible modes of adsorption of CO on small stable palladium clusters obtained in Chapter 3. Symmetry unrestricted geometry optimizations have been performed for all the complexes in different spin multiplicities. The results indicate that the binding of CO molecule to neutral and cationic palladium clusters takes place via 1-, 2- and 3-fold coordination. On the other hand, only terminal adsorption of CO molecule is possible in anionic clusters barring bridging adsorption in Pd_7^- cluster [Kalita and Deka, *Eur. Phys. J. D* **53**, 51 (2009)].

4.1 INTRODUCTION

Adsorption on metal surfaces has been extensively studied due to its importance in understanding surface phenomena and catalysis. The chemisorptions of CO on metal surfaces have become a subject of great interest as part of the necessary activation steps during the catalytic reduction/oxidation of these molecules in industrial processes. Previous theoretical [105,116-129] and experimental [131,132] investigations on different nanosized neutral and charged palladium clusters have concluded that these clusters exhibit a variety of binding sites for CO including a-top, bridge and hollow positions.

In spite of these theoretical and experimental studies, a systematic theoretical study of CO adsorption on anionic Pd clusters is still missing and till date, there have been no theoretical reports on Pd_nCO^+ clusters to the best of our knowledge. In the present work, we have carried out a systematic investigation of the adsorption

properties of CO on neutral, cationic and anionic Pd_n (n=1–7) clusters using density functional calculations.

4.2 COMPUTATIONAL DETAILS

All the density functional calculations reported here have been carried out using the DMol³ package [209,210]. Relativistic calculations are performed using a local pseudopotential (VPSR) [217]. Self consistent field procedures are performed with a convergence criterion of 2×10^{-5} a.u. on the total energy and 10^{-6} a.u. on electron density. We have used the DNP basis set [209] and the generalized gradient approximation (GGA) implemented in the exchange-correlation functional, BLYP [205,207]. Values of binding energy, bond length and vibrational frequency for free CO molecule are found to be 11.01 eV, 1.16 Å and 2111.7 cm⁻¹, respectively. These results are in well agreement with the experimental values [66] of 11.23 eV, 1.14 Å and 2143 cm⁻¹. Stability of all the structures has been confirmed by the absence of any imaginary frequency. The zero-point vibrational energy corrections have been included in all calculations.

In the results to follow, the binding energies of CO molecule onto bare Pd_n^q (n=1–7, q=1, 0, -1) clusters are computed as,

$$BE = E (Pd_n^q) + E (CO) - E (Pd_n^q-CO \text{ adduct}) \quad (4.1)$$

4.3 RESULTS AND DISCUSSION

4.3.1 Geometries and energetics

The lowest energy structures of Pd_n^q (n=1–7 and q=0, 1, -1) clusters have been taken from our recent work [Chapter 3] to study their interaction with CO molecule. Symmetry unrestricted full geometry optimization have been carried out on a large number of possible structural isomers of CO adsorbed palladium complexes corresponding to the on-top, atop, bridge and hollow adsorption sites for the adsorbed CO molecule in the complexes. In this study, we have examined two different spin multiplicities (M=1 and 3) for all the isomers of each cluster size of the neutral clusters. For cationic and anionic clusters, the isomers of each cluster size have been fully optimized in spin multiplicities, M=2 and 4. The resulting most stable structures of palladium monocarbonyl complexes are shown in Figures 4.1

and 4.2. Computed data for bare and CO adsorbed Pd_n^q ($n=1-7$, $q=0, 1, -1$) clusters are reported in Table 4.1, 4.2 and 4.3, respectively. The elongation of Pd–Pd bond lengths of the bare clusters upon CO adsorption shows that there is a bonding interaction between the cluster and the CO molecule.

$\text{Pd}_1\text{CO}^{0,\pm}$ complexes

The lowest energy structure of neutral Pd_1CO is a singlet with linear on-top geometry and $C_{\infty v}$ symmetry (Figure 4.1). The structure retains a-top geometry in triplet state with C_s symmetry, which lies 2.095 eV higher in energy (Table B1 in Appendix B). The cationic Pd_1CO also has the linear on-top geometry with $C_{\infty v}$ symmetry (Figure 4.1), but it is a doublet. The next higher energy structure (3.790 eV higher in energy) is in a-top geometry in the quartet state with C_s symmetry (Table B2 in Appendix B). The Pd–CO distance and C–O bond length in Pd_1CO are 1.87 and 1.16 Å, respectively (Table 4.1) which overestimate the experimental values [241] of 1.843 ± 0.003 Å and 1.138 ± 0.002 Å. However, these values are in good agreement with the B3LYP/TZVPP results of Nava *et al.* [242] and with the recent results of Zanti and Peeters [105]. The lowest energy structure of Pd_1CO^- is found to be a doublet with a-top geometry ($\angle \text{Pd-C-O} = 143.8^\circ$) and C_s symmetry (Figure 4.1). A-top geometry (C_s symmetry) of this structure in quartet state lies 2.559 eV higher in energy (Table B3 in Appendix B). Calculated values of Pd–CO distances in Pd_1CO^+ and Pd_1CO^- clusters are 1.98 and 1.92 Å, respectively. Values of C–O bond lengths are found to be 1.13 and 1.20 Å, respectively for Pd_1CO^+ and Pd_1CO^- clusters. Changes in bond distances are found to be $\Delta r_{\text{Pd-(CO)}} = 0.048$ Å and $\Delta r_{\text{C-O}} = 0.036$ Å, in transition from neutral to anionic complex. The increment in bond distances from neutral to anion is not very different from the earlier result [243]. CO binding energies with neutral, cationic and anionic Pd atom are 1.86, 1.72 and 1.54 eV, respectively. Binding energy value for neutral Pd_1CO agrees well with the B3LYP/TZVPP results of an earlier study [242].

$\text{Pd}_2\text{CO}^{0,\pm}$ complexes

CO molecule prefers the bridge adsorption site in neutral Pd_2CO . The structure is a singlet with C_{2v} symmetry. This observation is similar with other reported works [105,244]. A structure with a-top adsorption site for CO ($M=1$ with C_s symmetry) is

0.994 eV higher in energy than the lowest energy state (Table B1 in Appendix B). A-top (C_s symmetry) and bridge (C_{2v} symmetry) structures in triplet states are found to be 1.360 and 1.590 eV higher in energy, respectively than the most stable state. For cationic Pd_2CO ($M=2$ with C_{2v} symmetry), CO occupies the bridge adsorption site of Pd_2 . The structure with CO adsorbing in the a-top site ($M=2$ with $C_{\infty v}$ symmetry) lies 0.874 eV higher in energy (Table B2 in Appendix B). In anionic Pd_2CO complex, the structure is a doublet with $C_{\infty v}$ symmetry, in which CO prefers to be singly coordinated in the on-top adsorption site (Figure 4.1). The values of Pd–Pd bond lengths in neutral, cationic and anionic clusters are 2.67, 2.68 and 2.63 Å, respectively. In neutral Pd_2CO cluster, Pd–CO distance and C–O bond length are 1.97 and 1.18 Å, respectively. For cationic cluster, these distances are found to be 2.03 and 1.16 Å, respectively and for anionic cluster the corresponding values are 1.86 and 1.18 Å. The Pd–CO and C–O distances of neutral Pd_2CO complex agree well with some reported results [129,242]. CO binding energies for neutral, cationic and anionic Pd_2 clusters are 2.49, 2.06 and 1.98 eV, respectively. This value in neutral Pd_2CO complex is in well agreement with some earlier results [242,244,245] and slightly lower than that reported by Dai *et al.* [246].

$Pd_3CO^{0,\pm}$ complexes

For Pd_3CO , the lowest energy state of the neutral complex is a singlet with C_{3v} symmetry, in which CO is adsorbed through the threefold hollow adsorption site (Figure 4.1). This is similar to the observation of Joshi *et al.* [244]. It is seen from Table 4.1 that values of CO binding energy and C–O bond length are 1.93 eV and 1.20 Å, respectively, which are lower than the earlier results [244]. Energy of the structure corresponding to a-top adsorption of CO in singlet state with C_s symmetry is 0.704 eV higher in energy than the ground state. Two more structures (C_s symmetry) in triplet states with a-top and bridge adsorption sites for CO lie 0.823 and 0.933 eV higher in energy, respectively than the most stable structure. The ground state of cationic Pd_3CO complex is a doublet (C_{3v} symmetry) with threefold hollow adsorption site for CO. A-top ($M=2$) and bridge ($M=4$) geometry with C_s symmetry of Pd_3CO^+ are found to be 1.033 and 1.497 eV higher in energy, respectively, than the corresponding lowest energy structure. All the bond distances and CO binding energy values of the lowest energy Pd_3CO^+ structure are reported in

Table 4.2. It is seen that binding energy value of Pd_3CO^+ (2.24 eV) is higher than that of Pd_3CO . Anionic Pd_3CO ground state has a doublet with C_1 symmetry and CO is adsorbed in the a-top adsorption site ($\angle\text{Pd-C-O}=174.2^\circ$). Binding energy value of CO in this complex is 1.84 eV (Table 4.3), which is close to the experimental result [247] of 1.78 ± 0.32 eV. Bridge (with C_s symmetry) and three-fold (C_{3v} symmetry) adsorption of CO in doublet state for this structure are 0.321 and 0.422 eV higher in energy, respectively. The structures and relative energies of all low energy isomers are shown in Tables B1–B3 in Appendix B.

$\text{Pd}_4\text{CO}^{0,\pm}$ complexes

CO molecule is adsorbed in the threefold hollow adsorption site for both neutral and cationic Pd_4CO complexes, in their lowest energy states (Figure 4.1). Both the structures are found to be in C_{3v} symmetry (singlet for neutral and doublet for cationic complex). For neutral Pd_4CO cluster, energies of a-top (C_1 symmetry) and bridge (C_s symmetry) adsorption geometry of CO in singlet states are 0.130–0.132 eV (structures 4a–4d in Table B1 of Appendix B) and 0.263–0.264 eV (structures 4e–4g in Table B1 of Appendix B) higher in energy, respectively, than the lowest energy structure. CO adsorption geometries in a-top (C_s symmetry) and bridge sites (C_1 symmetry) with doublet state for cationic Pd_4CO , lie 0.400 and 0.149 eV higher in energy, respectively, than the corresponding lowest energy structure. Value of C–O bond length for the ground state neutral cluster is found to be 1.21 Å, which is close to the earlier results [118,129]. Our computed value of Pd–CO distance (2.03 Å) agrees well with Bertin *et al.* [129] and slightly less than the observation of Pacchioni and Koutecky [120]. CO binding energy in neutral Pd_4CO (1.321 eV) is found to be less than other observations [118,129]. Anionic Pd_4CO ground state is a doublet (C_s symmetry) with single coordination of the CO molecule in a slightly tilted on-top site ($\angle\text{Pd-C-O}=179.634^\circ$) (Figure 4.1). Table 4.3 summarizes all the bond distances and the CO binding energy values for all the anionic complexes. Three-fold adsorptions of CO in doublet and quartet states with C_{3v} symmetry are found to be 0.580 and 1.136 eV higher in energy, respectively than the anionic Pd_4CO ground state. Tables B1–B3 of Appendix B summarizes the structures and relative energies of all structural and spin isomers of neutral, cationic and anionic Pd_4CO complexes.

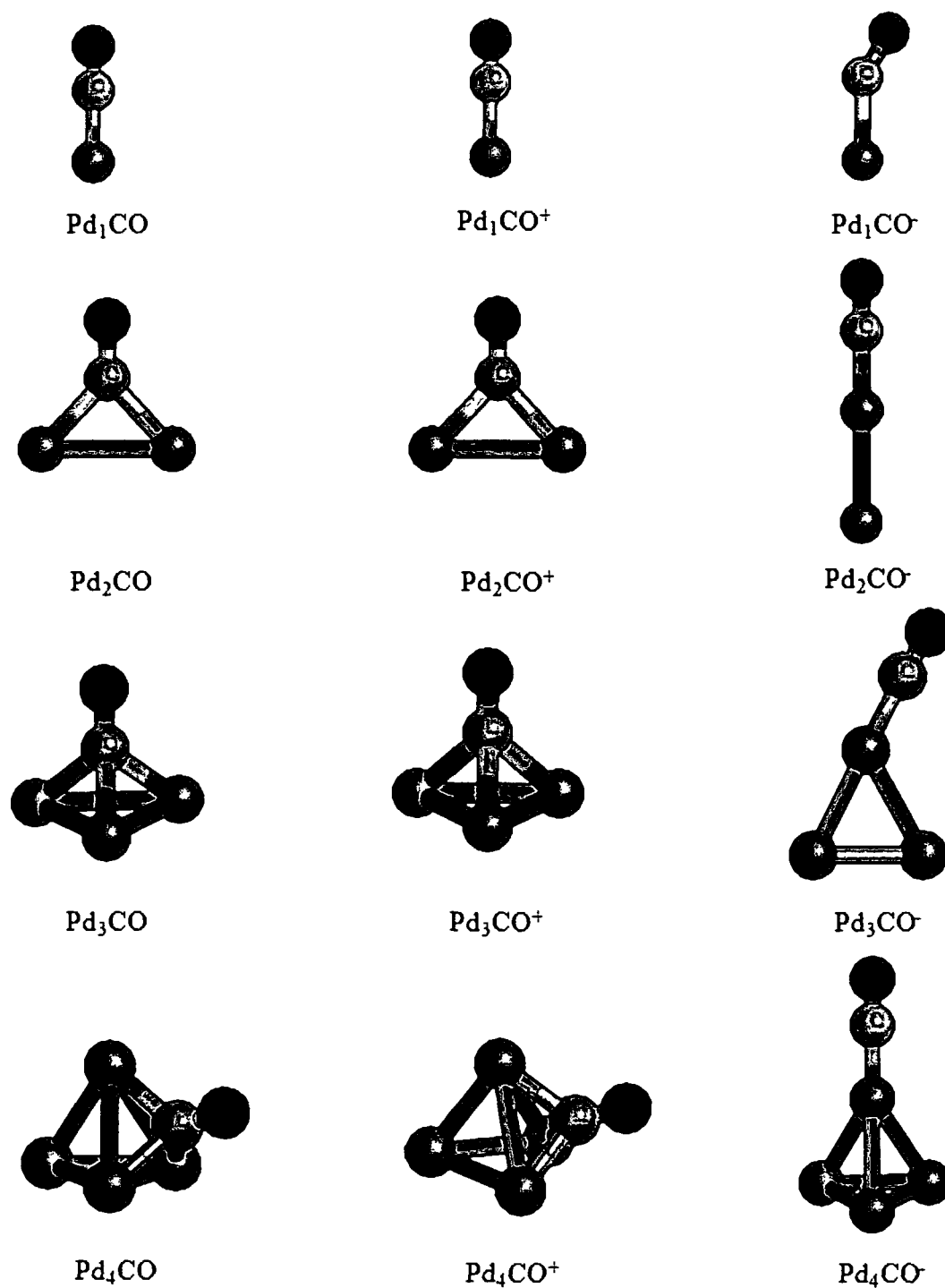


Figure 4.1: Optimized structures for the most stable geometries of Pd_n^qCO ($q=0, 1$ and $-1, n=1-4$) clusters. Blue, gray and red spheres represent palladium, carbon and oxygen atoms, respectively.

Table 4.1: Calculated parameters of the most stable adsorption complexes of CO on neutral Pd_n (n=1-7) clusters.

Complex	Geometry	Spin state	CO BE (eV)	Pd-Pd bond length (Å)	Pd-C distance (Å)	C-O bond length (Å)	C-O freq. (cm ⁻¹)
Pd ₁ CO	On-top	Singlet	1.86	—	1.87	1.16	2004.5
Pd ₂ CO	Bridge	Singlet	2.49	2.67	1.97	1.18	1827.9
Pd ₃ CO	Three-fold	Singlet	1.93	2.74	2.04	1.20	1707.9
Pd ₄ CO	Three-fold	Singlet	1.32	2.78	2.03	1.21	1660.3
Pd ₅ CO	On-top	Singlet	1.46	2.71	1.91	1.16	1986.2
Pd ₆ CO	A-top	Singlet	1.35	2.73	1.91	1.16	1971.0
Pd ₇ CO	Bridge	Singlet	1.62	2.76	2.00	1.18	1814.8

Pd₅CO^{0,±} complexes

Figure 4.2 shows the most stable structures of Pd₅CO, Pd₅CO⁺ and Pd₅CO⁻. The lowest energy structure of neutral Pd₅CO cluster has on-top geometry with C_{3v} symmetry (M=1) and structure of Pd₅CO⁻ cluster is close to the on-top geometry (<Pd-C-O=179.9°) with C₁ symmetry (M=2). The lowest energy structure of cationic Pd₅CO⁺ cluster is a doublet with C_s symmetry, in which, CO molecule coordinates to three palladium atoms through the carbon atom. For neutral Pd₅CO complex, bridge and three-fold adsorption of CO in singlet states (C_s symmetry) are 0.093 and 0.174 eV higher in energy, respectively, than the most stable structure (Table B1 in Appendix B). Two more structures in triplet states with on-top (C_{3v} symmetry) and bridge (C_s symmetry) site adsorption of CO are found to be 0.014 and 0.146 eV higher in energy, respectively, than the lowest energy state. In cationic Pd₅CO complex, a-top adsorption of CO in doublet and quartet states with C_s symmetries are 0.125 and 0.136 eV higher in energy, respectively, than the

corresponding ground state (Table B2 in Appendix B). Doublet states of one a-top and bridge sites adsorption of CO (C_1 symmetry) in anionic Pd_5CO complex lie 0.207 and 0.212 eV higher in energy, respectively, than the corresponding most stable structure (Table B3 in Appendix B). A higher binding energy value of CO is observed for anionic Pd_5CO complex (1.97 eV), followed by neutral (1.46 eV) and cationic (1.32 eV) clusters, respectively.

Table 4.2: Calculated parameters of the most stable adsorption complexes of CO on cationic Pd_n ($n=1-7$) clusters.

Complex	Geometry	Spin state	CO BE (eV)	Pd-Pd bond length (Å)	Pd-C distance (Å)	C-O bond length (Å)	C-O freq. (cm^{-1})
Pd_1CO^+	On-top	Doublet	1.72	—	1.98	1.13	2160.5
Pd_2CO^+	Bridge	Doublet	2.06	2.72	2.68	1.16	1964.8
Pd_3CO^+	Three-fold	Doublet	2.24	2.67	2.09	1.18	1848.5
Pd_4CO^+	Three-fold	Doublet	1.37	2.77	2.05	1.19	1753.7
Pd_5CO^+	Three-fold	Doublet	1.32	2.76	2.05	1.20	1725.8
Pd_6CO^+	A-top	Doublet	1.07	2.72	1.96	1.15	2057.9
Pd_7CO^+	Bridge	Doublet	1.42	2.76	2.01	1.17	1883.1

$Pd_6CO^{0\pm}$ complexes

For Pd_6CO , CO prefers to be singly coordinated in all the neutral, cationic and anionic clusters (Figure 4.2). CO adsorption is slightly tilted from the on-top position ($\angle Pd-C-O=179.1^\circ$) in the neutral cluster, which is in singlet state with C_s symmetry. One structure with a-top geometry ($M=3$ with \tilde{C}_1 symmetry) (Table B1

in Appendix B) and one with bridge geometry (M=1 with C_s symmetry) (structure 6c in Table B1 of Appendix B) for the neutral complex are found to be 0.062 and 0.190 eV higher in energy, respectively, than the ground state. A-top adsorption sites are favorable for CO in Pd_6CO^+ (doublet with C_1 symmetry) and Pd_6CO^- (doublet with C_s symmetry) with $\angle Pd-C-O=178.9^\circ$ and 178.8° , respectively.

For cationic complex, a-top adsorption geometry (C_1 symmetry) in quartet state and three-fold adsorption geometry (C_{3v} symmetry) in doublet state are only 0.046 and 0.089 eV higher in energy, respectively, than the corresponding ground state (Appendix B). In anionic Pd_6CO complex, a-top adsorption geometry (M=4) and bridge adsorption geometry (M=2) with C_s symmetry are found to be 0.204 and 0.231 eV higher in energy, respectively, than the most stable structure (Table B3 in Appendix B). Our calculated bond lengths and CO binding energies of all these clusters are tabulated in Tables 4.1, 4.2 and 4.3. The calculated C-O bond lengths and CO binding energies follow the trend: cationic < neutral < anionic clusters.

Table 4.3: Calculated parameters of the most stable adsorption complexes of CO on anionic Pd_n (n=1-7) clusters.

Complex	Geometry	Spin state	CO BE (eV)	Pd-Pd bond length (Å)	Pd-C distance (Å)	C-O bond length (Å)	C-O freq. (cm^{-1})
Pd_1CO^-	A-top	Doublet	1.54	—	1.92	1.20	1740.7
Pd_2CO^-	On-top	Doublet	1.98	2.63	1.86	1.18	1868.6
Pd_3CO^-	A-top	Doublet	1.84	2.67	1.88	1.18	1870.5
Pd_4CO^-	A-top	Doublet	1.95	2.76	1.88	1.18	1863.2
Pd_5CO^-	A-top	Doublet	1.97	2.74	1.87	1.18	1877.6
Pd_6CO^-	A-top	Doublet	1.85	2.75	1.88	1.18	1877.3
Pd_7CO^-	Bridge	Doublet	1.89	2.77	2.01	1.19	1756.6

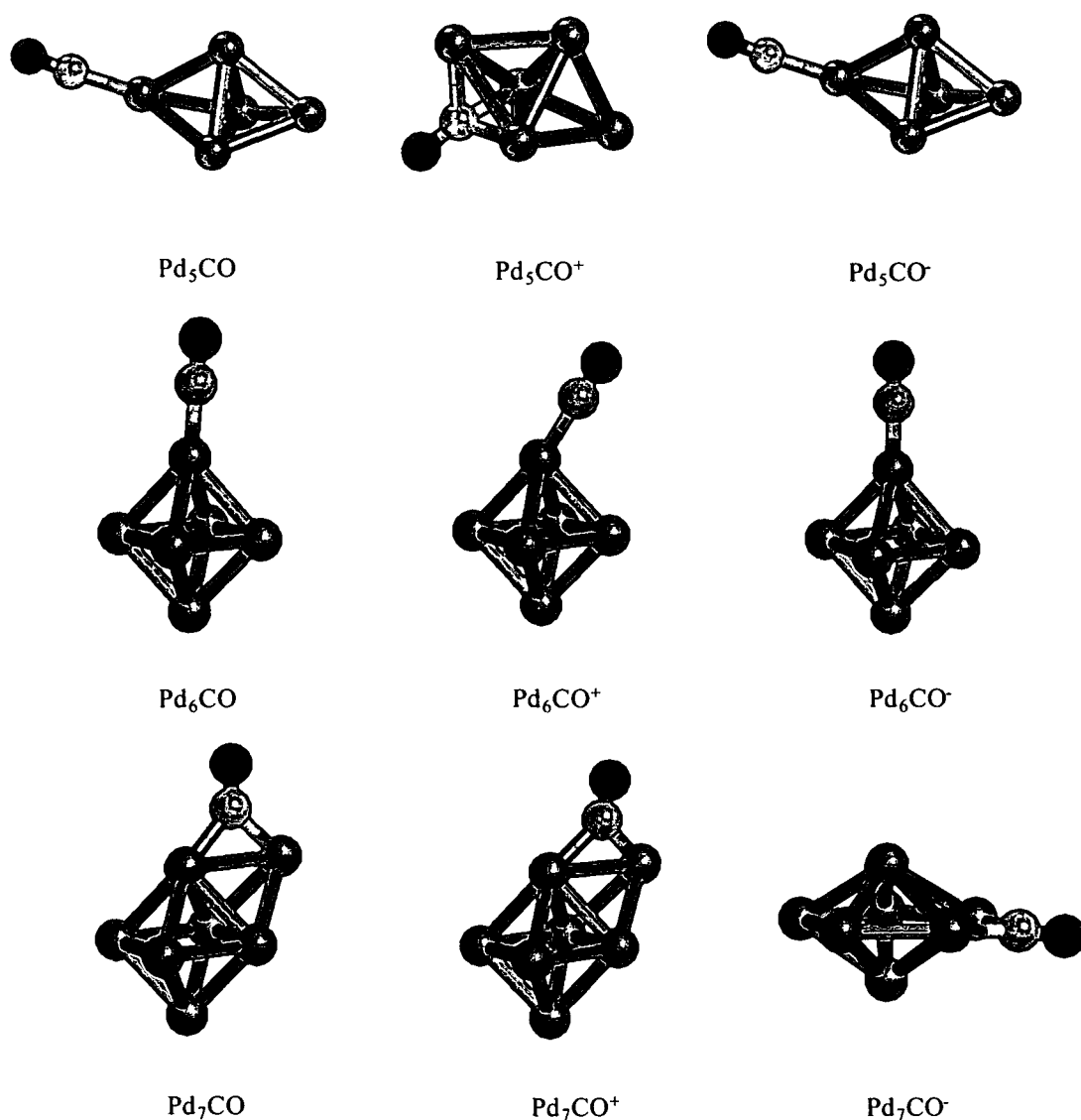


Figure 4.2: Optimized structures for the most stable geometries of Pd_n^qCO ($q=0, 1$ and $-1, n=5-7$) clusters. Blue, gray and red spheres represent palladium, carbon and oxygen atoms, respectively.

$\text{Pd}_7\text{CO}^{0,\pm}$ complexes

Adsorption of CO takes place in the bridge site of neutral, cationic and anionic Pd_7CO complexes. Pentagonal bipyramid structures of bare Pd_7 and Pd_7^+ change to monocapped octahedra upon CO adsorption, but for Pd_7^- , the structure remains the same as that of the bare cluster (Figure 4.2). The lowest energy structures of both Pd_7CO (singlet) and Pd_7CO^+ (doublet) have C_1 symmetry while the ground state Pd_7CO^- is a doublet with C_s symmetry. In neutral Pd_7CO complex, three structures

corresponding to the bridge site adsorption of CO are close in energy to the ground state. The differences in energy of these structures from those of the ground states are 0.029 eV (for structure in singlet state with C_s symmetry), 0.043 and 0.083 eV (for structures in triplet states with C_s symmetry). Bridge site adsorption of CO in quartet state with C_1 symmetry, in cationic Pd_7CO complex, is close in energy to the corresponding ground state (the difference in energy is only 0.045 eV). Other two structures in doublet states with a-top and bridge (C_s symmetry) site adsorption are found to be 0.189 and 0.112 eV higher in energy, respectively, than the lowest energy structure. In anionic complex, on-top (C_1 symmetry), a-top (C_1 symmetry) and bridge (C_s symmetry) adsorption of CO in doublet states are only 0.083, 0.421 and 0.098 eV higher in energy, respectively, than the corresponding most stable structure. CO binding energy and C–O bond length values follow the same pattern as that of the Pd_6CO complexes (Tables 4.1, 4.2 and 4.3). The structures and relative energies of all the structural and spin isomers of $Pd_7CO^{0,\pm}$ complexes are shown in Tables B1–B3 of Appendix B.

4.3.2 Variation in bond lengths and adsorption properties

From Tables 4.1, 4.2 and 4.3, it is observed that both the Pd–CO distance and C–O bond length increase in going from top to bridge to 3-fold adsorption sites in all the clusters. The increment of intermolecular CO interactions due to high coverage leads to the lengthening of the metal–CO distances. On the other hand, lengthening of C–O bonds in moving from top to bridge to hollow sites may be related to the increased metal $\rightarrow \pi^*$ back-donation, which progressively weakens the C–O bond.

From the pertinent calculations, it has been observed that the binding energies of CO with palladium clusters follow the trend: $Pd_nCO^+ < Pd_nCO < Pd_nCO^-$ (only $n = 5$ onwards). This may be due to the increased metal $\rightarrow CO$ back-donation in anionic clusters followed by neutral and cationic clusters. It suggests that metal $\rightarrow CO$ back-donation is the probable dominant mechanism for CO adsorption in larger three dimensional palladium clusters. No pronounced correlation is observed between the frontier orbital energies of the gas phase palladium clusters and their binding energies with CO. This is similar to the observation in case of gold clusters [248].

4.3.3 Vibrational properties

Calculated C–O vibrational frequencies for neutral, cationic and anionic Pd_nCO (n=1-7) complexes are given in Tables 4.1, 4.2 and 4.3, respectively. It is found from Table 4.1 that C–O stretching frequency of Pd₁CO complex is 2004.2 cm⁻¹, which lies in the range of some earlier observations [122,123,249]. However, this value is less than the experimental value of 2050 cm⁻¹ [250]. As the C–O bond lengths in cationic and anionic Pd₁CO complexes are shorter and longer, respectively, than free CO molecule, the corresponding C–O vibrational frequencies (Table 4.2 and Table 4.3) are found to be larger and smaller than the free C–O stretch frequency. Value of C–O stretch frequency decreases from Pd₁CO to Pd₂CO cluster (1827.9 cm⁻¹). This value is slightly less in comparison with the value reported by Andzelm and Salaňub [118] and the experimental range of 1880–2000 cm⁻¹ [251]. Values of C–O vibrational frequencies in cationic and anionic Pd₂CO complexes are higher than that the neutral complex. For Pd₃CO, C–O bond lengths in anionic and cationic clusters are shorter than the neutral cluster. As a result, C–O vibrational frequencies are found to be higher in the charged clusters than in the neutral cluster (Tables 4.1, 4.2 and 4.3). Our calculated value of C–O frequency in neutral Pd₃CO cluster (1707.9 cm⁻¹) is less than that of Joshi *et al.* (1825 cm⁻¹) [244]. C–O bond length successively decreases from neutral to cationic to anionic clusters in case of Pd₄CO. Accordingly, the C–O stretch frequencies follow the trend of anionic > cationic > neutral. C–O frequency value for neutral Pd₄CO cluster is found to be less than the earlier observations [126,129]. C–O bond length values in Pd₅CO clusters suggest that the C–O interaction is the weakest in cationic followed by that in anionic and neutral clusters. Following this trend, C–O frequencies (Tables 4.1, 4.2 and 4.3) show an increasing pattern from cationic to anionic to neutral Pd₅CO clusters. C–O vibrational frequency trends in case of Pd₆CO and Pd₇CO clusters are found to be in the order: cationic > neutral > anionic clusters. It has been observed that the C–O frequency values in Pd₄CO⁺ (1753.7 cm⁻¹) and Pd₅CO⁺ (1725.8 cm⁻¹) clusters are close to the experimental values (1735 cm⁻¹) [132] of adsorbed CO in three-fold site of cationic Pd clusters. Similarly, C–O frequency for bridge site adsorption of CO in Pd₇CO⁺ (1883.1 cm⁻¹) agrees well with the corresponding experimental value (1855 cm⁻¹) [132].

Figure 4.3 displays the linear correlation between the changes in C–O bond length and shift in C–O stretch frequencies of adsorbed CO in Pd_n^qCO ($q=0, 1$ and -1 , $n=1-7$) complexes.

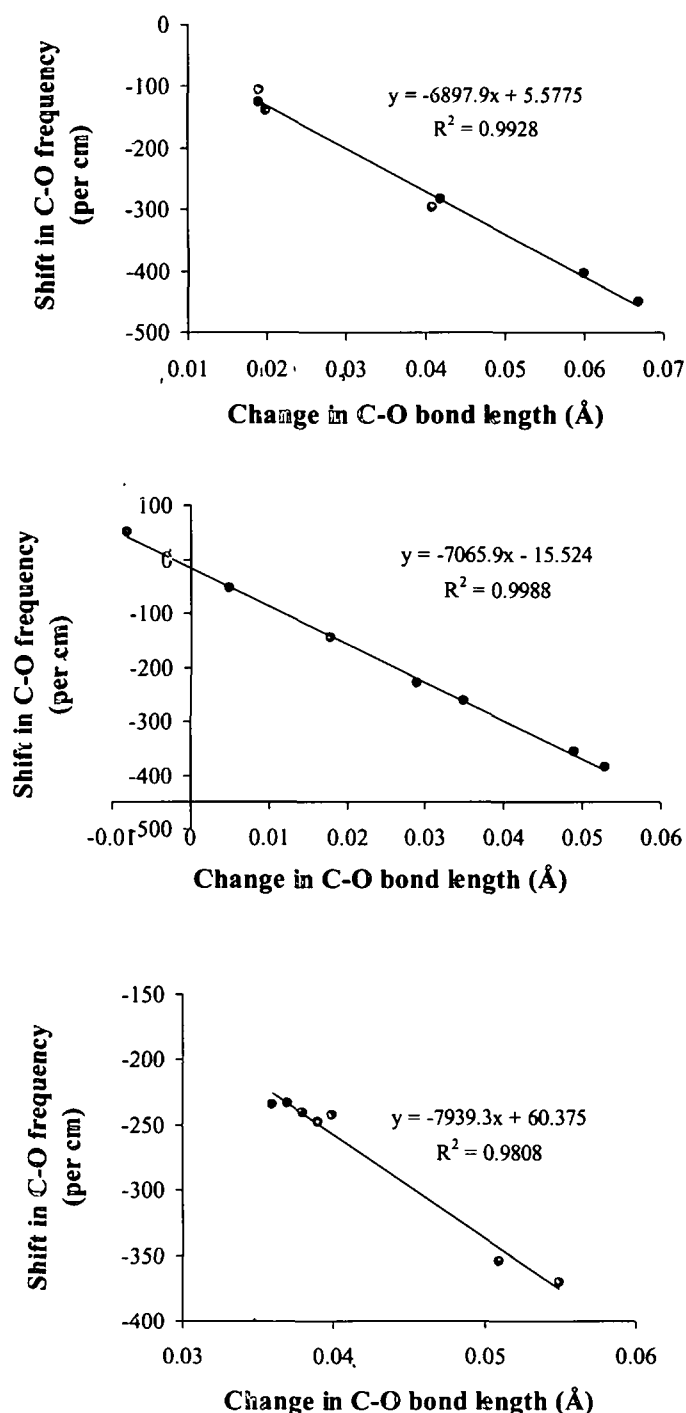


Figure 4.3: Linear correlation between change in the C–O bond length and shift in the C–O stretching frequency for adsorbed CO molecule in neutral (upper panel), cationic (middle panel), and anionic (lower panel) Pd_nCO clusters.

The red shift in the C–O stretching frequency upon adsorption correlates linearly with the elongation of the C–O bond in case of neutral and anionic clusters (upper and lower panel of Figure 4.3) with correlation coefficients of 0.9928 and 0.9808, respectively. In Pd_1CO^+ complex, C–O bond length is smaller and vibrational frequency is larger than the corresponding values of free CO molecule. This effect is essentially as a result of the electrostatic interaction due to a change in polarization of the bond orbitals caused by the positive charge of the cationic clusters [252]. However, for the larger cationic clusters, the trends are same as that of the neutral and anionic clusters. The correlation coefficient for the cationic clusters is 0.9988.

4.4 SALIENT OBSERVATIONS

We have carried out a systematic relativistic density functional calculation within the generalized gradient approximation to investigate the geometry and electronic properties of CO adsorption on small neutral and charged palladium clusters. Adsorption of CO on neutral clusters are examined with multiplicities $M=1$ and 3 , while the calculations for cationic and anionic clusters have been performed with multiplicities $M=2$ and 4 . Our results indicate that both for neutral and cationic complexes, all the 1-, 2- and 3-fold coordination are preferred by the CO molecule. But CO adsorption takes place mostly in single coordination (2-fold coordination only for Pd_7^- cluster) in case of anionic clusters, i.e., charge states of small palladium clusters have strong influence on the adsorption configurations. Cluster charges are also found to play an important role on the CO to metal forward donation and metal to CO back-donation, which is related to the C–O bond length and the CO binding energy in the metal clusters. CO binding energies of the larger three dimensional palladium clusters follow a trend like $\text{Pd}_n\text{CO}^+ < \text{Pd}_n\text{CO} < \text{Pd}_n\text{CO}^-$, in which metal→CO back-donation is the dominant factor. For all the clusters, CO binding energies oscillate with cluster size. Neutral Pd_4 cluster is found to have the lowest binding with CO, which implies least reactivity of bare Pd_4 cluster towards CO or higher stability of Pd_4 as predicted in Chapter 3. Based on these observations, we can say that CO binding on small palladium clusters can be tuned by the charge and size of the clusters. Advantage of this property can be taken in the catalytic $\text{CO} \rightarrow \text{CO}_2$ conversion process.

CO-ADSORPTION OF CO, O₂ AND OXIDATION OF CO ON GAS PHASE Pd₄ CLUSTERS

Neutral Pd₄ has been found to have higher stability from our investigations presented in the previous two chapters. Therefore, in the present chapter we have chosen Pd₄ as a model cluster to study the catalytic activity of small palladium clusters in catalyzing carbon monoxide oxidation. Moreover, recent experimental studies [253-255] have shown that small clusters can dominate catalytic activity although most of the metal is present in form of much larger particles. In this chapter, various adsorption modes of molecular, dissociative and atomic forms of oxygen on neutral, cationic and anionic Pd₄ clusters have been studied. The lowest energy structures of these calculations have been taken for investigating co-adsorption of carbon monoxide with pre-adsorbed oxygen. The different optimized co-adsorbed complexes form all possible reaction intermediates of oxidation of carbon monoxide by oxygen. Reaction energy profiles of these reactions show better catalytic activity of neutral and cationic Pd₄ clusters than that of anionic Pd₄ cluster for carbon monoxide oxidation process [Kalita and Deka, *J. Am. Chem. Soc.* **131**, 13252 (2009)].

5.1 INTRODUCTION

Removal of poisonous carbon monoxide gas emitted mainly in automobile exhaust is a major challenge in catalysis research and has been a subject of many investigations. This is a very simple oxidation process ($\text{CO} + \frac{1}{2}\text{O}_2 \rightarrow \text{CO}_2$), which has a relatively slow reaction rate in a gaseous mixture. Transition metals such as palladium, platinum and rhodium are well known for speeding up the oxidation process significantly [256,257]. Thus understanding adsorption mechanism,

dissociation of oxygen and oxidation of CO at molecular level are of great importance in designing suitable catalysts. Recently, Moseler and co-workers [145,146] reported an extensive density functional theory (DFT) study of the oxidation of magnesia-supported Pd_N clusters (N=4-9) and their behavior in catalytic oxidation of CO. Their study revealed that adsorption of dissociated oxygen is preferred on Pd₄/MgO with dissociation barrier of only 0.5 eV, lower than the corresponding value of 1.0 eV on a Pd(111) surface [258]. The dissociation of O₂ is accompanied by a strong relaxation of the Pd cluster. Moreover, adsorption site of CO changes from hollow on Pd₄ to top on Pd₄O₂ and the stretching frequency of CO is enhanced upon dissociation of O₂. Another important observation of this study [145] is that pre-adsorption of CO inhibits subsequent O₂ dissociation giving rise to the poisoning effect [259]. Charges of small palladium clusters are also found to play significant roles in controlling their catalytic activity [68,260,261]. Keeping this in mind, we have studied the affect of charge of small palladium clusters on various adsorption sites of CO molecule. Further investigation of the co-adsorption of O₂ and CO on neutral and charged Pd clusters will certainly clarify catalytic activities of these clusters towards CO oxidation. The present chapter is focused on the nature of O₂ adsorption as well as their co-adsorption with CO leading to formation of CO₂ on neutral, cationic and anionic Pd₄ clusters.

5.2 COMPUTATIONAL DETAILS

We performed scalar relativistic DFT calculation as implemented in the DMol³ package [209,210] using DNP [209] basis set and BLYP [205,207] functional. The reliability of this basis set and functional can be judged from the binding energy values of O₂ (5.72 eV), CO (11.01 eV) and CO₂ (5.76 eV), that are in agreement with the experimental values [66,262]: 5.12, 11.23 and 5.50 eV, respectively. In our calculations, self consistent field procedures are performed with a convergence criterion of 2×10^{-5} a.u. on the total energy and 10^{-6} a.u. on the electron density. None of the complex is found to exhibit any imaginary frequency from the frequency calculations. The zero point vibrational energy corrections have been included in all calculations. Transition state structures have been located with the help of transition state search option available in DMol³. This calculation is based on the linear (LST) and quadratic synchronous transit (QST) methods proposed by

Halgren and Lipscomb [263]. In the LST approach, a series of single point energy calculations are performed on a set of linearly interpolated structures between a given set of reactants and products. The maximum energy structure along this path provides a first estimate to the transition state structure. A single refinement in an orthogonal direction to the LST path is then performed, which is then used as an intermediate to define a QST pathway. This procedure yields a further refined estimate to transition state geometry. This new robust and fast scheme [264] allows rapid location of the transition states.

We have defined the binding energy (BE) of the adsorbates, X (O₂, 2O, O, CO, CO₂), as

$$BE = E(Pd_4^q) + E(X) - E(Pd_4^q-X), q=0, 1, -1 \quad (5.1)$$

and the binding energy of the co-adsorbates, X2 (CO and CO₂) with X1 (O₂, 2O and O), as

$$BE = E(Pd_4^q-X1) + E(X2) - E(Pd_4^q-X1-X2), q=0, 1, -1 \quad (5.2)$$

5.3 RESULTS AND DISCUSSION

In this work, we have performed full geometry optimizations of all possible structural isomers of Pd₄O₂^{0,±} corresponding to the different adsorption sites of molecular and dissociative adsorption of O₂ on Pd₄^{0,±}. We have examined the neutral Pd₄O₂ complexes with multiplicities, M=1, 3, 5 and 7 while the cationic and anionic Pd₄O₂ complexes have been optimized in multiplicities, M=2, 4, 6 and 8 (Appendix B). The initial geometries of bare Pd₄^q (q=0, 1, -1) clusters have been taken from our previous work (Chapter 3). The lowest energy structures of Pd₄O₂^{0,±} have been chosen to study co-adsorption of CO on these complexes. Full geometry optimizations have been performed on various possible adsorption sites of CO on palladium oxide clusters. The results of oxygen adsorbed Pd₄ complexes and their co-adsorbed complexes with CO have been compared with the lowest energy CO adsorbed bare Pd₄ complexes obtained in Chapter 4.

5.3.1 Adsorption of oxygen on Pd₄ clusters

Figures 5.1, 5.2 and 5.3 display optimized structures of the lowest energy isomers of neutral, cationic and anionic complexes, respectively, of Pd₄ corresponding to the adsorption of molecular (Pd₄O₂) and dissociated (Pd₄2O) forms of oxygen. Table

5.1 presents more details of these geometries, binding energies as well as the electronic properties of the adsorbates.

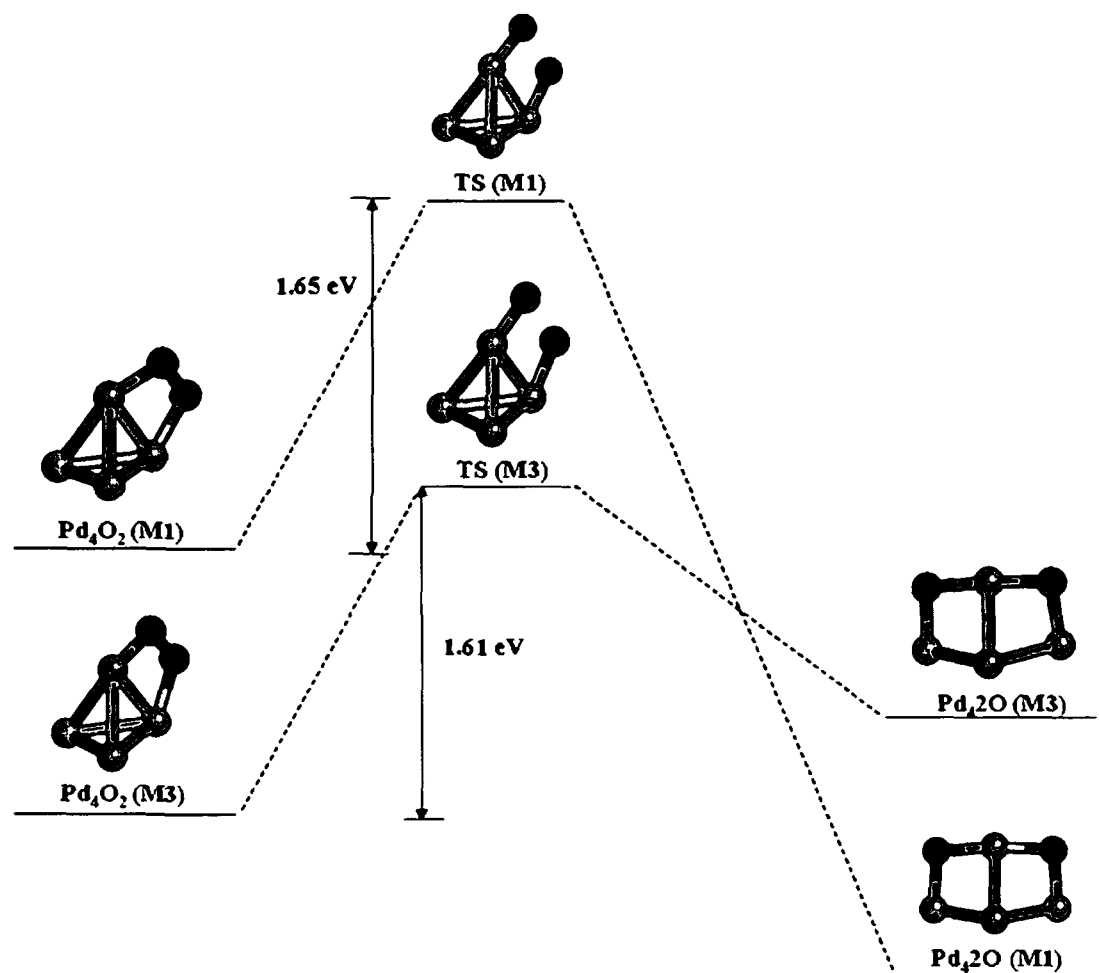


Figure 5.1: Reaction energy profile for dissociation of oxygen on gas phase neutral Pd₄ cluster for singlet and triplet states. The spin multiplicities are shown in parentheses.

Molecular adsorption (MA) of O₂ takes place preferably in bridge position of neutral and anionic Pd₄ with spin multiplicities M=3 and 4, respectively. For cationic Pd₄, adsorption of O₂ takes place in a-top position ($\angle \text{Pd-O-O} = 126.7^\circ$) of Pd₄ with multiplicity M=2. The lowest energy Pd₄O₂^{0,±} complexes are in C₁ symmetry. Dissociative adsorption (DA) of O₂ with the oxygen atoms occupying bridge sites of palladium clusters appears to be energetically most favourable for all the complexes. All the lowest energy complexes (C_s symmetry) are highly distorted from the gas phase tetrahedral Pd₄ clusters. For neutral Pd₄O₂, the lowest energy DA structure

with multiplicity $M=1$ lies 0.813 eV lower in energy than the MA complex. Energy difference of the lowest energy structure from a similar one with multiplicity $M=3$ is only 0.015 eV (Table B5 in Appendix B). This signifies the co-existence of these structures in the lowest energy state within the accuracy limit of DFT functional. Two more DA complexes with oxygen atoms sitting in bridge and hollow adsorption sites of Pd_4 cluster with multiplicities $M=1$ and 3 are found to be 0.147 and 0.191 eV higher in energy, respectively than the most stable structure (Table B5 in Appendix B).

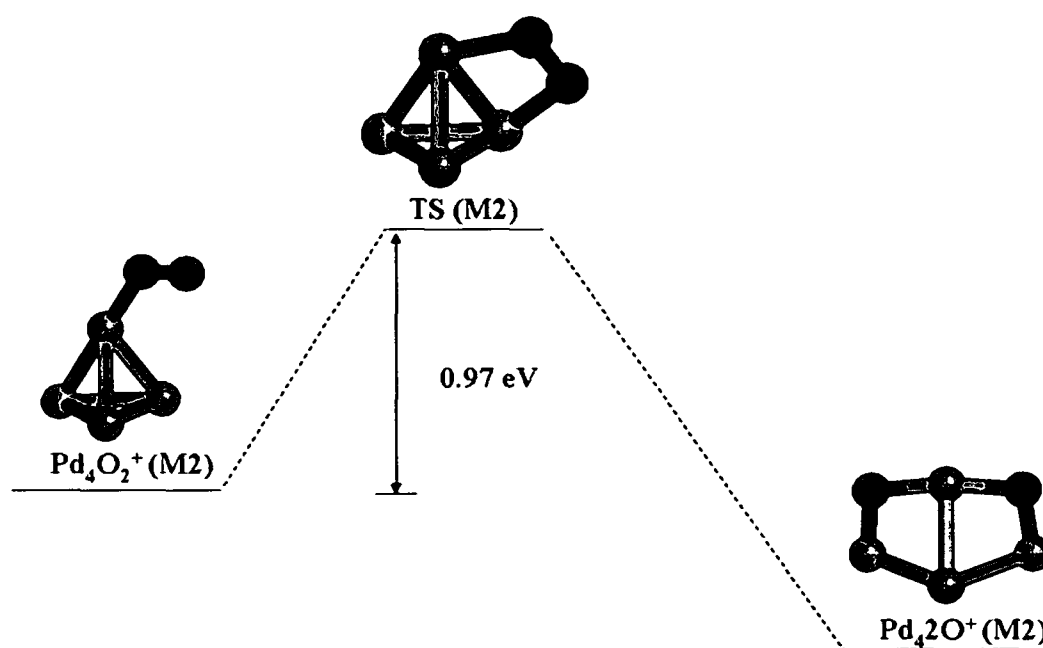


Figure 5.2: Reaction energy profile for dissociation of oxygen on gas phase cationic Pd_4 cluster. The spin multiplicities are shown in parentheses.

In case of cationic Pd_4O_2 complexes, highly distorted lowest energy DA structure ($M=2$) is 0.231 eV lower in energy than another structure ($M=2$) with similar adsorption configuration, which is slightly distorted from the gas phase Pd_4^+ cluster (Table B7 in Appendix B). The lowest energy MA structure of Pd_4O_2^+ lies 0.831 eV higher in energy than the lowest energy DA complex. One of the cationic complexes ($M=2$), in which, both the dissociated oxygen atoms gets adsorbed in three-fold co-ordination of the Pd_4^+ cluster has energy difference of only 0.082 eV from the most stable one. For anionic Pd_4O_2^- complexes, the lowest energy DA structure ($M=2$) has a similar isomer with multiplicity $M=4$ having an energy

difference of only 0.081 eV. The lowest energy MA anionic complex lies 1.125 eV higher in energy than the most stable DA structure. The structural and spin isomers with their relative stability are shown in Appendix B.

Table 5.1: Spin multiplicity (M), bond distances (d) of the adsorbates in Å, binding energy (BE) and activation energy (E_a) in eV, vibrational frequency in cm⁻¹ and Mulliken charge (q) of the adsorbates for the lowest energy isomers of oxygen adsorbed neutral, cationic and anionic Pd₄ clusters.

Complexes	M	d _{O-O}	BE (O ₂ /2O/O)	E _a	ν _{O2}	q _O /q _{O2}
Pd ₄ O ₂	3	1.35	0.82	—	960.4	-0.40
TS _N	3	2.06	—	1.66	—	—
Pd ₄ 2O	1	3.86	1.63	—	—	-1.22
Pd ₄ O	1	—	0.66	—	—	-0.59
Pd ₄ O ₂ ⁺	2	1.25	1.14	—	1318.1	-0.03
TS _C	2	1.60	—	0.97	—	—
Pd ₄ 2O ⁺	2	3.80	1.98	—	—	-1.06
Pd ₄ O ⁺	2	—	0.67	—	—	-0.61
Pd ₄ O ₂ ⁻	4	1.40	2.27	—	841.70	-0.62
TS _A	4	2.03	—	0.71	—	—
Pd ₄ 2O ⁻	2	3.90	3.39	—	—	-1.35
Pd ₄ O ⁻	2	—	1.19	—	—	-0.68

The transition state structures, termed TS_N (C₁ symmetry) (Figures 5.1), TS_C (C₁ symmetry) (Figures 5.2) and TS_A (C_{2v} symmetry) (Figures 5.3) associate with the dissociation of O₂ on neutral, cationic and anionic Pd₄ clusters, respectively. The magnitudes of the corresponding imaginary frequencies are 609 cm⁻¹, 287 cm⁻¹ and 250 cm⁻¹. The geometry and energetics of the transition state structures are given in Table 5.1. The neutral gas phase Pd₄ cluster is found to retain its tetrahedral shape during the O₂ dissociation reaction with a high activation barrier of 1.66 eV. This value is slightly lower than the activation barrier of 1.9 eV as observed by Huber *et*

al. [265]. The energy difference (2.43 eV) between TS_N and $Pd_4O_2^*$ complex is close to the value (2.3 eV) observed by Huber *et al.* [265]. The activation barriers for cationic and anionic Pd_4 clusters are calculated to be 0.97 eV and 0.71 eV, respectively. Low value of activation barrier for O_2 dissociation on Pd_4^- is similar to the experimental finding [68] of small activation barriers for O_2 chemisorption on Pd clusters anions (Pd_n^- , $n < 11$). It is seen that in case of neutral and anionic clusters, the transition state structures retain the spin multiplicity of the reactants ($Pd_4O_2^{0,-}$ complexes). However, the corresponding products are found to be stable in multiplicities other than those of the reactants and transition states. The surface crossing (singlet \rightarrow triplet and doublet \rightarrow quartet) is an indication of the two-state reactivity ($\dot{T}SR$) [266] processes, characterized accurately by DFT approaches in some other transition metal clusters [267]. The trend in activation barriers among the clusters is similar with the trend in binding energies of oxygen with the clusters.

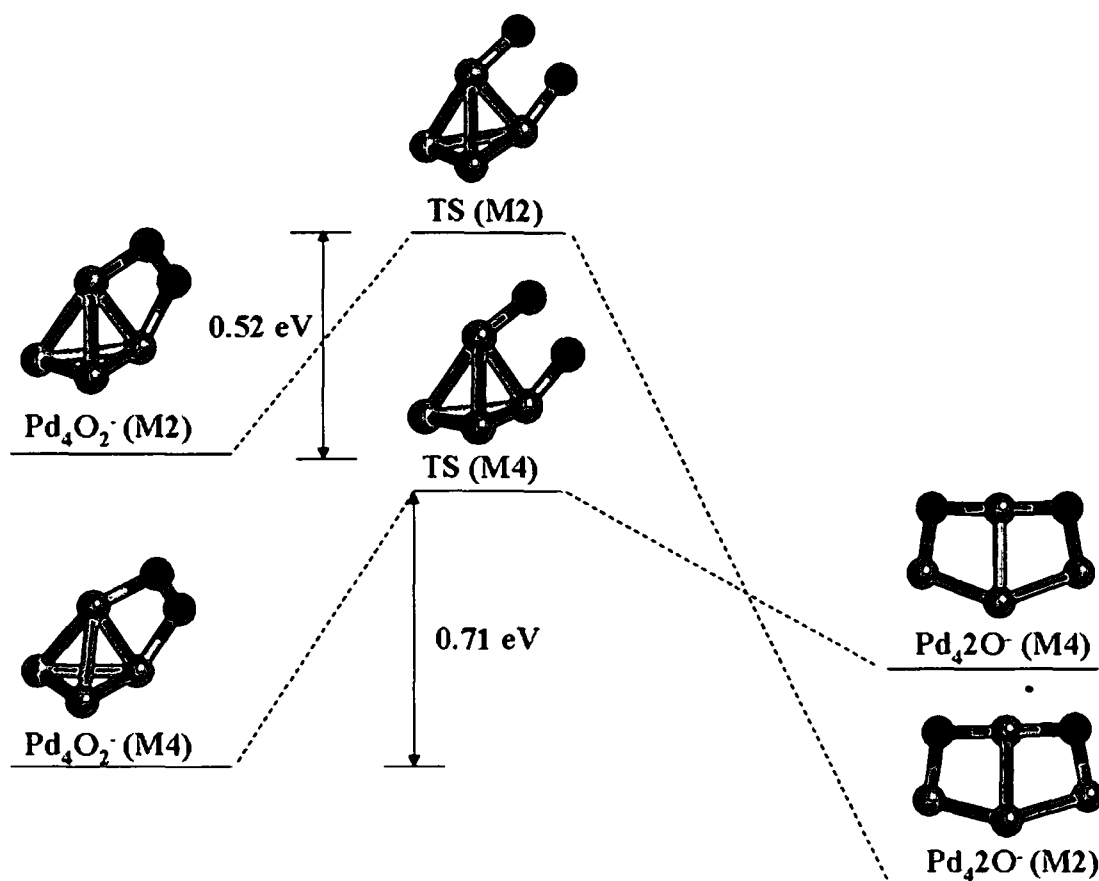


Figure 5.3: Reaction energy profile for dissociation of oxygen on gas phase anionic Pd_4 cluster. The spin multiplicities are shown in parentheses.

Calculation of binding energies of O₂ (Table 5.1) in all the structures shows maximum value for Pd₄⁻ cluster followed by Pd₄⁺ and Pd₄ clusters. Our calculated binding energies for structures Pd₄O₂ and Pd₄2O (0.82 eV and 1.63, respectively) are in agreement with the results of Huber *et al.* [265]. We have observed that O–O bond distance is larger in case of adsorbed O₂ (both in MA and DA mode) than in the free molecule (1.21 Å), being maximum for the dissociative adsorption of oxygen on anionic Pd₄ cluster. Mulliken charge analysis shows that electron charge transfer from palladium to dissociatively adsorbed O₂ takes place in the order: Pd₄⁻ > Pd₄ > Pd₄⁺. This trend is similar to that of O–O bond distance, which is due to fact that metal→oxygen back-donation increases the population of π* orbital leading to weakening of O–O bonds and thereby lengthen these bonds. Our computed O–O bond length values of structures Pd₄O₂ and Pd₄2O (Table 5.1) are in excellent agreement with those of Huber *et al.* [265]. No clear relation is visible between the oxygen binding energy and the Mulliken charge on adsorbed oxygen in its dissociative mode, probably due to the very complicated electron density transfer process during dissociative adsorption of oxygen. Similarly, in the lowest energy MA structures, trend of O₂ binding energy does not tally with the trend of Pd→O₂ back-donation (Table 5.1). For all the MA adsorption complexes, we obtain more charge transfer from palladium to O₂ adsorbed in the bridge position than that in the a-top sites.

The lowest energy adsorption complexes of Pd₄O^{0,±} complexes are shown in Figure 5.4.

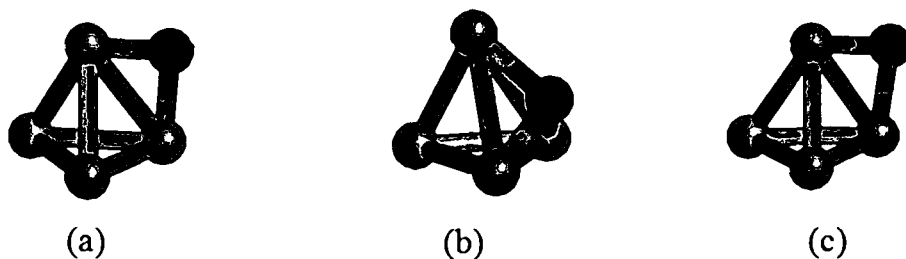


Figure 5.4: Lowest energy structures of: (a) neutral, (b) cationic and (c) anionic Pd₄O complexes.

Adsorption of atomic oxygen takes place in the bridge sites of neutral (singlet state) and anionic Pd₄ (doublet state) clusters, while hollow site adsorption is preferred by O in cationic Pd₄–O complex (doublet state). The adsorption site as well as the Pd–

O bond length (1.94 Å) of neutral Pd₄-O complex is in agreement with that of Rösch and co-workers [268]. Several other structural and spin isomers of Pd₄O^{0,±} complexes with their relative energies are shown in Table B10 of Appendix B. Binding energies of O with neutral, cationic and anionic Pd₄ clusters are found to be -0.66 eV, -0.67 eV and -1.19 eV, respectively (Table 5.1).

5.3.2 Adsorption of CO₂ on Pd₄ clusters

Figure 5.5 shows the lowest energy structures of Pd₄-CO₂^{0,±} complexes. It is seen from the figures that CO₂ molecule binds to neutral and anionic Pd₄ clusters through C atom, while CO₂ adsorption in the cationic Pd₄ cluster takes place through one of its O atoms. The geometry and energetics of these complexes are given in Table 5.2. Mulliken charge analysis shows that in neutral and anionic Pd₄-CO₂ complexes, C atom of CO₂ withdraws charge from the palladium atom to which it is connected. On the other hand, there occurs charge transfer from the O to the Pd atom of Pd₄⁺, which participates in Pd-O bonding. This charge transfer is accompanied by a flow of electron inside the CO₂ molecule in the direction of O→C→O→Pd.

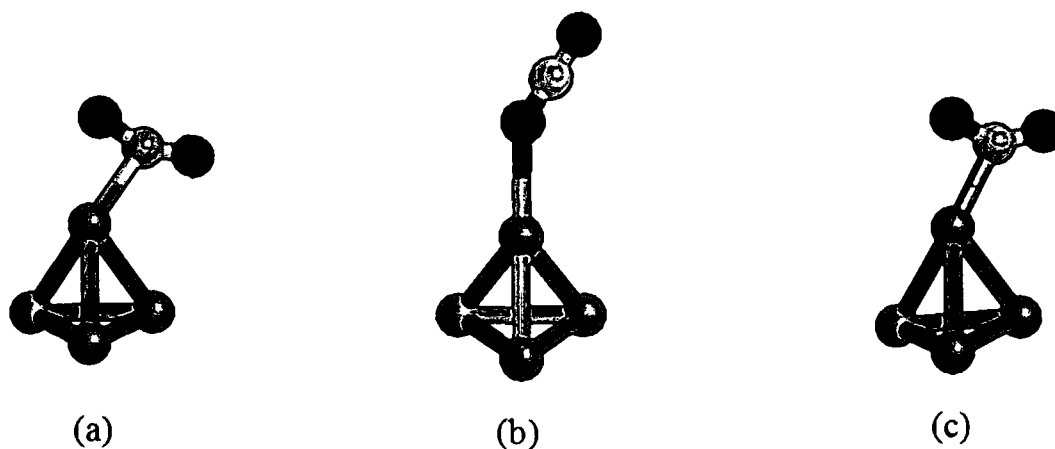


Figure 5.5: Lowest energy structures of: (a) neutral, (b) cationic and (c) anionic Pd₄CO₂ complexes.

BE of the adsorbates with neutral and anionic Pd₄ clusters follows the order: CO>O₂>O>CO₂. This observation agrees well with the previous experimental study [260] on reactivity order of palladium cluster, anions. Small negative value of BE for CO₂ with neutral Pd₄ cluster signifies repulsive nature of the adsorption process (Table 5.2). This is in agreement with the observation that surface reactions of

nickel group metals with CO₂ at room temperature result in no adsorption or dissociation of CO₂ [269-271].

5.3.3 Co-adsorption of O₂, 2O, O, CO and CO₂ on Pd₄ clusters

Adsorption of CO on neutral, cationic and anionic Pd₄ clusters has been studied in Chapter 4. The lowest energy structures of these complexes are shown in Figure 4.1. The corresponding structural characteristics and energetics are given in Tables 4.1–4.3. The important observations of this investigation are that CO binds to hollow adsorption sites in neutral and cationic Pd₄ clusters, whereas adsorption of CO takes place in a-top position of anionic Pd₄ cluster. Moreover, the trend of CO binding energy in these clusters is: Pd₄⁻ > Pd₄⁺ > Pd₄. We will make a comparison of these results with those of the co-adsorption complexes of CO with oxygen pre-adsorbed Pd₄^{0,±} clusters as discussed in the following sections.

Co-adsorption of O₂ and CO on Pd₄ clusters

The lowest energy structures of O₂ and CO co-adsorbed Pd₄^{0,±} complexes are shown in Figure 5.6. It is seen from the figure that the adsorption sites of CO on O₂ pre-adsorbed Pd₄⁺ changes to bridge position from the hollow position in gas phase Pd₄⁺ cluster. However, the adsorption sites of CO in neutral and anionic Pd₄O₂ complexes remain the same as those in Pd₄^{0,-} clusters (Figure 4.1). For neutral Pd₄ cluster, a-top and bridge adsorptions of CO lie 0.329 and 0.056 eV higher in energy, respectively, than the lowest energy structure. Two structural isomers with a-top adsorption of CO lie 0.306 and 0.336 eV higher in energy than the lowest energy structure of cationic Pd₄O₂CO complex. A number of structural isomers with adsorption of CO in various ways in neutral, cationic and anionic Pd₄O₂ complexes have been shown in Table B11 of Appendix B. CO binding energies for the O₂ pre-adsorbed Pd₄^{0,±} complexes follow the trend: Pd₄⁻ > Pd₄ > Pd₄⁺, which is similar to that of Pd→O₂ and Pd→CO back-donations. This means that pre-adsorption of O₂ changes the trend of CO binding energy from that in gas phase Pd₄ clusters. Moreover, comparison of Table 4.1 and 5.2 shows that binding of CO is strengthened in case of neutral Pd₄O₂ complex from that of gas phase Pd₄ cluster.

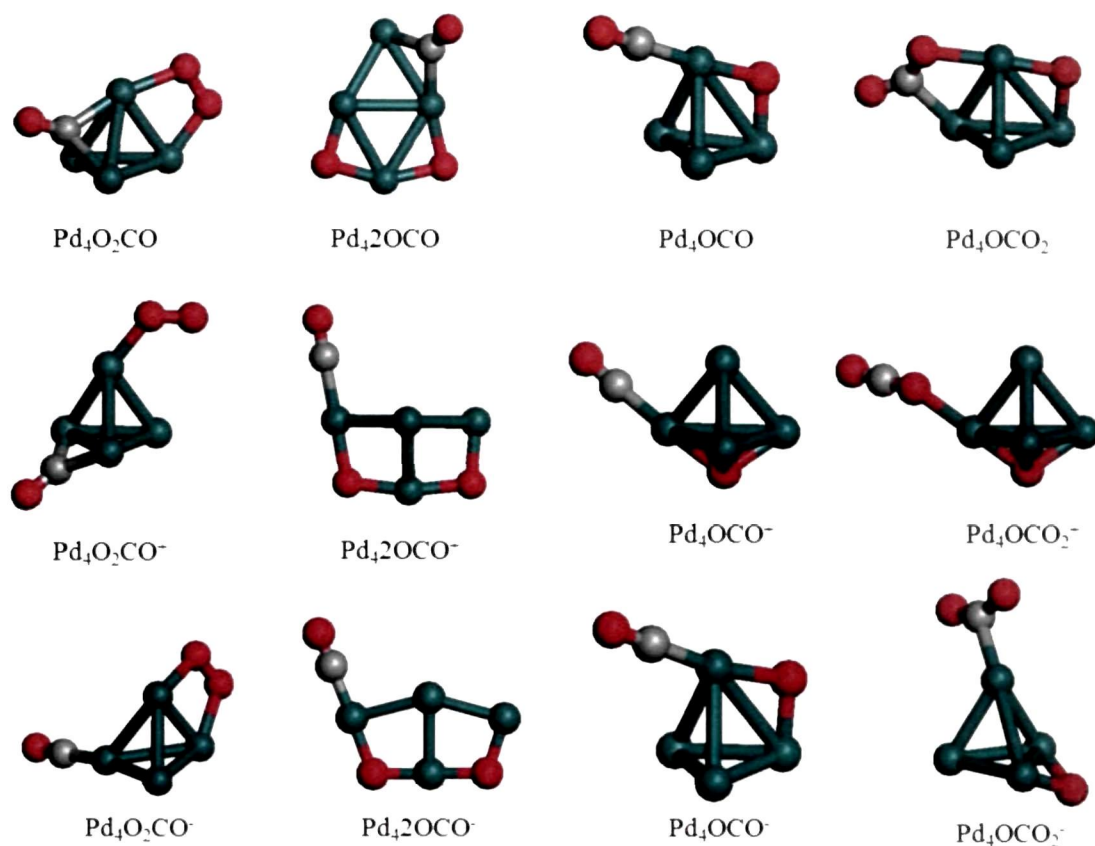


Figure 5.6: The lowest energy structures corresponding to the co-adsorption of O_2+CO , $2\text{O}+\text{CO}$, $\text{O}+\text{CO}$ and $\text{O}+\text{CO}_2$ on gas phase neutral (first row), cationic (second row) and anionic (third row) Pd_4 clusters.

Co-adsorption of 2O and CO on Pd₄ clusters

The optimized structures of two lowest energy adsorption complexes of CO on 2O pre-adsorbed palladium clusters are shown in Figure 5.6. It has been observed that three-fold adsorption site of CO in gas phase neutral and cationic Pd_42O clusters change to bridge and a-top position, respectively (Figure 4.1). However in anionic cluster, CO retains the same a-top adsorption site in oxide of palladium as that in bare cluster with a very small deviation in the orientation of the CO molecule ($\langle \text{Pd}-\text{C}-\text{O} = 179.8^\circ$). In case of neutral complexes, a structure with a-top adsorption of CO ($\langle \text{Pd}-\text{C}-\text{O} = 178.7^\circ$) on Pd_42O is only 0.018 eV higher in energy than the lowest energy structure. It means that these structures exist simultaneously within the accuracy limit of density functional theory. Experimental studies [146] have confirmed the change of CO adsorption sites from three-fold to top site in MgO supported bare and oxidized neutral Pd_4 cluster, respectively. In cationic complexes,

bridge site adsorption of CO lies 0.238 eV higher in energy than the corresponding most stable structure. Again, CO adsorption in a-top site of Pd₄2O⁻ with $\langle \text{Pd-C-O} \rangle = 169.8^\circ$ is found to be 0.397 eV higher in energy than the corresponding lowest energy structure. Several structural isomers with different adsorption modes of CO with their relative energies are summarized in Table B12 of Appendix B.

Table 5.2: Bond distances (Å), binding energies BE (eV), vibrational frequencies (cm⁻¹) and Mulliken charges (q) of the adsorbates for the co-adsorption complexes of Pd₄^q (q=0, 1, -1) clusters.

Complexes	O-O bond length (Å)	C-O bond length (Å)	BE of CO/CO ₂ (eV)	O-O freq (cm ⁻¹)	C-O freq (cm ⁻¹)	q _{O2} /q _O	q _{CO} /q _{CO2}
Pd ₄ O ₂ CO	1.38	1.20	1.46	913.4	1709.8	-0.49	-0.24
Pd ₄ 2OCO	3.76	1.18	1.65	576.9	1878.6	-1.22	-0.06
Pd ₄ OCO	–	1.16	1.58	–	1996.6	-0.64	0.02
Pd ₄ OCO ₂	–	1.24	0.04	–	–	-0.60	-0.27
Pd ₄ CO ₂	–	1.21	-0.08	–	–	–	-0.16
Pd ₄ O ₂ CO ⁺	1.27	1.18	1.34	1272.6	1860.1	-0.07	0.02
Pd ₄ 2OCO ⁺	3.78	1.14	1.48	562.1	2087.5	-1.10	0.18
Pd ₄ OCO ⁺	–	1.14	1.58	–	2080.0	-0.64	0.16
Pd ₄ OCO ₂ ⁺	–	1.18	0.46	–	–	-0.63	0.09
Pd ₄ CO ₂ ⁺	–	1.18	0.18	–	–	–	0.07
Pd ₄ O ₂ CO ⁻	1.38	1.18	1.83	887.3	1894.3	-0.56	-0.13
Pd ₄ 2OCO ⁻	3.89	1.17	2.14	520.5	1913.2	-1.40	-0.11
Pd ₄ OCO ⁻	–	1.18	1.94	–	1884.6	-0.70	-0.13
Pd ₄ OCO ₂ ⁻	–	1.24	0.73	–	–	-0.65	-0.46
Pd ₄ CO ₂ ⁻	–	1.24	0.99	–	–	–	-0.49

Table 5.2 shows the geometry, energetic and the electronic properties of the lowest energy co-adsorption complexes. In all the complexes, red-shift of CO frequency is reduced from that in $\text{Pd}_4\text{CO}^{0,\pm}$ complexes, irrespective of charge state of the complexes and co-ordination mode of adsorbed CO. This observation resembles the recent observation in Ni_4 clusters [272]. It is observed from Table 5.2 that binding energy of CO on palladium with co-adsorbed O_2 follows the trend: anionic > neutral > cationic. This trend is found to be similar to the $\text{Pd}\rightarrow\text{CO}$ and $\text{Pd}\rightarrow\text{O}_2$ back-donation as calculated from the Mulliken charge analysis in the complexes. Analysis of atomic charges also shows that charge transfer from palladium clusters to O_2 with CO co-adsorption is within the same quantity as that of without CO adsorption. However, charge transfer from palladium to CO decreases with pre-adsorbed oxygen than that in bare clusters. It is also observed from the comparison of Tables 4.1–4.3 with Table 5.2 that CO binding energy is enhanced in oxygen pre-adsorbed palladium clusters than that in gas phase palladium clusters irrespective of their charge.

Co-adsorption of O and CO on Pd_4 clusters

The lowest energy structures of the co-adsorption complexes of neutral, cationic and anionic Pd_4 clusters are shown in Figure 5.6. Several other structural isomers with different orientation of CO lying in different energies relative to the most stable isomers have been observed and they are shown in Table B13 of Appendix B. The maximum value of CO binding energy is found to be for anionic Pd_4O complex followed by neutral and cationic Pd_4O complexes (Table 5.2). $\text{Pd}\rightarrow\text{CO}$ back-donation follows the order: $\text{Pd}_4\text{O}^- > \text{Pd}_4\text{O} > \text{Pd}_4\text{O}^+$ which is reflected in the C–O bond lengths in the three complexes.

From the above discussion, it is seen that pre-adsorption of oxygen effects the adsorption configuration as well as the binding energy of co-adsorbed CO. This is due to the changes in the local electronic structure of palladium clusters induced by pre-adsorption of oxygen, thereby influencing the subsequent adsorption of CO. A change in electronic structure of anionic palladium clusters has been verified by Kim and his co-workers [68] using Time-of-Flight (ToF) mass spectrometry and Ultraviolet Photoelectron Spectroscopy (UPS). Figure 5.7 shows the frontier orbital pictures of $\text{Pd}_4^{0,\pm}$ and oxygen adsorbed $\text{Pd}_4^{0,\pm}$ complexes. A change in charge

localization is observed in all the clusters as a result of oxygen adsorption on palladium. This signifies the change in electronic structure of palladium clusters due to adsorption of oxygen.

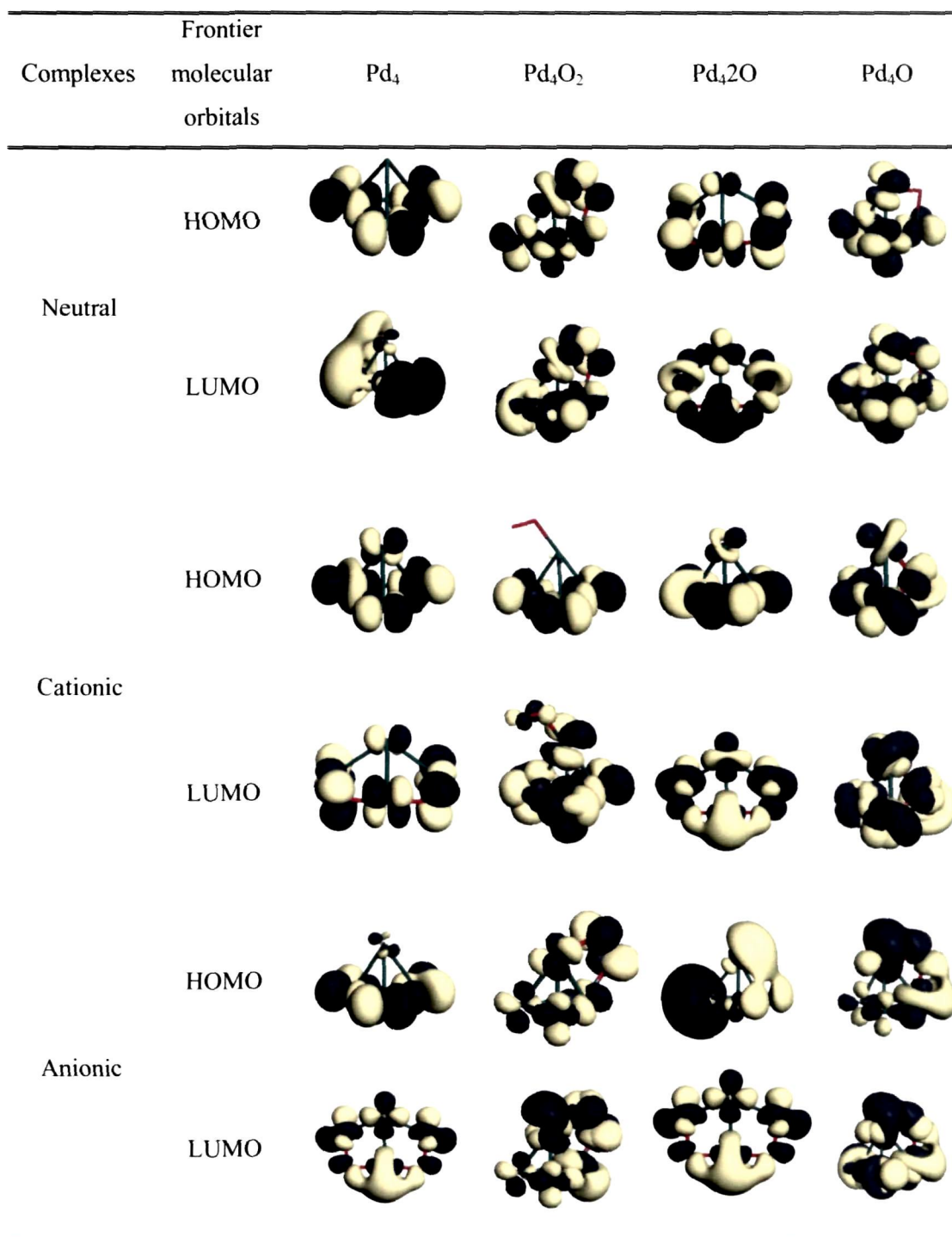


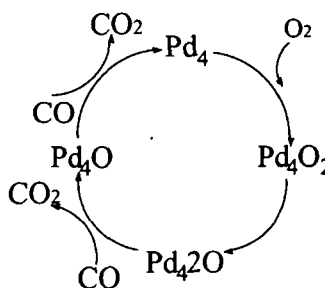
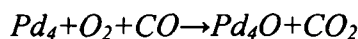
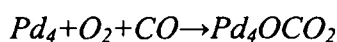
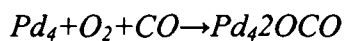
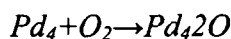
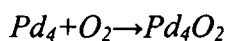
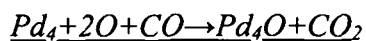
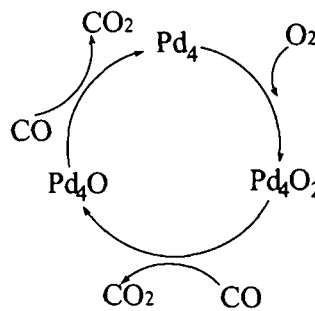
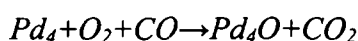
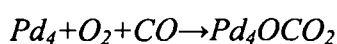
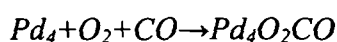
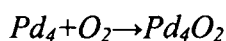
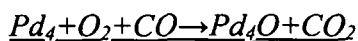
Figure 5.7: Frontier molecular orbitals of lowest energy gas phase and oxygen adsorbed Pd₄^{0±} clusters.

Co-adsorption of O and CO₂ on Pd₄ clusters

The lowest energy complexes of Pd₄^{0,±} corresponding to the co-adsorption of atomic oxygen and CO₂ are shown in Figure 5.6. It is observed that among the Pd₄-O-CO₂ co-adsorption complexes, CO₂ molecule binds through one of its O atoms and the C atom in cationic and anionic Pd₄O, respectively. The charge transfer processes in these two complexes are similar to those of Pd₄-CO₂[±] complexes. In case of neutral Pd₄-O-CO₂ complex, binding of CO₂ molecule with Pd₄O takes place through C and one O atom. In this complex, both the C and O atoms withdraw charge from the Pd atoms to which they are coordinated. Value of CO₂ binding energy is found to be maximum for anionic Pd₄O complex followed by the corresponding cationic and neutral complexes, which do not match the Pd→CO₂ back-donation trend.

5.3.4 CO oxidation reaction energy profiles

With the available data, we have constructed and compared three different reaction pathways, which combine CO with molecular, dissociated and atomic form of oxygen on neutral, cationic and anionic Pd₄ clusters to produce CO₂ in the following ways:



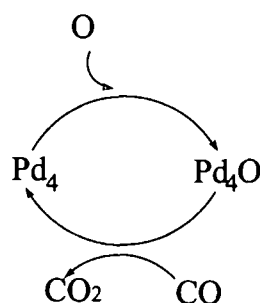
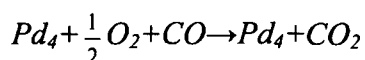
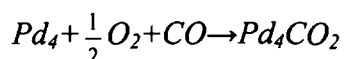
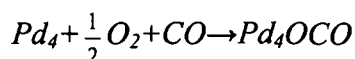
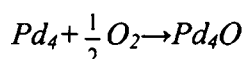
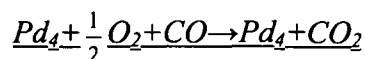


Figure 5.8 shows the calculated energy profiles of these reactions. It is seen from the figure that there is a deep energy sink on the potential energy surface of the CO oxidation process on anionic Pd₄ cluster due to its strong binding energies with CO and CO₂. This indicates worse reaction energetic for CO oxidation process by Pd₄⁻ cluster hindering the formation and desorption of CO₂ in comparison with those of neutral and cationic Pd₄ clusters. Further, among the three reaction channels (Figure 5.8 (a), (b) and (c)), reaction energy profile for dissociated oxygen is found to be more exothermic in nature and it exhibits shallower sink than those for molecular and atomic oxygens. Therefore, dissociated oxygen may be considered as a superior oxidant for CO oxidation on gas-phase tetra palladium clusters.

5.4 SALIENT OBSERVATIONS

Our results indicate that dissociative adsorption of oxygen is preferable on all the clusters. Pre-adsorption of O₂ is found to affect the adsorption geometry as well as the binding energy of CO in the co-adsorption complexes. CO adsorption sites change to bridge and a-top position in the co-adsorption complexes of neutral and cationic palladium clusters, respectively, from the three-fold position in the corresponding gas phase clusters. There is no change in the adsorption position of CO in case of anionic palladium cluster. Binding energy of CO with oxygen pre-adsorption on palladium clusters follows the trend: anionic > neutral > cationic. Based on these observations, oxygen adsorbed anionic palladium cluster is found to be more reactive towards CO followed by neutral and cationic clusters. On the basis of Mulliken charge analysis, it is found that metal→O₂ and metal→CO back-donation mechanism plays the key role in the co-adsorption process. Comparison of frontier orbitals of gas phase clusters with those of oxidized clusters shows a

significant change in the electronic structure of palladium clusters due to adsorption of oxygen. This change in electronic structure is responsible for the observed discrepancy in the structural as well as electronic properties of co-adsorption of CO on these clusters.

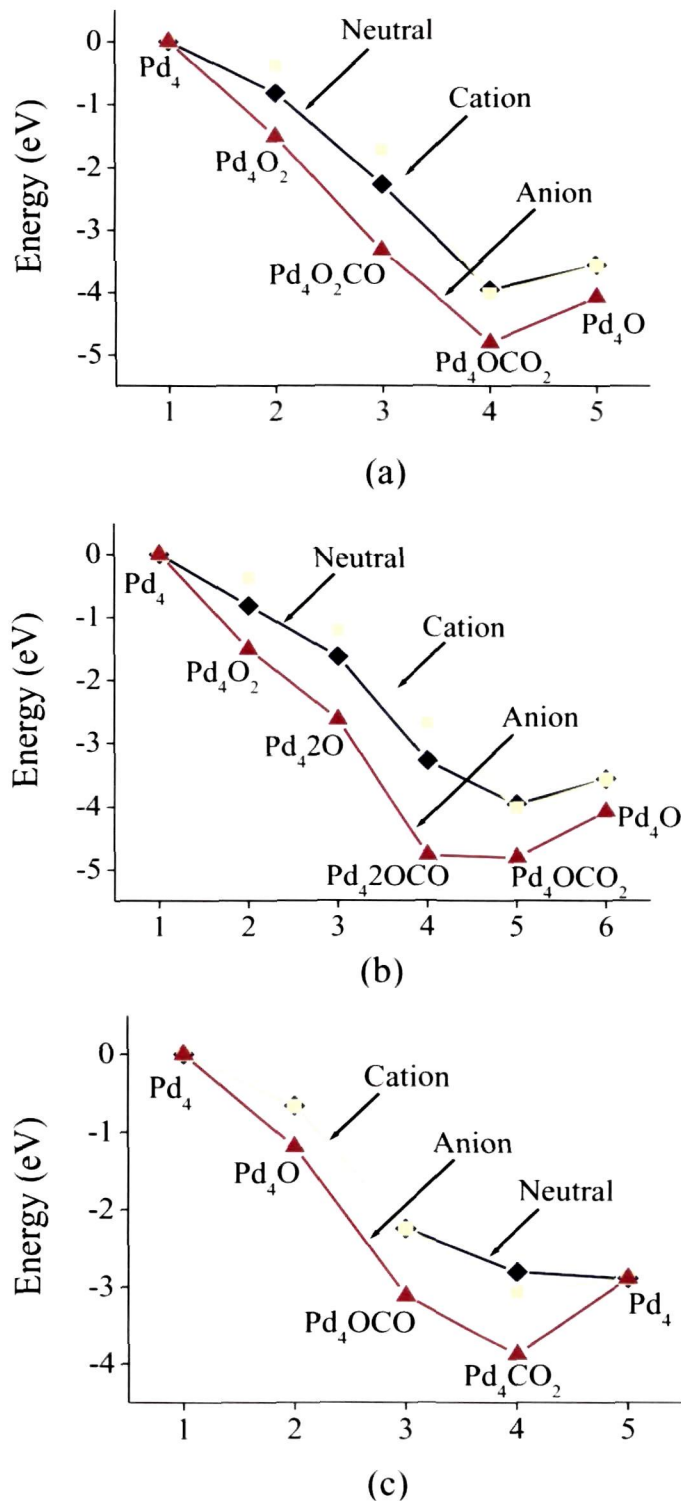


Figure 5.8: The energetic profiles of complete reaction cycles for CO oxidation on Pd₄^{0,±} clusters: (a) molecular O₂, (b) dissociated O₂ and (c) a single atomic O reacting with CO.

By investigating the possible reaction paths for CO oxidation over Pd₄ clusters, we have found that Pd₄⁰ and Pd₄⁺ clusters are more suitable catalysts compared to Pd₄⁻. In addition, dissociated form of oxygen molecule is found to be a better oxidant than its molecular and atomic forms. These arguments could be utilized in studying clusters with larger size, clusters of other metals as well as supported metal clusters. Experiments using neutral and cationic palladium clusters as catalysts for oxidation of CO would be instructive.

CHAPTER

6

SMALL PALLADIUM CLUSTERS ON ZEOLITE SUPPORT

In the present chapter, we have investigated the change in electronic structure of small palladium clusters in the presence of oxide support such as zeolites. The first part deals with the study of electronic structure of single palladium atom on H-ZSM-5 zeolite support via cluster model and embedded cluster models using CO and NO as probe molecules. It is found that the Pd atom interacts with a Brønsted proton as well as a nearby oxygen atom of the zeolite framework. Embedded cluster study has resulted in stronger interaction of Pd atom with H-ZSM-5 zeolite than that with the cluster model study. Adsorption energy values as well as thermodynamic analyses have shown preferable adsorption of CO over NO on Pd-H-ZSM-5. In the second part of the present work, we have intended to study the effect of zeolites on the electronic structure of Pd₄, which has been shown to be the most stable cluster form our previous gas phase studies in Chapters 3 and 4. To carry out this investigation, we have chosen faujasite (FAU) zeolite as the support due to its larger pore size to host Pd₄ cluster. This section summarizes the results of reverse hydrogen spillover from the hydroxyl groups of FAU zeolite onto the Pd₄ cluster by extended modelling of the support. This study shows that hydrogenated Pd₄/FAU complex with single proton transfer is the most stable form of faujasite supported tetrapalladium cluster [Kalita and Deka, *J. Phys. Chem. C* **113**, 16070 (2009)]. The calculations in this chapter have been performed using QM/MM approach implemented in the ONIOM scheme of Gaussian 03 program for the first time.

6.1 INTRODUCTION

Removal of carbon monoxide, nitrogen oxides and other green house gases is a major challenge in the field of catalysis as these are among the most harmful

chemicals produced in automobile exhausts, cigarette smoke and several industrial processes. Zeolite supported Pd catalysts, especially, Pd-ZSM-5 and Pd-H-ZSM-5 show excellent catalytic activity in NO reduction by CH₄ in presence of O₂ [161]. Similarly, small palladium clusters on faujasite zeolite (FAU) support have drawn a worldwide attention [172-184,188] due to their important catalytic activity. A fundamental study on the interaction between metal and support surface may serve to understand the effect of support on the oxidation state, structure and catalytic performance of the metal particle. In spite of the theoretical [154,165,187] and experimental studies [156,170,171], the interaction between Pd and H-ZSM-5 system and their interaction with CO and NO molecules have not been studied yet with proper modelling of the H-ZSM-5 zeolite support. In first part of the present study, we attempt to understand the structural and electronic properties of palladium particles on H-ZSM-5 support. Further, we have investigated the adsorption of highly favoured IR probe molecules, CO and NO to examine the nature of electronic state of the supported Pd. In the second part of our study, we have investigated the reverse spillover of hydrogen from the hydroxyl groups of faujasite zeolite support onto the Pd₄ cluster as no such study for tetrapalladium cluster has been explored till date either experimentally or theoretically to the best of our knowledge. In the present study, we apply QM/MM approach implemented in the ONIOM2 scheme of Gaussian 03 program for proper modelling of the supports.

6.2 COMPUTATIONAL DETAILS

In the first part of the present work, the T8 site among the 12 crystallographically distinct T-sites in the two different-sized cluster models (7T and 93T, where T is the tetrahedral sites) of MFI framework has been substituted by an aluminium atom. This site has been found to be one of the most probable acid sites in zeolite ZSM-5 by previous quantum chemical study [273]. The optimized structures of these clusters are shown in Figure 6.1. The net negative charge of the zeolite framework due to Al substitution is compensated by a proton to preserve neutrality. In the second part of our study, the zeolite support is represented by three 60T (T=tetrahedral atoms) model clusters Zeo1, Zeo2 and Zeo3 of faujasite structure (Figures 6.3 (b), (c); 6.4 (a), (b) and 6.5 (a), (b)), each including one super-cage, where the metal species and adsorbates can be trapped inside. One, two and three Si

atoms of the 6T ring of Zeo1, Zeo2 and Zeo3 are isomorphously substituted by one, two and three Al atoms, respectively. Substitutions of Si by Al in Zeo2(2H) and Zeo3(3H) are made in an alternating sequence according to the Löwenstein rule [274]. The extra negative charges generated due to Al substitution are balanced by adding one, two and three protons to corresponding number of oxygen atoms at O1 crystallographic positions of Zeo1, Zeo2 and Zeo3, respectively. There are six bridging oxygens in the six-ring of the zeolite clusters with alternating bending in and out positions and are denoted throughout as O2 and O1, respectively (Figure 6.3 (b), 6.4 (a) and 6.5 (a)). The atomic coordinates of Si and O atoms of the zeolites are taken from the MFI and FAU zeolite data stored in Accelrys MS Modeling 3.2 software package [275].

All calculations have been performed using the Gaussian 03 programs [276]. Full quantum mechanical calculations have been carried out for all the molecular structures associated with the 7T cluster (HZ7) of H-ZSM-5. It is computationally too expensive and even impractical to use pure DFT based QM calculations for the large 93T (HZ93) and 60T clusters of H-ZSM-5 and FAU zeolite, respectively. Therefore, we have used QM/MM modeling for these clusters by use of two-layer ONIOM scheme [212]. According to this method, the entire complex of Pd-H-ZSM-5 has been divided into two regions: (i) inner core region consists of 7T sites including the T8 site along with the adsorbed Pd atom and CO, NO molecules and (ii) outer region consists of 86T sites. Similarly, in Pd₄/FAU complex, the inner core region consists of a 6T ring facing the super-cage of FAU zeolite and the Pd₄ cluster, while the rest of the zeolite framework constitutes the outer region. A high level DFT based QM calculations has been used to treat the inner region of the complexes using the B3LYP [204,205,207] density functional with 6-31G(d,p) basis set on all electrons in H, O, Al, Si and relativistic LANL2DZ basis for Pd atom. The outer region has been modeled by molecular mechanics using the universal force field (UFF) [277]. From earlier studies on adsorption in MFI [278] and FAU [279] zeolites, it has been observed that the ONIOM2 (B3LYP/6-31G(d,p):UFF) method provides reasonable values corresponding to the experimental prediction. Following the justifications of Joshi *et al.* [280], we have fixed all the outer layer atoms to their respective crystallographic positions. Only the core region of the zeolite along with the adsorbates is allowed to relax during structure optimization. At the QM/MM boundary, link H atoms are placed along the Si–O covalent bonds and O atoms at the

boundary of the MM layer have been replaced by H atoms along the Si–O bonds and the Si–H bond distance is fixed to 1.47 Å.

In the results to follow, adsorption energies of Pd with HZN (N=7 and 93) zeolite clusters have been evaluated as

$$E_{ads} = E(\text{PdHZN}) - E(\text{HZN}) - E(\text{Pd}) \quad (6.1)$$

Similarly, adsorption energies of CO and NO molecules with PdHZN (N=7 and 93) zeolite clusters have been calculated using the following formula

$$E_{ads} = E(\text{PdHZN-CO/NO}) - E(\text{PdHZN}) - E(\text{CO/NO}) \quad (6.2)$$

To determine the reactivity of the metal clusters with OH group of the zeolite fragment, we have calculated the energy of reverse hydrogen spillover (E_{RS}) from the bridging OH groups of FAU zeolite to Pd₄ cluster using the following formula

$$E_{RS} = \{E[\text{Pd}_4\text{H}_n/\text{Zeo}((m-n)\text{H})] - E[\text{Pd}_4/\text{Zeo}(m\text{H})]\} / n, m, n = 1-3 \quad (6.3)$$

The individual energy (E_{trans}) in stepwise (n=1–3) spillover process of each hydrogen transfer is calculated as

$$E_{trans} = E[\text{Pd}_4\text{H}_n/\text{Zeo}((m-n)\text{H})] - E[\text{Pd}_4\text{H}_{n-1}/\text{Zeo}((m+1)-n)\text{H}] \quad (6.4)$$

In addition, adsorption energy (E_{ads}) of bare Pd₄ cluster on the neutral zeolite fragment has been evaluated as

$$E_{ads} = E[\text{Pd}_4/\text{Zeo}(m\text{H})] - E[\text{Zeo}(m\text{H})] - E[\text{Pd}_4] \quad (6.5)$$

6.3 RESULTS AND DISCUSSION

6.3.1 Pd atom supported on H-ZSM-5 zeolite

6.3.1.1 Structure and energetics

The optimized structures of 7T and 93T clusters in singlet states are shown in Figures 6.1(a) and (e). Figures 6.1(b) and (f) show the optimized structures of PdHZ7 and PdHZ93 complexes: Pd atom adsorbed in 7T and 93T clusters of HZSM-5, respectively. We have performed vibrational analysis for all the complexes and none of them is found to exhibit any imaginary frequency. Positive values of all the vibrational frequencies verify the presented structures to be the lowest energy states. It is seen from the figure that the Pd atom interacts with the acidic hydrogen atom and one of the zeolite framework oxygen atoms (O_N) bound to Al. This is in agreement with the study of van Santen *et al.* [187]. Recently, a similar structure in singlet state has also been reported to be more stable than the

corresponding triple and quintet states [165]. Selected parameters of the optimized clusters are shown in Table 6.1.

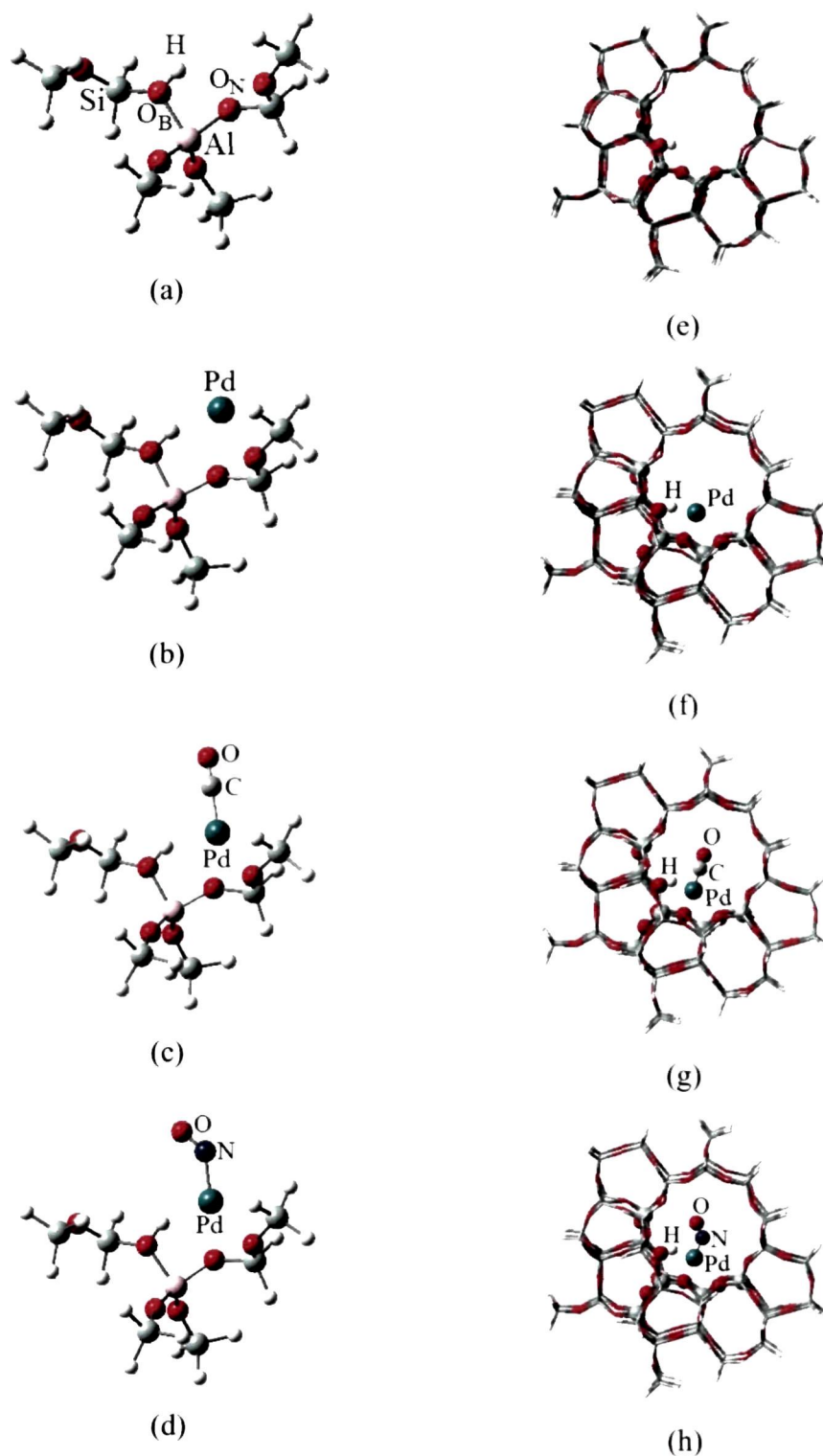


Figure 6.1: Optimized structures of H-ZSM-5; Pd on H-ZSM-5; CO and NO adsorption on Pd-H-ZSM-5: (a)-(d) 7T cluster model and (e)-(h) 93T embedded cluster model. The quantum and molecular mechanics regions have been designated by ball-stick and only stick representation, respectively.

The oxygen atom connected to the acidic proton is denoted as O_B . The elongation of the O_B-H bond length in Pd adsorbed HZSM-5 complexes from that in bare HZSM-5 framework confirm a bonding interaction between the Pd atom and the proton. The nature of the interaction of Pd atom with O_N is shown by the lengthening of the other two bonds of O_N with Si and Al atoms (Table 6.1). The calculated values of O_B-H , Pd-H and Pd- O_N bond distances in PdHZ7 (1.02 Å, 2.34 Å and 1.92 Å) and PdHZ93 (1.03 Å, 2.24 Å and 2.00 Å) complexes agree well with the available results [165] of 1.08 Å, 2.31 Å and 1.91 Å, respectively. The negligible changes in Al-O and Si-O bond distances surrounding the acid site indicate only local perturbation in the zeolite structure due to the adsorption of Pd atom.

The Pd atom interacts weakly with the HZ7 cluster with E_{ads} value of -1.83 kcal/mol. The value becomes positive (2.40 kcal/mol) due to the inclusion of BSSE correction. The increased size of the zeolite model (from 7T to 93T) can stabilize the adsorption of Pd more (E_{ads} is -5.18 kcal/mol) although it has little effect on the geometry (Table 6.1). It emphasizes the need of a realistic model to represent the zeolite support [281]. However, E_{ads} for 93T clusters optimized at ONIOM2 level do not include BSSE as the facility of performing counterpoise corrections in ONIOM calculations is not available in Gaussian 03 at this point. The difference in the E_{ads} values is due to the more realistic environment in HZ93 clusters than that in HZ7 cluster of the HZSM-5 framework.

6.3.1.2 Interaction of CO and NO with Pd-H-ZSM-5

The optimized structures of the adsorption complexes of CO and NO on PdHZ7 and PdHZ93 clusters are shown in Figures 6.1 (c), (d) and 6.1 (g), (h), respectively. Important geometrical parameters of these structures are reported in Table 6.1. The CO molecule gets adsorbed on the Pd atom in HZSM-5 framework in a linear configuration with Pd-C-O angles of 179.2° and 178.3°, respectively, in PdHZ7 and PdHZ93 clusters. The geometries of these structures are similar to those of CO adsorbed Au-ZSM-5 complexes [167] and Pt-H-Mordenite complexes [168]. Values of Pd-C bond lengths in the two clusters are found to be 1.85 Å and 1.86 Å, respectively. C-O bond distance in both the clusters are increased to 1.15 Å from the experimental value of free C-O bond distance of 1.13 Å [66].

TABLE 6.1: Important geometrical parameters: bond distances R (Å), bond angles <Pd-C/N-O (deg) and calculated adsorption energies E_{ads} (kcal/mol) of the optimized Pd-HZSM-5 complexes^a.

Geometrical parameters and E_{ads} (kcal/mol)	HZ7	PdHZ7	PdHZ7-CO	PdHZ7-NO	HZ93	PdHZ93	PdHZ93-CO	PdHZ93-NO
E_{ads}^b	–	-1.83 (2.40) ^c	-46.76 ^d (-44.73) ^c	-31.77 ^c (-30.02) ^c	–	-5.18	-46.93 ^d	-32.29 ^c
R(Al-O _B)	1.91	1.88	1.89	1.89	1.91	1.88	1.89	1.89
R(Al-O _N)	1.72	1.76	1.77	1.78	1.71	1.74	1.76	1.76
R(Si-O _B)	1.71	1.69	1.71	1.70	1.70	1.69	1.70	1.69
R(Si-O _N)	1.62	1.63	1.65	1.65	1.61	1.62	1.64	1.64
R(O _B -H)	0.97	1.02	1.00	1.01	0.97	1.03	1.01	1.02
R(Pd···H)	–	1.92	2.04	2.07	1.90	1.90	2.00	1.99
R(Pd···O _N)	–	2.34	2.25	2.26	2.33	2.24	2.25	2.25
R(Pd···C/N)	–	–	1.85	1.91	–	–	1.86	1.91
<Pd-C/N-O	–	–	179.2	136.5	–	–	178.3	136.6
R(C/N-O)	–	–	1.15	1.18	–	–	1.15	1.17

^a HZ7 denotes the fully optimized 7T cluster of H-ZSM-5 and HZ93 denotes the ONIOM optimized 93T cluster of H-ZSM-5. ^b Zero point correction included. ^c Values in parentheses have been BSSE corrected. ^d Calculated BE of CO with Pd-H-ZSM-5. ^e Calculated E_{ads} of NO with Pd-H-ZSM-5.

An NO molecule adsorbs on a Pd atom in HZSM-5 support in a bent configuration. The bent adsorption geometry is a characteristic of the nitrosyls of Ni group metals [282] and noble metals [283]. The values of Pd–N–O angles in PdHZ7 and PdHZ93 clusters are found to be 136.5° and 136.6° , respectively. This result agrees well with the recent observation by Hafner *et al.* [169]. The Pd–N bond length in the two complexes (1.91 Å) are comparable to the reported value (1.89 Å) [169]. There is an increment in the N–O bond distances in the Pd-HZSM-5 complexes (1.18 Å and 1.17 Å) from the experimental free N–O bond distance (1.15 Å) [284]. Lengthening of Pd–H (~0.1–0.2 Å) in Pd-HZSM-5-CO and Pd-HZSM-5-NO complexes clearly shows significant weakening of the interaction between Pd atom and the acid site of HZSM-5 upon adsorption of CO and NO (Table 6.1). However, very little changes in the Pd–O_N distances are observed in the respective complexes (only in the PdHZ93 clusters).

Adsorption energies of CO on PdHZ7 and PdHZ93 clusters are found to be -44.73 kcal/mol and -46.93 kcal/mol, respectively. E_{ads} value for PdHZ93-CO complex agrees very well with the earlier result [187]. NO adsorption energies in Pd adsorbed HZ7 and HZ93 complexes are -30.02 kcal/mol and -32.29 kcal/mol, respectively. These values are in agreement with the reported values [169]. Comparison between the E_{ads} values for CO and NO adsorption indicates stronger interaction of CO than NO with Pd-HZSM-5. Moreover, binding of CO and NO with Pd-HZSM-5 are much larger than the binding of PdCO and PdNO adducts with HZSM-5 (E_{ads} values for PdCO-HZSM-5 are 6.52 kcal/mol in HZ7 and 10.04 kcal/mol in HZ93; E_{ads} values for PdNO-HZSM-5 are 4.46 kcal/mol in HZ7 and 8.33 kcal/mol in HZ93). The strong Pd–CO and Pd–NO interactions probably result in carbonyl and nitrosyl complexes of Pd, which is also suggested by IR and FTIR studies [155,156].

6.3.1.3 Charge analysis

Partial charges of CO and NO adsorbed Pd-HZSM-5 complexes have been examined by using Natural Population (NPA) scheme of the Natural Bond Orbital (NBO) methods [285]. However, NBO analysis in ONIOM is not available in Gaussian 03 at this point. Therefore, the NAO partial charges and the electronic configurations of only PdHZ7 complexes calculated by NBO analysis are presented in Table 6.2.

Our results indicate that electron transfer takes place among the Pd atom, the Brønsted acid site (H) and the framework oxygen atom (O_N) through bonding. There is an increase of electron density in s- and p- orbitals of Pd atom due to interaction with O_N , which destabilizes the Pd atom. On the other hand, interaction with the Brønsted proton stabilizes the Pd atom by withdrawing excess electron density (Table 6.2) leading to the decrease of electron density from the d- orbitals of the Pd atom. Electron transfer from the Pd atom to the Brønsted proton is a straightforward explanation for the electron-deficient states of Pd, which is supported by earlier investigations [156].

In PdHZ7-CO complex, the bonding orbitals are formed via electron transfer from the occupied 5σ molecular orbital (HOMO) of CO to the unoccupied spd-hybrid orbitals (LUMO) of PdHZ7 complex, which is mainly concentrated on Pd- O_N (Figure 6.2). The σ donation is accompanied by π back-donation from occupied d-orbitals of Pd metal atom to the unoccupied $2\pi^*$ orbital of CO. Table 6.2 shows the increment and decrement of electronic charge in 5s and 4d orbitals of Pd due to the donation and back-donation process. Increment of electron density in π^* orbitals of CO can be seen from the lengthening of C-O bond. Wiberg bond index value of Pd-C bond (0.98) based on NBO analysis indicates it as a strong bond. On the other hand, bonding mechanism in bent PdHZ7-NO complex is different from linear PdHZ7-CO complex (Figure 6.1). The bonding of NO molecule in the complex can be explained similar to a bent bare transition metal nitrosyl (TM-NO) complex, in which, NO $2\pi^*$ electron (SOMO) is spin paired with a metal d_σ electron to form an M-N covalent σ bond but there is little or no NO 5σ donation occurs to the metal empty d orbitals (Figure 6.2). Occupancy of 5σ orbital of N (0.92~1) from NBO analysis confirms the absence of σ -donation from NO adsorbate to Pd atom on HZSM-5 support. Moreover, low Wiberg index value of 0.19 signifies weaker Pd-N bond in PdHZ7-NO complex compared to the Pd-C bond in PdHZ7-CO complex. However, NBO analysis characterizes electron deficient states of Pd in both of the CO and NO adsorbed Pd-HZSM-5 complexes.

TABLE 6.2: Partial charges (au) and the electronic configurations based on NPA from NBO analysis of the optimized Pd-HZSM-5 complexes.

Complexes	Partial charge					Electronic configuration	
	O _B	O _N	H	Pd	CO/NO	O _N	Pd
HZ7	-1.139	-1.322	0.570	-	-	2s(1.77)2p(5.54)3d(0.01)	-
PdHZ7	-1.166	-1.301	0.466	0.115	-	2s(1.77)2p(5.52)	5s(0.12)4d(9.76)5p(0.01)6p(0.01)
PdHZ7-CO	-1.159	-1.301	0.509	0.003	0.010	2s(1.77)2p(5.52)3p(0.01)	5s(0.60)4d(9.39)6p(0.01)
PdHZ7-NO	-1.160	-1.299	0.487	0.160	-0.118	2s(1.77)2p(5.52)3p(0.01)	5s(0.50)4d(9.33)5p(0.02)

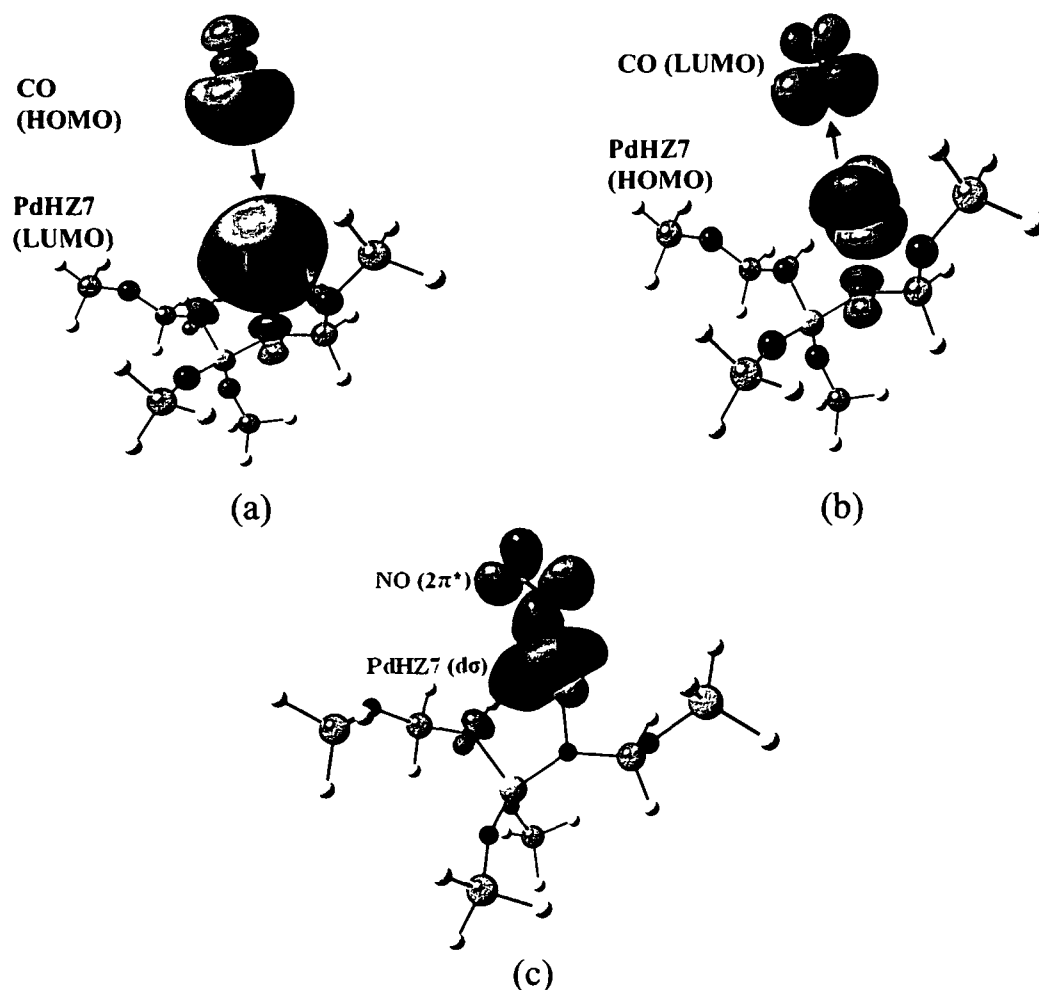


Figure 6.2: The interaction of Pd-HZSM-5 with: a CO molecule through (a) σ donation and (b) π back-donation (the arrows show the directions of electron transfer); a NO molecule through (c) forming a covalent σ bond via sharing NO $2\pi^*$ and Pd d_σ electrons.

6.3.1.4 Vibrational and thermodynamic analysis

Table 6.3 presents the calculated vibrational frequencies for carbonyl and nitrosyl adsorbed on Pd supported on HZSM-5. The results show that both CO and NO vibrational frequencies in smaller (PdHZ7-CO and PdHZ7-NO) as well as in larger (PdHZ93-CO and PdHZ93-NO) sized model clusters are nearly same. This means that frequency of adsorbed CO and NO is almost independent of the size of the zeolite model cluster. These results confirm that small 7T cluster model would provide cost-effective model for studying adsorption and reaction on Pd-HZSM-5

system. The similar conclusion has been drawn from earlier studies of CO adsorption on Cu-ZSM-5 [286] and Pt-ZSM-5 [168].

TABLE 6.3: Vibrational and thermodynamic property analysis of CO and NO adsorbed Pd-HZSM-5 complexes at 298.15 K.

Complexes	CO and NO vibrational frequencies $\nu(\text{cm}^{-1})$	Reaction	ΔH kcal/mol	ΔG kcal/mol
PdHZ7-CO	2131.0	$\text{PdHZ7} + \text{CO} \rightarrow \text{PdHZ7-CO}$	-47.28	-37.67
PdHZ7-NO	1830.2	$\text{PdHZ7} + \text{NO} \rightarrow \text{PdHZ7-NO}$	-32.49	-20.97
PdHZ93-CO	2138.3	$\text{PdHZ93} + \text{CO} \rightarrow \text{PdHZ93-CO}$	-50.05	-39.65
PdHZ93-NO	1835.5	$\text{PdHZ93} + \text{NO} \rightarrow \text{PdHZ93-NO}$	-34.22	-24.62

Vibrational frequency of adsorbed CO in PdHZ7-CO (2131.0 cm^{-1}) and PdHZ93-CO (2138.3 cm^{-1}) complexes undergo small red shift from that of free CO molecule (2143 cm^{-1}). Our calculated values of CO vibrational frequencies are close to the experimental value [157] of $\text{Pd}^+ \text{-CO}$ (2126 cm^{-1}) species. NO vibrational frequency in PdHZ7-NO and PdHZ93-NO complexes are found to be 1830.2 cm^{-1} and 1835.5 cm^{-1} , respectively. These values agree well with the experimentally determined [155] NO frequency (1881 cm^{-1}) of $\text{Pd}^+ \text{-NO}$ species. Our computed values are also close to the NO stretching frequency (1840 cm^{-1}) in Pd-Mordenite [166]. Moreover, there is a red shift in frequency of adsorbed NO in Pd-HZSM-5 complexes compared to that in free NO molecule (1876 cm^{-1}) [284]. Comparison of our calculated frequencies of adsorbed CO and NO molecules with the available IR data have identified the formation of cationic Pd(I) carbonyl and nitrosyl complexes on H-ZSM-5 support.

Table 6.3 shows the thermodynamic properties at standard conditions (298.15 K and 1 atm), i.e., the heat of adsorption (ΔH) and the Gibbs free energy of adsorption (ΔG). It is important to account for the entropic effects, which are included in the ΔG values. Negative values of ΔG indicate favorable adsorption processes. Our calculated values of ΔH and ΔG in PdHZ7-CO complex are close to those for CO adsorption on Au (T8)/ZSM-5 [167]. The adsorption processes of CO and NO on Pd-HZSM-5 are found to be more favorable in PdHZ93 complexes than in PdHZ7 complexes. Moreover, magnitude of ΔH and ΔG for CO adsorption are greater than the values for NO adsorption. It evidences the thermodynamically more favorable interaction of Pd-HZSM-5 with CO than with NO. The same conclusion has been drawn on the basis of adsorption energy values of CO and NO on Pd-HZSM-5. Therefore, NO can be displaced by CO from the adsorption site in Pd-HZSM-5. This observation is similar to that in Au-ZSM-5 complexes [167].

6.3.2 Pd₄ clusters supported on faujasite zeolite

6.3.2.1 Structure and energetics of zeolite supported bare Pd₄ clusters

In the present investigation, we have first optimized the structure of a gas phase Pd₄ cluster. A symmetry unrestricted full geometry optimization led bare Pd₄ to a distorted tetrahedron (C₁ symmetry) with triplet state as the lowest energy structure (Figure 6.3 (a)). Our previous DMol³ calculations have also established the ground electronic state of isolated Pd₄ to be as triplet in a slightly distorted tetrahedral shape (Chapter 3). We have computed the Pd–Pd bond distance of 2.61–2.72 Å in gas phase Pd₄ cluster. This value is in agreement with earlier studies [287,288]. From our calculations, it is found that the difference in energy between singlet (S) and triplet (T) states (C₁ symmetry) of Pd₄ is 68.99 kJ/mol and the singlet state has Pd–Pd distances of 2.58–2.82 Å. These values are close to the S–T difference of 70.29 kJ/mol and Pd–Pd distances of 2.58–2.84 Å in the singlet state of Pd₄, as observed by Moc *et al.* [287].

The ONIOM2 level optimized structures of faujasite zeolites (Zeo1, Zeo2 and Zeo3) are shown in Figures 6.3 (b), (c); 6.4 (a), (b) and 6.5 (a), (b); respectively. Important structural parameters of the QM regions are summarized in Tables 6.4–6.6.

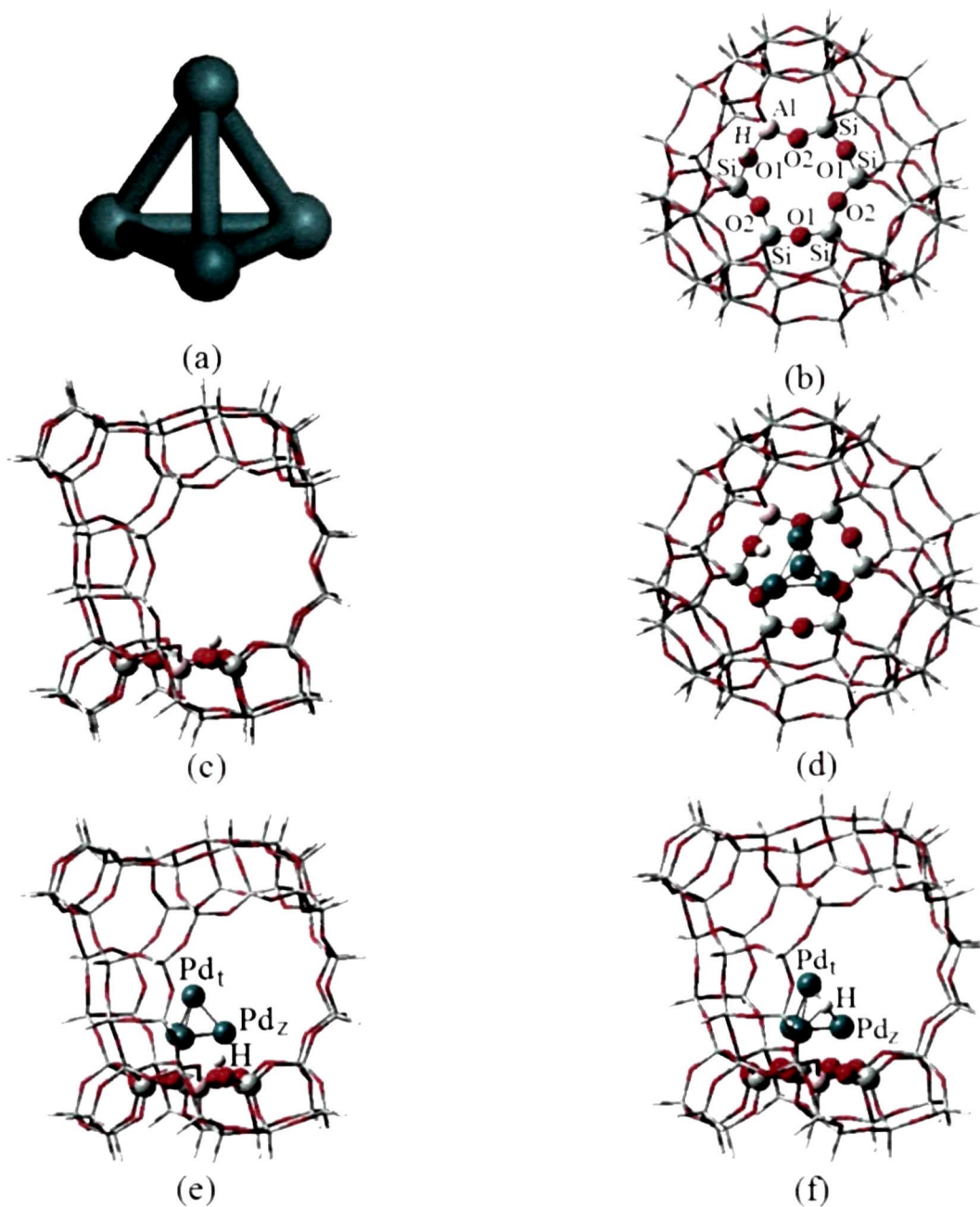


Figure 6.3: Lowest energy structures of (a) gas phase Pd₄ cluster; ONIOM2 model clusters of: (b) top and (c) side view of Zeol(1H); (d) top and (e) side view of Pd₄/Zeol(1H); (f) Pd₄H/Zeo1. The quantum and the molecular mechanics regions have been designated by ball-stick and only stick representations, respectively.

Table 6.4: Important structural parameters, Mulliken charges and energetics of gas phase Pd₄, Zeol and Pd₄/Zeol complexes.

Calculated parameters	Complexes			
	Pd ₄	Zeol(H)	Pd ₄ /Zeol(H)	Pd ₄ H/Zeol
Pd _z -Pd _z	-	-	2.72	2.72
Pd _z -Pd _t	-	-	2.61	2.73
<Pd-Pd>	2.66	-	2.66	2.73
Al-Si _{max}	-	6.38	6.42	6.41
Al(O1)-Si	-	3.44	3.43	3.27
Al(O2)-Si	-	3.09	3.16	3.22
Al-O1	-	1.89	1.86	1.75
Al-O2	-	1.73	1.77	1.82
Average Distances (Å)				
Si-O1	-	1.65	1.64	1.64
Si-O2	-	1.64	1.65	1.67
O2-O2	-	4.06	4.13	4.06
O1-H	-	0.97	1.04	-
Pd _z -O1	-	-	3.45	3.40
Pd _z -O2	-	-	2.48	2.30
Pd _z -Si	-	-	3.38	3.24
Pd _z -Al	-	-	3.20	3.08
Pd _z -H/Pd _t -H	-	-	-	1.87/1.69
Charges				
<Pd _z >	-	-	-0.19	-0.04
Pd _t	-	-	-0.05	0.02
Pd ₄	-	-	-0.62	-0.10
H ₁ /H ₂ /H ₃	-	0.39	0.39	0.05
Pd ₄ H _n	-	-	-0.23	-0.06
Energies (kJ/mol)				
E _{ads}	-	-	-48.75 (-8.75)	-
E _{RS}	-	-	-	-61.35
E _{trans}	-	-	-	-61.35

Our calculations reveal that Al–O1 distances (1.89 Å in Zeo1, 1.87 Å in Zeo2 and 1.85 Å in Zeo3) are higher than Al–O2 distances (1.73 Å in Zeo1, 1.74 Å in Zeo2 and 1.75 Å in Zeo3), which agrees with the earlier theoretical and experimental observations [289,290] that the Al–O distance associated with the acidic proton is significantly longer than the other Al–O distances, by up to 0.2 Å. The values of the Al–O1 distances are found to be close to that calculated from EXAFS multiple scattering studies of H-FAU [291]. Al(O1)–Si, Al(O2)–Si, O2–O2 and O1–H distances in Zeo1, Zeo2 and Zeo3 are in agreement with the observation of Rösch and co-workers [193]. Our calculated values of O1–H distances (0.97 Å) agrees well with ONIOM2 (B3LYP/6-31G(d,p):UFF) result of Kasuriya *et al.* [279].

The resulting structures of embedded-cluster models of 60T zeolites have been chosen to study the adsorption complexes of zeolite-supported palladium clusters. The lowest energy Pd₄ cluster is placed orienting its base towards the 6T ring of the optimized zeolite supercages. Orientation of Pd₄ cluster is so chosen that the Pd_z atoms are coordinated to the oxygen atoms at O2 positions, which do not participate in the bridging OH groups. Labeling of Pd_z and Pd_t atoms are shown in the lowest energy structures of zeolite-supported bare Pd₄ cluster, Pd₄/Zeo1(1H), Pd₄/Zeo2(2H) and Pd₄/Zeo3(3H), calculated at ONIOM2 (B3LYP/6-31G(d,p), LANL2DZ:UFF) level (Figures 6.3 (e), (f); 6.4 (c), (d), (e) and 6.5 (c), (d), (e), (f)). To test the spin multiplicity of Pd₄ cluster on zeolite-support, we have performed calculations for Pd₄/Zeo3(3H) system in singlet and triplet states. It has been observed that like isolated Pd₄, zeolite-supported Pd₄ cluster has a triplet ground state. The singlet state of Pd₄/Zeo3(3H) complex lies 79.07 kJ/mol higher in energy than the triplet state. Recent observation has also confirmed triplet ground state of Pd₄ on zeolite-support [188]. Therefore, we have carried out the calculations for Pd₄/Zeo1(1H) and Pd₄/Zeo2(2H) complexes in triplet states only. Our computed structural characteristics of the lowest energy Pd₄/Zeo1, Pd₄/Zeo2 and Pd₄/Zeo3 complexes are given in Tables 6.4, 6.5 and 6.6, respectively.

It is found that each of Pd₄/Zeo1(H), Pd₄/Zeo2(2H) and Pd₄/Zeo3(3H) complexes exhibits three shorter Pd–O2 bond distances of 2.31–2.59 Å, 2.32–2.58 Å and 2.36–2.37 Å (with longer Pd–O1 bond distances of 3.23–3.64 Å, 3.21–3.65 Å and 3.25–3.27 Å), respectively. These values are shorter in comparison with the study of Morokuma and co-workers [188].

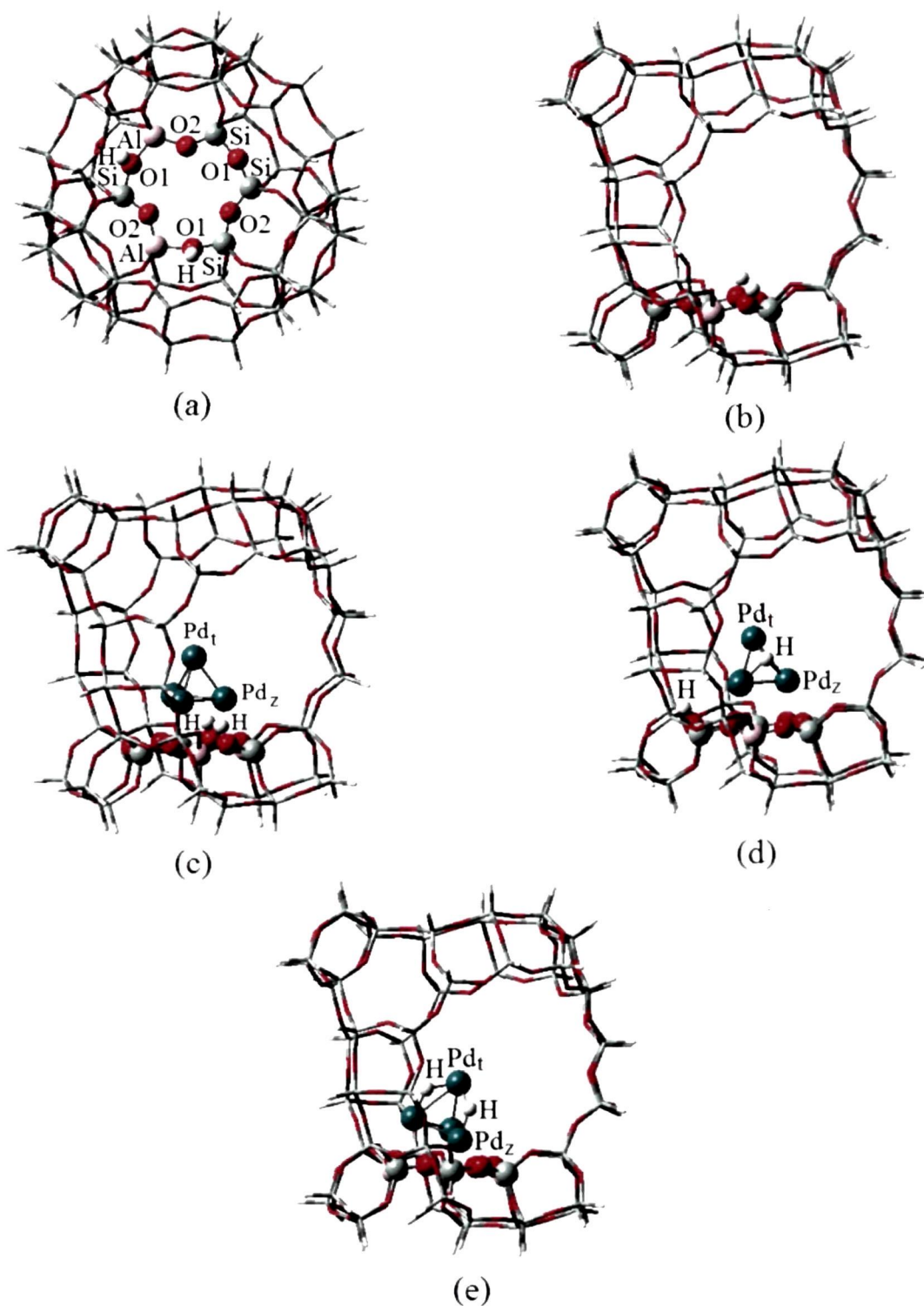


Figure 6.4: ONIOM2 optimized lowest energy structures of: (a) top and (b) side view Zeo2(2H); (c) Pd₄/Zeo2(2H); (d) Pd₄H/Zeo2(1H); (e) Pd₄H₂/Zeo2. The quantum and the molecular mechanics regions have been designated by ball-stick and only stick representations, respectively.

Table 6.5: Important structural parameters, Mulliken charges and energetics of Zeo2 and Pd₄/Zeo2 complexes.

Calculated parameters	Complexes			
	Zeo2(2H)	Pd ₄ / Zeo2(2H)	Pd ₄ H/ Zeo2(H)	Pd ₄ H ₂ / Zeo2
Pd _z -Pd _z	–	2.72	2.71	2.66
Pd _z -Pd _t	–	2.61	2.73	2.92
<Pd-Pd>	–	2.67	2.72	2.79
Al-Si _{max}	6.41	6.48	6.44	6.45
Al(O1)-Si	3.41	3.42	3.33	3.29
Al(O2)-Si	3.08	3.15	3.17	3.24
Al-O1	1.87	1.85	1.80	1.78
Al-O2	1.74	1.76	1.81	1.83
Average Distances (Å)				
Si-O1	1.67	1.66	1.67	1.64
Si-O2	1.62	1.64	1.66	1.66
O2-O2	3.99	4.14	4.01	4.08
O1-H	0.97	1.02	0.97	–
Pd _z -O1	–	3.35	3.41	3.28
Pd _z -O2	–	2.41	2.26	2.57
Pd _z -Si	–	3.34	3.22	3.00
Pd _z -Al	–	3.28	3.19	3.49
Pd _z -H/Pd _t -H	–	–	1.86/1.68	1.62/1.72, 1.66/1.66
Charges				
<Pd _z >	–	-0.21	-0.07	0.02
Pd _t	–	-0.04	0.03	0.07
Pd ₄	–	-0.68	-0.19	0.11
H ₁ /H ₂ /H ₃	0.39	0.39/0.39	0.05/0.38	0.02/0.07
Pd ₄ H _n	–	0.11	0.24	0.21
Energies (kJ/mol)				
E _{ads}	–	-74.09 (-11.30)	–	–
E _{RS}	–	–	-65.16	-10.16
E _{trans}	–	–	-65.16	44.84

Our calculated Pd–O distances are $\sim 0.15\text{--}0.40$ Å shorter than the values of $2.74\text{--}2.76$ Å derived from EXAFS measurements of NaX FAU zeolite-supported Pd_n (n=2–4) clusters [172]. However, this experiment gives 1.5 Pd and 2.1 O neighbors for each Pd atom, which is different from the present study. In spite of this, Pd₄/NaX FAU zeolite data are presented here for comparison because of the unavailability of EXAFS structural data for Pd₄/H-FAU zeolite system. The Pd–O₂ bond distances in Pd₄/Zeo(3H) complex are close to those reported by Vayssilov and Rösch [190] for Pd₆/Zeo(3H) complex (2.28 Å) and are essentially close to the corresponding distances of Pd₃ clusters supported on $\alpha\text{-Al}_2\text{O}_3$ (0001) surface, optimized without any symmetry constraints [292]. It is observed that Si–O₁, Al–O₁ bond lengths decrease and Si–O₂, Al–O₂ bond lengths increase in faujasite zeolite support due to the adsorption of Pd₄. As seen in Tables 6.4–6.6, Pd–Pd bond lengths of zeolite-supported Pd₄ clusters are $2.59\text{--}2.76$ Å, which are slightly deviated from those in the gas phase Pd₄ cluster. This finding is similar to the observation of Bussai *et al.* [293] that adsorption of a metal cluster in a zeolite cage does not change the structure of the cluster in a significant way compared with a tetrahedral structure in the gas phase. A similar observation has also been reported in case of purely siliceous FAU zeolite-supported palladium tetramer [188] as well as in Pd₆ cluster on a constrained six-ring model FAU zeolite cluster [190]. Almost unchanged structural parameters along with the preserved tetrahedral-shape of gas phase Pd₄ cluster on zeolite-support indicate a weak interaction between palladium cluster and the support.

6.3.2.2 Hydrogenated Pd₄ clusters on zeolite

Figures 6.3 (f); 6.4 (d), (e) and 6.5 (d), (e), (f) show the ONIOM2 model optimized adsorption complexes of Pd₄H/Zeo1; Pd₄H/Zeo2(1H), Pd₄H₂/Zeo2 and Pd₄H/Zeo3(2H), Pd₄H₂/Zeo3(1H), Pd₄H₃/Zeo3, respectively, corresponding to one, two and three proton transfer processes in Zeo1, Zeo2 and Zeo3. It is found that in the hydrogenated Pd₄ adsorbed zeolite complexes, the transfer of one and two hydrogen atoms get adsorbed in two-fold coordination between Pd_z and Pd_t atoms. However, the third hydrogen in Pd₄H₃/Zeo3 complex is coordinated with only Pd_z atom. Characteristic features of these complexes are given in Tables 6.4–6.6.

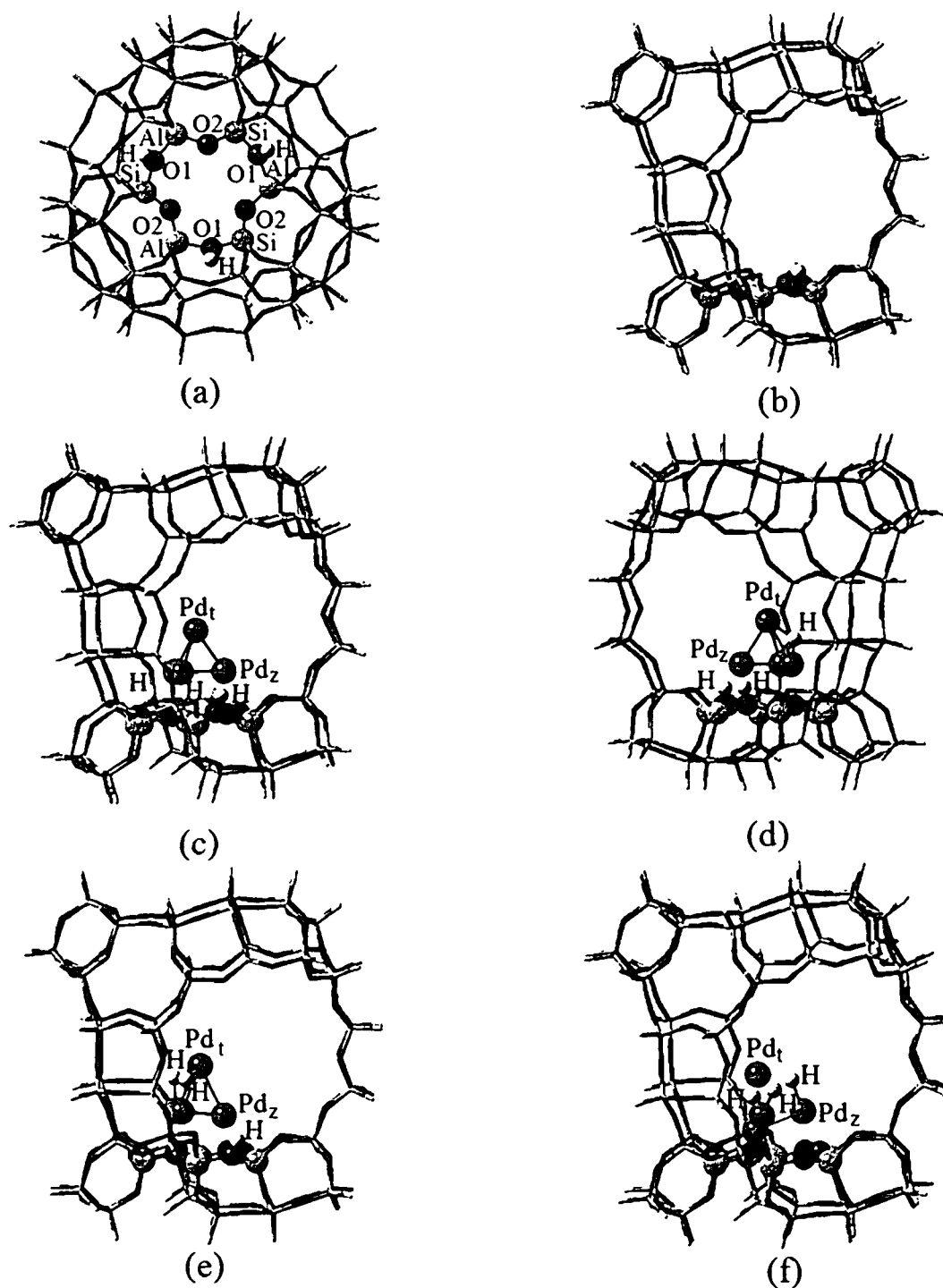


Figure 6.5: ONIOM2 optimized lowest energy structures of: (a) top and (b) side view Zeo3(3H); (c) Pd₄/Zeo3(3H); (d) Pd₄H/Zeo3(2H); (e) Pd₄H₂/Zeo3(1H); (f) Pd₄H₃/Zeo3. The quantum and the molecular mechanics regions have been designated by ball-stick and only stick representations, respectively.

Table 6.6: Important structural parameters, Mulliken charges and energetics of Zeo3 and Pd₄/Zeo3 complexes.

Calculated parameters	Complexes				
	Zeo3(3H)	Pd ₄ / Zeo(3H)	Pd ₄ H/ Zeo(2H)	Pd ₄ H ₂ / Zeo(1H)	Pd ₄ H ₃ / Zeo
Pd _z -Pd _z	-	2.72	2.72	2.68	2.81
Pd _z -Pd _t	-	2.61	2.74	2.83	2.84
<Pd-Pd>	-	2.67	2.73	2.76	2.83
Al-Si _{max}	6.45	6.55	6.50	6.48	6.43
Al(O1)- Si	3.38	3.41	3.34	3.29	3.25
Al(O2)- Si	3.07	3.14	3.15	3.19	3.22
Al-O1	1.85	1.83	1.81	1.77	1.73
Al-O2	1.75	1.76	1.79	1.80	1.79
Average Distances (Å)					
Si-O1	1.71	1.69	1.66	1.63	1.61
Si-O2	1.60	1.61	1.64	1.66	1.67
O2-O2	3.91	4.17	3.95	3.94	3.97
O1-H	0.97	1.01	0.97	0.97	-
Pd _z -O1	-	3.26	3.42	3.36	3.33
Pd _z -O2	-	2.36	2.24	2.20	2.23
Pd _z -Si	-	3.30	3.22	3.24	3.35
Pd _z -Al	-	3.33	3.20	3.10	2.97
Pd _z -H/ Pd _t -H	-	-	1.80/1.67	1.66/1.71, 1.62/1.70	1.65/1.68, 1.65/1.70, 1.52/2.64
Charges					
<Pd _z >	-	-0.26	-0.08	-0.01	0.01
Pd _t	-	0.01	0.08	0.13	0.12
Pd ₄	-	-0.78	-0.16	0.10	0.15
H ₁ /H ₂ /H ₃	0.38/0.38/ 0.38	0.39/0.39/ 0.39	-0.05/0.41/ 0.39	0.05/0.03/ 0.38	0.06/0.05/ 0.07
Pd ₄ H _n	-	-	0.59	0.56	0.33
Energies (kJ/mol)					
E _{ads}	-	-72.65 (-20.39)	-	-	-
E _{RS}	-	-	-33.32	12.40	42.07
E _{trans}	-	-	-33.32	58.12	101.40

In hydrogenated Pd₄/Zeo clusters, elongation of average Pd–Pd bond length is observed by 0.05–0.07 Å than that of adsorbed bare Pd₄ clusters. Strong interaction of the metal cluster with zeolite supports results due to reverse hydrogen spillover, which is reflected by the shorter Pd–O2 distances compared to adsorbed bare cluster (Table 6.4–6.6). Bond length values of T–O1 and T–O2 (T=Si, Al) in hydrogenated Pd₄ clusters are found to be less and greater, respectively, in comparison with those in bare Pd₄ clusters on zeolite support.

6.3.2.3 Charge analysis

Based on finite model as well as embedded cluster studies, it has been already established that most of the bare metal clusters (M₄, M₆) on zeolite supports are internally polarized, with uneven distribution of charges between M_z and M_t metal atoms. Mulliken charge analysis in the present work reveals a qualitatively similar charge polarization effect of Pd₄ on Zeo1, Zeo2 and Zeo3 supports (Tables 6.4–6.6). However, unlike earlier observations [190,191], we have found that metal atoms Pd_z close to the framework oxygen atoms O2 of a zeolite fragment carry higher negative charges while the apex Pd_t atom carries small negative or positive charges. A similar charge distribution has been observed in case of Au₆ cluster on zeolite support by Ivanova Shor *et al.* [193]. The adsorbed Pd₄ clusters in our study are found to carry a total negative charge of -0.62–-0.78 e, which is larger than the value of -0.18 e reported for adsorbed Pd₆ cluster in a finite zeolite model [190]. Further, in line with the earlier results [190,191,193], we have observed that Pd₄H_n (n=1–3) species formed as a result of reverse hydrogen spillover, carry positive charges, 0.21–0.59e (with small negative charge of -0.06 for Pd₄H/Zeo1). It is seen from Tables 6.4–6.6 that reverse hydrogen spillover results in decrement and increment of electron density of metal atoms and transferred hydrogen species, respectively. Therefore, the process of reverse hydrogen spillover is associated with a partial oxidation of the metal clusters. The shift of electron density from metal atoms to hydrogens is larger for Pd_z atoms, which can interact with the transferred protons easily than apex Pd_t atoms. Electron density is less polarized in the adsorbed metal hydride species, Pd₄H_n (n=1–3) compared to adsorbed bare Pd₄ species. This redistribution of electron density in zeolite-supported metal clusters may be important for their reactivity and catalytic activity.

6.3.2.4 Energies of adsorption and reverse hydrogen spillover

The calculated energies of adsorption and reverse hydrogen spillover are tabulated in Tables 6.4–6.6. It should be noted that the energy values do not include basis-set superposition error (BSSE) corrections. The facility of performing counter-poise corrections in ONIOM calculations of Gaussian 03 is not available at this point. However, we have calculated the BSSE using counterpoise method in the fully optimized QM geometries of Pd₄ adsorbed zeolite complexes as reported by Joshi *et al.* [280]. We have performed pure QM calculations on Pd₄ adsorbed in 6T ring of faujasite zeolite clusters. In the first step of these calculations, we have allowed to relax only the terminating Si–H bonds by keeping all other atoms fixed to their respective crystallographic positions. In the subsequent step, the terminating hydrogen atoms are kept fixed and all other atoms are allowed to relax. The values of BSSE in Pd₄/Zeo1(1H), Pd₄/Zeo2(2H) and Pd₄/Zeo3(3H), estimated from pure QM calculations are 50.56 kJ/mol, 70.00 kJ/mol and 71.41 kJ/mol, respectively, giving positive values of corrected E_{ads}. These are only approximated corrections as they have been calculated from pure QM calculations on adsorption complexes of Pd₄ with small zeolite clusters and not from QM/MM calculations on more realistic Pd₄ adsorption zeolite model complexes. Therefore, we have not included the BSSE corrected adsorption energies in Tables 6.4–6.6. BSSE value of 54 kJ/mol has been reported by Moc *et al.* [188] for the adsorption energy of Pd₄ cluster on 24T model cluster of purely siliceous faujasite zeolite. We have calculated the MM contribution (E_{ads,MM}) to the total QM/MM adsorption energy (E_{ads}) as $E_{ads,MM} = E_{ads} - E_{ads,QM}$, where E_{ads,QM} is the pure QM adsorption energy. These values are shown in parentheses of Tables 6.4–6.6. Adsorption energies of Pd₄ on Zeo1, Zeo2 and Zeo3 have been found to be -48.75 kJ/mol, -74.09 kJ/mol and -72.65 kJ/mol, respectively, using equation (6.5). These values are less than the adsorption energy (BSSE uncorrected) of -84.94 kJ/mol for Pd₄ on 24T model cluster of purely siliceous FAU zeolite [188]. An earlier study showed that adsorption energy of six atom octahedral Pd₆ cluster on 6T zeolite cluster is -56 kJ/mol [190]. It suggests that Pd₄ has stronger binding than that of Pd₆ with FAU zeolite. This difference in adsorption energy may be due to the lower coordination saturation of the metal atoms in the free Pd₄ cluster which results in a comparatively stronger interaction with oxygen atoms of the zeolite support. A similar observation has been reported in case of Ir₄ and Ir₆

clusters [190,191]. Our calculations reveal that binding of a Pd tetramer to the zeolite is thus weaker than that to a MgO support (-164.03 kJ/mol) [294].

In the present study, zeolite-supported Pd₄ clusters in triplet ground state is found to be more stable in the configurations with 1H impurity (Figures 6.3 (f), 6.4 (d) and 6.5 (d)). We have calculated that proton migration from bridging OH group of the Zeo1 support to the Pd₄ cluster is exothermic, which is given by E_{RS} value of -61.35 kJ/mol (Table 6.4). The corresponding process in the singlet state of Pd₄/Zeo(3H) is more exothermic with E_{RS} value of -54.28 kJ/mol. Values of E_{RS} corresponding to single proton transfer in Pd₄H/Zeo2(1H) and Pd₄H/Zeo3(2H) complexes are calculated to be -65.16 kJ/mol and -33.32 kJ/mol, respectively (Tables 6.5 and 6.6), showing exothermic nature of these processes. Migration of both the protons from Zeo2 support to Pd₄ is found to be less exothermic, with E_{RS} of -10.16 kJ/mol (Table 6.5). On the other hand, transfer processes of two and three protons in Pd₄H₂/Zeo3(1H) and Pd₄H₃/Zeo3, respectively, take place at the expense of energies (E_{RS}), 12.40 kJ/mol and 42.07 kJ/mol, respectively (Table 6.6). However, in the singlet excited states of Zeo3 adsorption complexes, reverse hydrogen spillover processes for transferring two and three protons are found to be exothermic (E_{RS}=-4.30 kJ/mol) and endothermic (E_{RS}=19.51 kJ/mol), respectively. This observation contradicts the previous finding of exothermicity of three hydrogen transfer process in case of Pd₆/Zeo(3H) complex with finite models of the zeolite framework [190]. Recently, elaborate embedded cluster model study computed reduced E_{RS} values in comparison with finite model studies [193]. This study showed that zeolite-supported hydrogenated M₆H₃ (M=Rh, Ir, Au) species are not always energetically favorable over supported bare M₆ clusters. In this study, it is also established that nature of reverse hydrogen spillover depends on the acidity of the corresponding OH groups and the process proceeds easier from the most acidic hydroxyl groups. Having these results in mind, there is a possibility of changing in the nature of spillover process in Pd₄/Zeo(mH), m=1–3 systems with the change of corresponding OH group, which may be a subject of further investigations. However, there is no theoretical study on zeolite-supported metal tetramers with proper modeling of extended zeolite framework till date. On the basis of the present investigation, we can conclude that reverse hydrogen spillover processes of more than one proton transfer are energetically not favorable for Pd₄ cluster on faujasite zeolite support.

6.4 SALIENT OBSERVATIONS

We have used cluster model and embedded cluster model based on DFT/B3LYP method to study the interaction of palladium atom with H-ZSM-5 support using 7T and 93T model clusters of the zeolite fragment, respectively. It is observed that the Pd atom interacts with a Brønsted proton and a nearby oxygen atom of the zeolite framework. As a result of this interaction, electron transfer takes place from the oxygen atom to the palladium atom, increasing the electron density in s- and p-orbitals of the Pd atom. Simultaneous withdrawal of this excess electron density by the Brønsted proton stabilizes the palladium atom with a decrement in its d-orbital electron density. The adsorption energy of Pd in HZ7 and HZ93 systems are found to be -1.83 and -5.18 kcal/mol, respectively. This implies the greater stability of Pd-HZSM-5 complex with proper modeling of the support. Both the cluster and embedded cluster model are equally efficient in terms of the adsorption of CO and NO molecules on Pd-HZSM-5. NBO analysis gives insight to bonding characteristics of the probe molecules with the supported Pd systems. CO gets adsorbed linearly on Pd-HZSM-5 through the σ donation and π back-donation mechanism. Whereas, adsorption NO molecule takes place in a bent configuration via a covalent σ bond formed between the NO $2\pi^*$ electron and metal d_σ electron. Our calculated vibrational frequency values for these adsorbed species are close to the corresponding experimental values of $\text{Pd}^+\text{-CO}$ and $\text{Pd}^+\text{-NO}$ species, respectively. These results indicate the presence of Pd(I) species in Pd-HZSM-5 complex, which is also reflected by the NAO partial charge analysis.

We have also studied faujasite supported bare Pd_4 clusters and their interaction with OH groups of the support to form hydrogenated Pd_4 clusters. The average Pd-Pd bond length of gas phase Pd_4 cluster remains almost unchanged in $\text{Pd}_4/\text{Zeo}(m\text{H})$, $m=1-3$ complexes. Elongation of the Pd-Pd bond lengths are found to be $\sim 0.05-0.07$ Å, in going from $\text{Pd}_4/\text{Zeo}(m\text{H})$ to $\text{Pd}_4\text{H}_n/\text{Zeo}((m-1)\text{H})$ ($m, n=1-3$) complexes. The presence of the support is effective in producing internal charge polarization in bare as well as in hydrogenated Pd_4 clusters. Pd_4 clusters has been observed to undergo partial oxidation due to proton transfer process, the metal atoms closer to zeolite oxygens are more oxidized than those located at far away. Taking into account the effects of zeolite environment properly, it has been found that reverse hydrogen spillover processes for single proton transfer from zeolite OH

groups to the metal clusters are exothermic with E_{RS} values of -61.35 kJ/mol, -65.16 kJ/mol and -33.32 kJ/mol in case of Zeo1, Zeo2 and Zeo3, respectively. On the other hand, stepwise transfer processes of two protons in Zeo2 and Zeo3 are endothermic with E_{trans} values of 44.84 kJ/mol and 58.12 kJ/mol, respectively, in the triplet states. Value of E_{trans} for the third proton transfer in $Pd_4H_2/Zeo3$ complex is 101.40 kJ/mol. In summary, we have observed that for zeolite-supported tetranuclear palladium clusters, $Pd_4H/Zeo((m-1)H)$, $m=1-3$ in the triplet states is the more stable complex and may be useful as an active species in catalytic processes.

CHAPTER

7

CONCLUSIONS AND FUTURE SCOPES

CONCLUSIONS

In the present thesis, we aimed to reach four goals: first, to investigate the structure and stability of small gas phase palladium clusters; second, to study the nature of adsorption of carbon monoxide on small stable gas phase palladium clusters; third, to study the catalytic activity of gas phase palladium clusters towards oxidation of carbon monoxide; fourth, change in electronic structure of small palladium clusters in presence of oxide supports like zeolites. We have used the most popular density functional theory (DFT) method to carry out our investigations. The calculations in gas phase have been performed with the help of DMol³ program, whereas QM/MM based ONIOM method of Gaussian 03 have been used to study zeolite supported palladium clusters.

Symmetry unrestricted full geometry optimizations have been performed on a randomly chosen large number of gas phase neutral Pd_n (n=1–13) clusters in different spin multiplicities. The lowest energy structures of these clusters are in agreement with the earlier reported results. Further, we have systematically investigated the structural and electronic properties of cationic and anionic Pd_n (n=1–13) clusters for the first time. The corresponding cationic and anionic clusters have been constructed by removing and adding one electron, respectively, from the lowest energy neutral clusters. These clusters have been fully optimized in different spin multiplicities. From the calculations, we have computed electronic properties such as binding energy, fragmentation energy, bond dissociation energy, ionization potential, electron affinity, chemical hardness and dipole moment of the optimized clusters. Based on these parameters, we have predicted the four-atom palladium cluster (Pd₄) in triplet state to be a magic number cluster.

The various adsorption modes of carbon monoxide (CO) on gas phase neutral, cationic and anionic Pd_n (n=1–7) clusters have been investigated. It has

been observed that both for neutral and cationic complexes, all the 1-, 2- and 3-fold coordination are preferred by the CO molecule. But CO adsorption takes place mostly in single coordination (2-fold coordination only for Pd₇⁻ cluster) in case of anionic clusters. i.e., charge states of small palladium clusters have strong influence on the adsorption configurations. Both cluster charge and adsorption configuration are found to effect Pd→CO back-donation. It is observed that Pd–CO and C–O bond distances increase in going from top to bridge to 3-fold adsorption sites in all the clusters. The increment of intermolecular CO interactions due to high coverage leads to the lengthening of the metal–CO distances. On the other hand, lengthening of C–O bonds in moving from top to bridge to hollow sites may be related to the increased metal→π* back-donation, which progressively weakens the C–O bond. Moreover, CO binding energies of the larger three dimensional Pd_n clusters (from n=5 onwards) follow a trend like Pd_nCO⁺ < Pd_nCO < Pd_nCO⁻, in which metal→CO back-donation is the dominant factor. For all the clusters, CO binding energies oscillate with cluster size. Neutral Pd₄ cluster is found to have the lowest binding with CO, which implies least reactivity of bare Pd₄ cluster towards CO or higher stability of Pd₄. Based on these observations, we can say that CO binding on small palladium clusters can be tuned by the charge and size of the clusters. Advantage of this property can be taken in the catalytic CO→CO₂ conversion process.

Due to the higher stability, Pd₄ cluster has been considered to study the catalytic activity of small palladium clusters in removing carbon monoxide. Among the different adsorption modes of molecular (O₂), dissociative (2O) and atomic (O) oxygen on Pd₄^{0,±} clusters, dissociative adsorption with the oxygen atoms occupying bridge sites of Pd₄ clusters appears to be energetically most favorable for all the complexes. All these complexes are highly distorted from the gas phase tetrahedral Pd₄ clusters. All of O₂, 2O and O are found to have the highest binding energy with anionic Pd₄ cluster. Pre-adsorption of oxygen effect the adsorption configuration as well as the binding energy of co-adsorbed carbon monoxide. This is due to the change in electronic structure of gas phase of Pd₄ clusters by adsorption of oxygen. The co-adsorbed complexes form all possible reaction intermediates of the oxidation of carbon monoxide. From the study of three reaction pathways, which combine CO with O₂, 2O and O to form CO₂, it is observed that neutral and cationic Pd₄ clusters are more effective in catalyzing CO oxidation reaction than that of anionic Pd₄

cluster. Further, dissociated oxygen is found to be a superior oxidant for CO oxidation on gas phase tetra palladium clusters.

To study the change in electronic structure of small palladium clusters in presence of oxide support, we have employed the ONIOM method implemented in Gaussian 03 for the first time for proper modelling of the support. In our study, zeolite has been considered as a model oxide support because of its advantageous higher thermal stability, size, shape selectivity of reactants and products, ease separation of products etc. We have first studied the electronic structure of single Pd atom on MFI zeolite support using CO and NO as probe molecules. It is observed that the Pd atom interacts with a Brønsted proton and a nearby oxygen atom of the zeolite framework, as a result of which, electron transfer takes place from the oxygen atom to the palladium atom, increasing the electron density in *s*- and *p*-orbitals of the Pd atom. Simultaneous withdrawal of this excess electron density by the Brønsted proton stabilizes the palladium atom with a decrement in its *d*-orbital electron density. Higher adsorption energy of Pd in HZ7 than HZ93 cluster implies greater stability of Pd-HZSM-5 complex with proper modeling of the support. CO is found to adsorb linearly on Pd-HZSM-5 through the σ donation and π back-donation mechanism. Whereas, adsorption of NO molecule takes place in a bent configuration via a covalent σ bond formed between the NO $2\pi^*$ electron and metal d_σ electron. Our calculated vibrational frequency values for these adsorbed species are close to the corresponding experimental values of $\text{Pd}^+\text{-CO}$ and $\text{Pd}^+\text{-NO}$ species, respectively. These results indicate the presence of Pd(I) species in Pd-HZSM-5 complex.

Next we attempted to investigate the effect of zeolite support on the electronic structure of Pd_4 , which is found to be the most stable cluster from the gas phase calculations. For this study, we have chosen FAU zeolite as support due to its large pore size to accommodate Pd_4 in it. The results show that the structure of gas phase Pd_4 cluster remains almost unchanged in the presence of FAU zeolite support. However, the presence of the support is effective in producing internal charge polarization in bare as well as in hydrogenated Pd_4 clusters. Moreover, Pd_4 cluster has been observed to undergo partial oxidation due to proton transfer process in hydrogenated Pd_4/FAU complexes. The Pd atoms closer to zeolite framework oxygens are more oxidized than those located far away. It has been found that the reverse spillover of single proton from zeolite OH group to Pd_4 cluster is the most

exothermic process or Pd₄H/FAU in the triplet state is the most stable complex and may be useful as an active species in catalytic processes.

FUTURE SCOPES

Recently, there is a trend of growing interest both in theoretical and experimental research based on palladium because of its wide application and the several issues related to it that have remained unexplored. In the present thesis, we have dealt with some of the important structural and electronic properties of small palladium clusters in gas phase as well as on oxide support such as zeolite. Moreover, we have investigated the effect of palladium cluster charge on its catalytic activity in oxidation of carbon monoxide. Still there are a large number of directions left on palladium research for future investigations, some of which have been mentioned below:

- i) The present study can be extended to higher atomic clusters and even to Pd metal surfaces.
- ii) Studies can be made to elucidate the structure and properties of bimetallic palladium clusters with different charge states.
- iii) There is a possibility for the study of these clusters for various catalytic reactions other than CO oxidation.
- iv) Effect of different supports like MgO, Al₂O₃, CNT etc. on the structural and electronic properties of these clusters can be studied.
- v) DFT studies of various catalytic reactions on supported metal clusters will be useful in fabrication of suitable catalysts based on these clusters.

BIBLIOGRAPHY:

- [1] A. W. Castleman and K. H. Bowen, *J. Phys. Chem.* **100**, 12911 (1996).
- [2] R. L. Johnston, *Atomic and Molecular Clusters*, Taylor & Francis, London, 2002.
- [3] K. H. Meiwes-Broer and H. O. Lutz, *Phys. Blätter* **47**, 283 (1991).
- [4] R. Boyle, *The Sceptical Chymist: or Chymico-Physical Doubts and Paradoxes*, London (1661).
- [5] U. Landman, "Small is Different", *Book of Abstracts ISSPIC 11*; Strasbourg, Sept. 9-13 (2002).
- [6] J. P. Wilcoxon and B. L. Abrams, *Chem. Soc. Rev.* **35**, 1162 (2006).
- [7] T. Pradeep, *Nano: The essentials*, Tata Mcgraw-Hill, 2008.
- [8] A. W. Castleman, Jr. and P. Jena, *PNAS* **103**, 10552 (2006).
- [9] P. Jena and A. W. Castleman, Jr., *PNAS*, **103**, 10560 (2006).
- [10] L. -S. Wang, Chapter C1.1, *Encyclopedia of Chemical Physics and Physical Chemistry*, Volume III: Applications, Editors: J. H. Moore and N. D. Spenceer, Publisher: The Institute of Physics, London, 2001.
- [11] T. Hihara, S. Pokrant and J. A. Becker, *Chem. Phys. Lett.* **294**, 357 (1998).
- [12] S. Nonose, Y. Sone, K. Onodera and K. Kaya, *J. Phys. C: Solid State Phys.* **94**, 2744 (1990).
- [13] K. Sattler, J. Muhlbach and E. Recknagel, *Phys. Rev. Lett.* **45**, 821 (1980).
- [14] T. P. Martin and H. Schaber, *J. Chem. Phys.* **83**, 855 (1985).
- [15] T. P. Martin, T. Bergmann, H. Gohlich and T. Lange, *Chem. Phys. Lett.* **172**, 209 (1990).
- [16] W. D. Knight, K. Clemenger, w. A. de Heer, W. A. Saunders, M. Y. Chou and M. L. Cohen, *Phys. Rev. Lett.* **52**, 2141 (1984).
- [17] H. W. Kroto, J. R. Heath, S. C. O'Brien, R. F. Curl and R. E. Smalley, *Nature* **318**, 162 (1985).
- [18] W. C. Wiley and I. H. McLaren, *Rev. Sci. Instrum.* **60**, 792 (1989).
- [19] M. B. Comisarow and A. g. Marshall, *Chem. Phys. Lett.* **25**, 282 (1974).
- [20] M. F. Jarrold, *J. Phys. C: Solid State Phys.* **99**, 11 (1995).
- [21] C. P. Poole, Jr. and F. J. Owens, *Introduction to Nanotechnology*, John Wiley & Sons, Inc., Hoboken, New Jersey (2003).

- [22] J. Jortner, *Physics and Chemistry of Finite Systems: From Clusters to Crystals*, Editors: P. Jena, S. N. Khanna & B. K. Rao, World Scientific, Singapore, p. 1-18, 1992.
- [23] G. Ganteför, M. Gausa, K. H. Meiwes-Broer and H. O. Lutz, *Faraday Discuss. Chem. Soc.* **86**, 197 (1988).
- [24] V. Kumar and Y. Kawazoe, *Phys. Rev. B* **66**, 144413 (2002).
- [25] C. R. Henry, *Surf. Sci. Rep.* **31**, 235 (1998).
- [26] I. Borgia, B. Brunetti, I. Mariani, A. Sgamellotti, F. Cariati, P. Fermo, M. Mellini, C. Viti and G. Padeletti, *Appl. Surf. Sci.* **185**, 206 (2002).
- [27] G. Padeletti and P. Fermo, *Appl. Phys. A: Mater. Sci. Process.* **76**, 515 (2003).
- [28] E. S. Kryachko and F. Remacle, *J. Phys. Chem. B* **109**, 22746 (2005).
- [29] C. -A. J. Lint, T. -Y. Yang, C. -H. Lee, S. H. Huang, R. A. Sperling, M. Zanella, J. K. Lit, J. -L. Shen, H. -H. Wang, H. -I. Yeh, W. J. Parak and W. H. Chang, *ACS Nano* **3**, 395 (2009).
- [30] D. J. Wales, *Energy Landscapes with Applications to Clusters, Biomolecules and Glasses*, Cambridge University, Cambridge, England, 2003.
- [31] L. D. Marks, *Rep. Prog. Phys.* **57**, 603 (1994).
- [32] M. Frank and M. Bäumer, *Phys. Chem. Chem. Phys.* **2**, 3723 (2000).
- [33] J. Guzman and B. C. Gates, *Dalton Trans.* 3303 (2003).
- [34] U. Heiz and E. L. Bullock, *J. Mater. Chem.* **14**, 564 (2004).
- [35] J. C. F. -Gonzalez, S. Kuba, Y. Hao and B. C. Gates, *J. Phys. Chem. B* **110**, 13326 (2006).
- [36] W. M. H. Sachtler, *Acc. Chem. Res.* **26**, 383 (1993).
- [37] D. Barthomeuf, *Catal. Rev. -Sci. Eng.* **38**, 521 (1996).
- [38] W. M. H. Sachtler and Z. Zhang, *Adv. Catal.* **39**, 129 (1993).
- [39] B. C. Gates, *Chem. Rev.* **95**, 511 (1995).
- [40] N. Rösch, G. N. Vayssilov and K. M. Neyman, Density Functional Model Cluster Studies of Metal Cations, Atoms, Complexes, and Clusters in Zeolites (p. 339-357), *Host-Guest-Systems Based on Nanoporous Crystals*, Editors: Dr. F. Laeri, F. Schüth, U. Simon and M. Wark, Wiley Interscience.
- [41] W. C. Conner, Jr. and J. L. Falconer, *Chem. Rev.* **95**, 759 (1995).
- [42] J. A. Alonso, *Chem. Rev.* **100**, 637 (2000).
- [43] F. Baletto and R. Ferrando, *Rev. Mod. Phys.* **77**, 371 (2005).

- [44] A. Fielicke, G. von Helden, G. Meijer, D. B. Pedersen, B. Simard and D. M. Rayner, *J. Phys. Chem. B* **108**, 14591 (2004).
- [45] H. Kietzmann, J. Morenzin, P. S. Bechthold, G. Gantefor, W. Eberhardt, D. -S. Yang, P. A. Hackett, R. Fournier, T. Pang and C. Chen, *Phys. Rev. Lett.* **77**, 4528 (1996).
- [46] M. B. Knickelbein and S. Yang, *J. Chem. Phys.* **93**, 5760 (1990).
- [47] I. Stara, V. Nehasil and V. Matolin, *Surf. Sci.* **173**, 331 (1995).
- [48] S. Tanabe and H. Matsumoto, *J. Mater. Sci. Lett.* **13**, 1540 (1994).
- [49] H. Matsumoto and S. Tanabe, *J. Phys. Chem.* **99**, 6951 (1995).
- [50] M. Valden, J. Aaltonen, E. Kuusisto, M. Pessa and C. J. Barnes, *Surf. Sci.* **193**, 307 (1994).
- [51] M. Che and C. O. Bennett, *Adv. Catal.* **36**, 55 (1989).
- [52] G. D. Zakumbaeva, N. F. Toktobaeva, A. G. Kubasheva and I. G. Efremenko, *Neftekhimija* **34**, 258 (1994) (in Russian).
- [53] K. Ihara and H. Oishi, *Jpn. Kokai Tokyo Koho* JP: 61234936 (1986).
- [54] H. Muraki, H. Sofugawa, M. Fukui, M. Kimura, S. Matsumoto and N. Miyoshi, *Jpn. Kokai Tokyo Koho* JP: 01011643 (1989).
- [55] D. C. Douglass, J. P. Bucher and L. A. Bloomfield, *Phys. Rev. B* **45**, 6341 (1992).
- [56] A. J. Cox, J. G. Louderback, S. E. Apsel and L. A. Bloomfield, *Phys. Rev. B* **49**, 12295 (1994).
- [57] T. Taniyama, E. Otha and T. Sato, *Europhys. Lett.* **38**, 195 (1997).
- [58] M. D. Morse, *Chem. Rev.* **86**, 1049 (1986).
- [59] J. Ho, K. M. Ervin, M.L. Polak, M.K. Gilles and W.C. Lineberger, *J. Chem. Phys.* **95**, 4845 (1991).
- [60] J. Ho, M. L. Polak, K. M. Ervin and W. C. Lineberger, *J. Chem. Phys.* **99**, 8542 (1993).
- [61] M. Harada and H. Dexpert, *J. Phys. Chem.* **100**, 565 (1996).
- [62] J. -M. Pénisson and A. Renou, *J. Cryst. Growth* **102**, 585 (1990).
- [63] M. José-Yacamán, M. Marín-Almazo and J. A. Ascencio, *J. Mol. Catal. A: Chem.* **173**, 61 (2001).
- [64] J. Colbert, A. Zangwill and M. Strongin, *Phys. Rev. B* **27**, 1378 (1983).

- [65] G. Ganteför, M. Gausa, K. -H. Meiwes-Broer and H. O. Lutz, *J. Chem. Soc. Farad. Trans.* **86**, 2483 (1990).
- [66] K. P. Huber and G. Herzberg, *Molecular Spectra and Molecular Structure, IV, Constants of Diatomic Molecules*, Van Nostrand Reinhold, New York (1979).
- [67] C. C. Yang, C. C. Wan and D. C. L. Lee, *Encyclopedia of Nanoscience and Nanotechnology*, American Scientific Publishers, California, Vol. 8, p. 397 (2004).
- [68] F. von Gynz-Rekowski, G. Ganteför and Y. D. Kim, *Eur. Phys. J. D* **43**, 81 (2007).
- [69] V. L. Moruzzi and P. M. Marcus, *Phys. Rev. B* **39**, 471 (1989).
- [70] V. Kumar, K. Esfarjani and Y. Kawazoe, *Clusters and Nanomaterials*, Springer Series in Cluster Physics, Springer-Verlag, Heidelberg, p. 9 (2002).
- [71] V. L. Moruzzi and P. M. Marcus, *Phys. Rev. B* **39**, 471 (1989).
- [72] B. V. Reddy, S. N. Khanna and B. I. Dunlap, *Phys. Rev. Lett.* **70**, 3323 (1993).
- [73] V. Kumar and Y. Kawazoe, *Eur. Phys. J. D* **24**, 81 (2003).
- [74] M. Moseler, H. Häkkinen, R. N. Barnett and U. Landman, *Phys. Rev. Lett.* **86**, 2545 (2001).
- [75] H. Zhang, D. Tian and J. Zhao, *J. Chem. Phys.* **129**, 114302 (2008).
- [76] F. Aguilera-Granja, A. Vega, J. Rogan, W. Orellana and G. García, *Eur. Phys. J. D* **44**, 125 (2007).
- [77] C. Barreteau, R. G. -López, D. Spanjaard, M. C. Desjonquères and A. M. Oleś, *Phys. Rev. B* **61**, 7781 (2000).
- [78] F. Aguilera-Granja, J. M. Montejano-Carrizales, E. O. Berlanga-Ramírez and A. Vega, *Physica B* **354**, 271 (2004).
- [79] F. Aguilera-Granja, J. M. Montejano-Carrizales and A. Vega, *Phys. Lett. A* **332**, 107 (2004).
- [80] M. Nawate, N. Nishimura, S. Honda and H. Tanaka, *IEEE Trans. Magn.* **41**, 3424 (2005).
- [81] D. C. Douglass, J. P. Bucher and L. A. Bloomfield, *Phys. Rev. Lett.* **68**, 1774 (1992).
- [82] A. J. Cox, J. G. Louderback, S. E. Apsel and L. A. Bloomfield, *Phys. Rev. B* **49**, 12295 (1994).
- [83] A. J. Cox, J. G. Louderback and L. A. Bloomfield, *Phys. Rev. Lett.* **71**, 923 (1993).

- [84] G. Ganteför and W. Eberhardt, *Phys. Rev. Lett.* **76**, 4975 (1996).
- [85] I. Efremenko and M. Sheintuch, *Surf. Sci.* **414**, 148 (1998).
- [86] I. Efremenko and M. Sheintuch, *J. Mol. Cat. A* **160**, 445 (2000).
- [87] D. Dai and K. Balasubramanian, *J. Chem. Phys.* **103**, 648 (1995).
- [88] D. Dai and K. Balasubramanian, *Chem. Phys. Lett.* **310**, 303 (1999).
- [89] K. Balasubramanian, *J. Chem. Phys.* **91**, 307 (1989).
- [90] S. Kürger, S. Vent, F. Nörtemann, M. Staufer and N. Rösch, *J. Chem. Phys.* **115**, 2082 (2001).
- [91] S. Lee, D. M. Bylander and L. Kleinman, *Phys. Rev. B* **39**, 4916 (1989).
- [92] G. Valerio and H. Toulhoat, *J. Phys. Chem.* **100**, 10827 (1996).
- [93] N. Watari and S. Onishi, *Phys. Rev. B* **58**, 1665 (1998).
- [94] K. Lee, *Phys. Rev. B* **58**, 2391 (1998).
- [95] C. Barreteau, R. Guirado-López, D. Spanjaard, M. S. Desjonquères and A. Oleś, *Phys. Rev. B* **61**, 7781 (2000).
- [96] M. Moseler, H. Häkkinen, R. N. Barnett and U. Landman, *Phys. Rev. Lett.* **86**, 2545 (2001).
- [97] J. M. Seminario, A. G. Zacarias and M. Castro, *Int. J. Quantum Chem.* **61**, 515 (1997).
- [98] T. Nakao, D. A. Dixon and H. Chen, *J. Phys. Chem.* **97**, 12665 (1993).
- [99] J. Rogan, G. García, J. A. Valdivia, W. Orellana, A. H. Romero, R. Ramírez and M. Kiwi, *Phys. Rev. B* **72**, 115421 (2005).
- [100] W. Zhang, Q. Ge and L. Wang, *J. Chem. Phys.* **118**, 5793 (2003).
- [101] J. Rogan, G. García, M. Ramírez, V. Muñoz, J. A. Valdivia, X. Andrade, R. Ramírez and M. Kiwi, *Nanotechnol.* **19**, 205701 (2008).
- [102] C. Luo, C. Zhou, J. Wu, T. J. D. Kumar, N. Balakrishnan, R. C. Forrey and H. Cheng, *Int. J. Quantum Chem.* **107**, 1632 (2007).
- [103] P. Nava, M. Sierka and R. Ahlrichs, *Phys. Chem. Chem. Phys.* **5**, 3372 (2003).
- [104] M. Böyükata and J. C. Belchior, *Croat. Chem. Acta* **81**, 289 (2008).
- [105] G. Zanti and D. Peeters, *Eur. J. Inorg. Chem.* **2009**, 3904 (2009).
- [106] S. Nigam, C. Majumder and S. K. Kulshreshtha, *Phys. Rev. B* **76**, 195430 (2007).
- [107] J. Rogan, G. García, C. Loyola, W. Orellana, R. Ramírez and M. Kiwi, *J. Chem. Phys.* **125**, 214708 (2006).

- [108] C. M. Chang and M. Y. Chou, *Phys. Rev. Lett.* **93**, 133401-1 (2004).
- [109] L. -L. Wang and D. D. Johnson, *Phys. Rev. B* **75**, 235405 (2007).
- [110] Y. Sun, M. Zhang and R. Fournier, *Phys. Rev. B* **77**, 075435 (2008).
- [111] Y. Sun, R. Fournier and M. Zhang, *Phys. Rev. A* **79**, 043202 (2009).
- [112] Y. -C. Bae, V. Kumar, H. Osanai and Y. Kawazoe, *Phys. Rev. B* **72**, 125427 (2005).
- [113] R. C. Longo and L. J. Gallego, *Phys. Rev. B* **74**, 193409 (2006).
- [114] G. Blyholder, *J. Chem. Phys.* **68**, 2772 (1964).
- [115] J. T. Yates, *Surf. Sci.* **731**, 299 (1994).
- [116] M. Kobayashi, *Bull. Chem. Soc. Jpn.* **56**, 831 (1983).
- [117] S. Katsuki and H. Taketa, *Solid State Commun.* **39**, 711 (1981).
- [118] J. Andzelm and D. R. Salahub, *Int. J. Quantum Chem.* **29**, 1091 (1986).
- [119] A. Gavezzotti, G. F. Tantardini and M. Simonetta, *Chem. Phys.* **105**, 333 (1986).
- [120] G. Pacchioni and J. Koutecky, *J. Phys. Chem.* **91**, 2658 (1987).
- [121] J. Koutecky, G. Pacchioni and P. Fantucci, *Chem. Phys.* **99**, 87 (1985).
- [122] G. W. Smith and E. A. Carter, *J. Phys. Chem.* **95**, 2327 (1991).
- [123] M. R. A. Blomberg, C. B. Lebrilla and P. E. M. Siegbahn, *Chem. Phys. Lett.* **150**, 522 (1988).
- [124] M. Filatov, *Chem. Phys. Lett.* **373**, 131 (2003).
- [125] G. Pacchioni and P. S. Bagus, *J. Chem. Phys.* **93**, 1209 (1990).
- [126] A. Goursot, I. Papai and D. R. Salahub, *J. Am. Chem. Soc.* **114**, 7452 (1992).
- [127] S. -C. Chung, S. Krüger, G. Pacchioni and N. Rösch, *J. Chem. Phys.* **102**, 3695 (1995).
- [128] I. V. Yudanov, R. Sahnoun, K. M. Neyman, N. Rösch, J. Hoffmann, S. Schauerermann, V. Johánek, H. Unterhalt, G. Rupprechter, J. Libuda and H.-J. Freund, *J. Phys. Chem. B* **107**, 255 (2003).
- [129] V. Bertin, E. Agacino, R. López-Rendon and E. Poulain, *J. Mol. Struct. (THEOCHEM)* **796**, 243 (2006).
- [130] I. V. Yudanov, R. Sahnoun, K. M. Neyman and N. Rösch, *J. Chem. Phys.* **117**, 9887 (2002).
- [131] V. A. Spasov and K. M. Ervin, *J. Chem. Phys.* **109**, 5344 (1998).

- [132] P. Gruene, A. Fielicke, G. Meijer and D. M. Rayner, *Phys. Chem. Chem. Phys.* **10**, 6144 (2008).
- [133] D. L. Trimm and Z. I. Önsan, *Catal. Rev. -Sci. Eng.* **43**, 31 (2001).
- [134] J. H. Lee and D. L. Trimm, *Fuel Process. Technol.* **42**, 339 (1995).
- [135] H. Conrad, G. Ertl and J. Küppers, *Surf. Sci.* **76**, 323 (1978).
- [136] T. Engel and G. Ertl, *Adv. Catal.* **28**, 1 (1979).
- [137] T. Engel and G. Ertl, *Chem. Phys. Lett.* **54**, 95 (1978).
- [138] K. Judai, S. Abbet, A. S. Wörz, M. A. Röttgen and U. Heiz, *Int. J. Mass Spec.* **229**, 99 (2003).
- [139] S. H. Kim, J. Méndez, J. Wintterlin and G. Ertl, *Phys. Rev. B* **72**, 155414 (2005).
- [140] J. Méndez, S. H. Kim, J. Cerdá, J. Wintterlin and G. Ertl, *Phys. Rev. B* **71**, 085409 (2005).
- [141] H. Gabasch, A. Knop-Gericke, R. Schlögl, M. Borasio, C. Weilach, G. Rupprechter, S. Penner, B. Jenewein, K. Hayek and B. Klötzer, *Phys. Chem. Chem. Phys.* **9**, 533 (2007).
- [142] L. Piccolo, C. Becker and C. R. Henry, *Appl. Surf. Sci.* **164**, 156 (2000).
- [143] R. -L. Kuittinen and K. Laasonen, *Chem. Phys.* **314**, 19 (2005).
- [144] S. Abbet, U. Heiz, H. Häkkinen and U. Landman, *Phys. Rev. Lett.* **86**, 5950 (2001).
- [145] B. Huber, P. Koskinen, H. Häkkinen and M. Moseler, *Nature Materials* **5**, 44 (2006).
- [146] B. Huber and M. Moseler, *Eur. Phys. J. D* **45**, 485 (2007).
- [147] E. Blomsma, J. A. Martens and P. A. Jacobs, *Stud. Surf. Sci. Catal. B* **105**, 909 (1997).
- [148] J. -L. Dong, J. -H. Zhu and Q. -H. Xu, *Appl. Catal. A* **112**, 105 (1994).
- [149] J. M. Silva, M. F. Ribeiro, F. R. Ribeiro, E. Benazzi and M. Guisnet, *Appl. Catal. A* **125**, 15 (1995).
- [150] L. B. Galperin, J. C. Bricker and J. R. Holmgren, *Appl. Catal. A* **239**, 297 (2003).
- [151] Y. Li, and J. N. Armor, *Air Products and Chemicals Inc.* US Pat. 5149512, (1992).

- [152] L. S. Stokes, D. M. Murphy, R. D. Farley, C. C. Rowlands and S. Bailey, *Phys. Chem. Chem. Phys.* **1**, 621 (1999).
- [153] K. Okumura, J. Amano, N. Yasunobu and M. Niwa, *J. Phys. Chem. B* **104**, 1050 (2000).
- [154] M. J. Rice, A. K. Chakraborty and A. T. Bell, *J. Phys. Chem. B* **104**, 9987 (2000).
- [155] B. Pommier and P. Gelin, *Phys. Chem. Chem. Phys.* **3**, 1138 (2001).
- [156] K. Okumura and M. Niwa, *Catal. Surv. Jpn.* **5**, 121 (2002).
- [157] K. Chakarova, E. Ivanova, K. Hadjiivanov, D. Klissurski and H. Knözinger, *Phys. Chem. Chem. Phys.* **6**, 3702 (2004).
- [158] K. Okumura, S. Matsumoto, N. Nishiaki and M. Niwa, *Appl. Catal. B* **40**, 151 (2003).
- [159] C. -J. Liu, K. Yu, Y. -P. Zhang, X. Zhu, F. He and B. Eliasson, *Appl. Catal. B* **47**, 95 (2004).
- [160] C. -K. Shi, L. -F. Yang, Z. -C. Wang, X. -E. He, -E., J. -X. Cai, G. Li and X. -S. Wang, *Appl. Catal. A* **243**, 379 (2003).
- [161] B. Wen, Q. Sun and W. M. H. Sachtler, *J. Catal.* **204**, 314 (2001).
- [162] M. Dams, L. Drijkoningen, B. Pauwels, G. V. Tendeloo, D. E. De Vos and P. A. Jacobs, *J. Catal.* **209**, 225 (2002).
- [163] Y. Nishizaka and M. Misono, *Chem. Lett.* **23**, 2237 (1994).
- [164] D. Berthomieu, J.-M. Ducéré and A. Goursot, *J. Phys. Chem. B* **106**, 7483 (2002).
- [165] G. Barone, N. Armata, A. Prestianni, T. Rubino, D. Duca and D. Yu. Murzin, *J. Chem. Theory Comput.* **5**, 1274 (2009) and the supporting information.
- [166] R. Grybos, J. Hafner, L. Benco and P. Raybaud, *J. Phys. Chem. C* **112**, 12349 (2008).
- [167] A. Sierralta, P. Alejos, E. Ehrmann, L. J. Rodriguez and Y. Ferrer, *J. Mol. Catal. A: Chem.* **301**, 61 (2009).
- [168] P. Treesukol, K. Srisuk, J. Limtrakul and T. N. Truong, *J. Phys. Chem. B* **109**, 11940 (2005).
- [169] R. Grybos, L. Benco, T. Bučko and J. Hafner, *J. Chem. Phys.* **130**, 104503 (2009).

- [170] L. J. Lobree, A. W. Aylor, J. A. Reimer and A. T. Bell, *J. Catal.* **181**, 189 (1999).
- [171] A. W. Aylor, L. J. Lobree, J. A. Reimer and A. T. Bell, *J. Catal.* **172**, 453 (1997).
- [172] K. Moller, D. C. Koningsberger and T. Bein, *J. Phys. Chem.* **93**, 6116 (1989).
- [173] K. Moller and T. Bein, *J. Phys. Chem.* **94**, 845 (1990).
- [174] Z. Zhang, H. Chen, L. -L. Sheu and W. M. H. Sachtler, *J. Catal.* **127**, 213 (1991).
- [175] X. Bai and W. M. H. Sachtler, *J. Catal.* **129**, 121 (1991).
- [176] Z. Zhang, H. Chen and W. M. H. Sachtler, *J. Chem. Soc. Faraday Trans.* **87**, 1413 (1991).
- [177] J. G. Kim, S. K. Ihm, J. Y. Lee and R. Ryoo *J. Phys. Chem.* **95**, 8546 (1991).
- [178] Z. Zhang and W. M. H. Sachtler, *J. Mol. Catal.* **67**, 349 (1991).
- [179] R. Ryoo, S. J. Cho, C. Pak, J. G. Kim, S. K. Ihm and J. Y. Lee, *J. Am. Chem. Soc.* **114**, 76 (1992).
- [180] A. Yu. Stakheev and W. M. H. Sachtler, *J. Chem. Soc. Faraday Trans.* **87**, 3703 (1991).
- [181] T. Beutel, Z. Zhang, W. M. H. Sachtler and H. Knözinger, *J. Phys. Chem.* **97**, 3579 (1993).
- [182] L. Sordelli, G. Martra, R. Psaro, C. Dossi and S. Coluccia, *J. Chem. Soc., Dalton Trans.* 765 (1996).
- [183] W. Vogel, H. Knözinger, B. T. Carvill, W. M. H. Sachtler and Z. C. Zhang, *J. Phys. Chem. B* **102**, 1750 (1998).
- [184] Y. -X. Jiang, W. -Z. Weng, D. Si and S. -G. Sun, *J. Phys. Chem. B* **109** (2005) 7637.
- [185] T. Yokoyama, S. Kimoto and T. Ohta, *Physica B* **158**, 255 (1989).
- [186] A. L. Yakovlev, G. M. Zhidomirov, K. M. Neyman, V. A. Nasluzov and N. Rösch, *Ber. Bunsen Ges. Phys. Chem.* **100**, 413 (1996).
- [187] R. Harmsen, S. Bates and R. A. van Santen, *Faraday Discuss.* **106**, 443 (1997).
- [188] J. Moc, D. G. Musaev and K. Morokuma, *J. Phys. Chem. A* **112**, 5973 (2008).
- [189] G. N. Vayssilov, B. C. Gates and N. Rösch, *Angew. Chem. Int. Ed.* **42**, 1391 (2003).

- [190] G. N. Vayssilov and N. Rösch, *Phys. Chem. Chem. Phys.* **7**, 4019 (2005).
- [191] G. P. Petrova, G. N. Vayssilov and N. Rösch, *Chem. Phys. Lett.* **444**, 215 (2007).
- [192] G. P. Petrova, G. N. Vayssilov and N. Rösch, *J. Phys. Chem. C* **111**, 14484 (2007).
- [193] E. A. Ivanova Shor, V. A. Nasluzov, A. M. Shor, G. N. Vayssilov and N. Rösch, *J. Phys. Chem. C* **111**, 12340 (2007).
- [194] N. Argaman and G. Makov, *Amer. J. Phys.* **68**, 69 (2000).
- [195] P. Hohenberg and W. Kohn, *Phys. Rev. B* **135**, 864 (1964).
- [196] W. Koch and M.C. Holthausen, *A Chemist's Guide to Density Functional Theory*, WILEY-VCH, Weinheim, Germany, second edition, (2000).
- [197] L. H. Thomas, *Proc. Camb. Phil. Soc.* **23**, 542 (1927).
- [198] E. Fermi *Z. Phys.* **48**, 73 (1928).
- [199] W. Kohn and L. J. Sham, *Phys. Rev. A* **140**, 1133 (1965).
- [200] P. A. M. Dirac, *Proc. Camb. Phil. Soc.* **26**, 376 (1930).
- [201] D. M. Ceperley and B. J. Alder, *Phys. Rev. Lett.* **45**, 566 (1980).
- [202] P. A. M. Dirac, *Proc. R. Soc. London, Ser. A*, **123**, 714, (1929).
- [203] J. C. Slater, *Phys. Rev.* **81**, 385 (1951).
- [204] S. J. Vosko, L. Wilk and M. Nusair, *Can. J. Phys.* **58**, 1200 (1980).
- [205] A. D. Becke, *Phys. Rev. A* **38**, 3098 (1988).
- [206] J. P. Perdew, *Electronic Structure of Solids*, Editors: P. Ziesche, H. Eschrig, Akademie Verlag, Berlin (1991).
- [207] C. Lee, W. Wang and R. G. Parr, *Phys. Rev. B* **37**, 785 (1988).
- [208] J. P. Perdew, K. Burke and M. Ernzerhof, *Phys. Rev. Lett.* **77**, 3865 (1996).
- [209] B. Delley, *J. Chem. Phys.* **92**, 508 (1990).
- [210] B. Delley, *J. Chem. Phys.* **113**, 7756 (2000).
- [211] S. F. Boys and F. Bernardi, *Mol. Phys.* **19**, 553 (1970).
- [212] S. Dapprich, I. Komaromi, K. S. Byun, K. Morokuma and M. J. Frisch, *J. Mol. Struct. (THEOCHEM)* **461**, 1 (1999).
- [213] M. Svensson, S. Humbel and K. Morokuma, *J. Chem. Phys.* **105**, 3654 (1996).
- [214] P. B. Karadakov and K. Morokuma, *Chem. Phys. Lett.* **317**, 589 (2000).
- [215] T. Vreven and K. Morokuma, *J. Comput. Chem.* **21**, 1419 (2000).
- [216] K. Morokuma, *Bull. Korean Chem. Soc.* **24**, 797 (2003).

- [217] B. Delley, *Int. J. Quantum Chem.* **69**, 423 (1998).
- [218] B. Delley, *Modern Density Functional Theory: A tool for Chemistry*, Elsevier, (1995).
- [219] J. M. Seminario and P. Politzer, *Theoretical and Computational Chemistry*, Vol. 2, Elsevier, Amsterdam, The Netherlands (1995).
- [220] C. W. Bock and M. Trachtman, *J. Phys. Chem.* **98**, 95 (1994).
- [221] M. S. Gordon, *Chem. Phys. Lett.* **76**, 163 (1980).
- [222] W. J. Hehre, R. Ditchfield and J. A. Pople, *J. Chem. Phys.* **56**, 2257 (1972).
- [223] R. G. Parr and R. G. Pearson, *J. Am. Chem. Soc.* **105**, 7512 (1983).
- [224] C. E. Moore, *Atomic Energy Levels*, Natl. Bur. Stand. (U.S.), U.S. GPO, Washington, D.C. (1971).
- [225] I. Shim and K. A. Gingerich, *J. Chem. Phys.* **80**, 5107 (1984).
- [226] A. G. Zacarias, M. Castro, J. M. Tour and J. M. Seminario, *J. Phys. Chem. A* **103**, 7692 (1999).
- [227] K. M. Ervin, J. Ho and W. C. Lineberger, *J. Chem. Phys.* **89**, 4514 (1988).
- [228] F. Aguilera-Granja, A. Vega, J. Rogan and G. García, *Nanotechnol.* **18**, 365706 (2009).
- [229] D. D. Wagman *et al.*, *J. Phys. Chem. Ref. Data* **11**, Suppl. 2 (1982).
- [230] S. N. Khanna and P. Jena, *Phys. Rev. B* **51**, 13705 (1995).
- [231] M. Brack, *Rev. Mod. Phys.* **65**, 677 (1993).
- [232] S. Krüger, S. Vent and N. Rösch, *Ber. Bunsenges. Phys. Chem.* **101**, 1640 (1997).
- [233] M. S. Stave and A. E. DePristo, *J. Chem. Phys.* **97**, 3386 (1992).
- [234] T. Ishikawa, *Jpn. J. Appl. Phys.* **32**, 4779 (1993).
- [235] D. R. Lide, *Handbook of Chemistry and Physics*, 74th ed.; CRC Press: Boca Raton, FL (1994).
- [236] K. A. Gingerich, *Naturwiss.* **54**, 43 (1967).
- [237] *CRC Handbook of Chemistry and Physics*, 55th ed., edited by R. C. Weast (CRC, Cleveland, OH, 1974).
- [238] H. Hotop and W. C. Lineberger, *J. Phys. Chem. Ref. Data* **14**, 731 (1985).
- [239] R. G. Pearson, *Inorg. Chem.* **27**, 734 (1988).
- [240] B. K. Rao, P. Jena, S. Burkart, G. Ganteför and G. Seifert, *Phys. Rev. Lett.* **86**, 692 (2001).

- [241] N. R. Walker, J. K. -H. Hui and M. C. L. Gerry, *J. Phys. Chem. A* **106**, 5803 (2002).
- [242] P. Nava, M. Sierka and R. Ahlrichs, *Phys. Chem. Chem. Phys.* **6**, 5338 (2004).
- [243] S. A. Klopčič, V. D. Moravec and C. C. Jarrold, *J. Chem. Phys.* **110**, 8986 (1999).
- [244] A. M. Joshi, M. H. Tucker, W. N. Delgass and K. T. Thomson, *J. Chem. Phys.* **125**, 194707 (2006).
- [245] M. Neurock, *Top. Catal.* **9**, 135 (1999).
- [246] D. Dai, S. Roszak and K. Balasubramanian, *J. Chem. Phys.* **104**, 1471 (1996).
- [247] E. Ozensoy, B. K. Min, A. K. Santra and D. W. Goodman, *J. Phys. Chem. B* **108**, 4351 (2004).
- [248] N. S. Phala, G. Klatt and E. van Steen, *Chem. Phys. Lett.* **395**, 33 (2004).
- [249] C. W. Bauschlicher, *Surf. Sci.* **154**, 70 (1985).
- [250] B. Tremblay and L. Manceron, *Chem. Phys.* **250**, 187 (1999).
- [251] A. M. Bradshaw and F. M. Hoffmann, *Surf. Sci.* **72**, 513 (1978).
- [252] A. J. Lupinetti, S. Fau, G. Frenking and S. H. Strauss, *J. Phys. Chem. A* **101**, 9551 (1997).
- [253] Q. Fu, H. Saltsburg and M. F. -Stephanopoulos, *Science* **301**, 935 (2003).
- [254] A. A. Herzing, C. J. Kiely, A. F. Carley, P. Landon and G. J. Hutchings, *Science* **321**, 1331(2008).
- [255] W. E. Kaden, T. Wu, W. A. Kunkel and S. L. Anderson, *Science* **326**, 826 (2009).
- [256] J. Rogal, K. Reuter and M. Scheffler, *Phys. Rev. B* **75**, 205433 (2007).
- [257] K. Reuter, *Oil & Gas Science and Technology – Rev. IFP* **61**, 471 (2006).
- [258] A. Eichler, F. Mittendorfer and J. Hafner, *Phys. Rev. B* **62**, 4744 (2000).
- [259] U. Heiz, A. Sanchez and S. Abbet, *Chem. Phys.* **262**, 189 (2000).
- [260] P. A. Hintz and K. M. Ervin, *J. Chem. Phys.* **103**, 7897 (1995).
- [261] M. P. Irion, A. Selinger and P. Schnabel, *Z. Phys. D* **19**, 393 (1991).
- [262] W. O. Davies, *J. Chem. Phys.* **43**, 2809 (1965).
- [263] T.A. Halgren and W. N. Lipscomb, *Chem. Phys. Lett.* **49**, 225 (1977).
- [264] N. Govind, M. Peterson, G. Fitzgerald, D. King-Smith and J. Andzelm, *J. Comput. Mat. Sci.* **28**, 250 (2003).

- [265] B. Huber, H. Häkkinen, U. Landman and M. Moseler, *Comp. Mat. Sci.* **35**, 371 (2006).
- [266] D. Schröder, S. Shaik and H. Schwarz, *Acc. Chem. Res.* **33**, 139 (2000).
- [267] A. Prestianni, A. Martorana, I. Ciofini, F. Labat and C. Adamo, *J. Phys. Chem. C* **112**, 18061 (2008).
- [268] A. Genest, S. Krüger and N. Rösch, *J. Phys. Chem. A* **112**, 7739 (2008).
- [269] D. E. A. Gordon and R. M. Lambert, *Surf. Sci.* **287-288**, 114 (1993).
- [270] Z. M. Liu, Y. Zhou, F. Solymosi and J. M. White, *Surf. Sci.* **245**, 289 (1991).
- [271] M. F. H. van Tol, A. Gielbert, R. M. Wolf, A. B. K. Lie and B. E. Neiuwenhuys, *Surf. Sci.* **287-288**, 201 (1993).
- [272] P. St. Petkov, G. N. Vayssilov, S. Krüger and N. Rösch, *J. Phys. Chem. A* **112**, 8523 (2008).
- [273] A. Chatterjee and R. Vetrivel, *Microporous Mater.* **3**, 211 (1994).
- [274] W. Löwenstein, *Am. Mineral.* **39**, 92 (1954)
- [275] *Material Studio*, Version 3.2; Accelrys Software, Inc.: San Diego, CA, 2005.
- [276] M. J. Frisch, G. W. Trucks, H. B. Schlegel, G. E. Scuseria, M. A. Robb, J. R. Cheeseman, J. A. Jr. Montgomery, T. Vreven, K. N. Kudin, J. C. Burant, J. M. Millam, S. S. Iyengar, J. Tomasi, V. Barone, B. Mennucci, M. Cossi, G. Scalmani, N. Rega, G. A. Petersson, H. Nakatsuji, M. Hada, M. Ehara, K. Toyota, R. Fukuda, J. Hasegawa, M. Ishida, T. Nakajima, Y. Honda, O. Kitao, H. Nakai, M. Klene, X. Li, J. E. Knox, H. P. Hratchian, J. B. Cross, V. Bakken, C. Adamo, J. Jaramillo, R. Gomperts, R. E. Stratmann, O. Yazyev, A. J. Austin, R. Cammi, C. Pomelli, J. W. Ochterski, P. Y. Ayala, K. Morokuma, G. A. Voth, P. Salvador, J. J. Dannenberg, V. G. Zakrzewski, S. Dapprich, A. D. Daniels, M. C. Strain, O. Farkas, D. K. Malick, A. D. Rabuck, K. Raghavachari, J. B. Foresman, J. V. Ortiz, Q. Cui, A. G. Baboul, S. Clifford, J. Cioslowski, B. B. Stefanov, G. Liu, A. Liashenko, P. Piskorz, I. Komaromi, R. L. Martin, D. J. Fox, T. Keith, M. A. Al-Laham, C. Y. Peng, A. Nanayakkara, M. Challacombe, P. M. W. Gill, B. Johnson, W. Chen, M. W. Wong, C. Gonzalez and J. A. Pople, *Gaussian 03*, revision A.1; Gaussian, Inc.: Pittsburgh PA, 2003.
- [277] A. K. Rappe, C. J. Casewit, K. S. Colwell, W. A. Goddard and W. M. Skiff, *J. Am. Chem. Soc.* **114**, 10024 (1992).
- [278] J. Sirijaraensre and J. Limtrakul, *Phys. Chem. Chem. Phys.* **11**, 578 (2009).



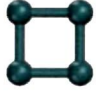

- [279] S. Kasuriya, S. Namuangruk, P. Treesukol, M. Tirtowidjojo and J. Limtrakul, *J. Catal.* **219**, 320 (2003).
- [280] A. M. Joshi, W. N. Delgass and K. T. Thomson, *J. Phys. Chem. C* **111**, 11888 (2007).
- [281] A. Y. Stakheev, E. S. Shpiro, N. I. Jaeger and G. Schulz-Ekloff, *Catal. Lett.* **34**, 293 (1995).
- [282] M. Zhou and L. Andrews, *J. Phys. Chem. A* **104**, 3915 (2000).
- [283] M. Zhou and L. Andrews, *J. Phys. Chem. A* **104**, 2618 (2000).
- [284] D. R. Lide, *Handbook of Chemistry and Physics*, 84th ed.; CRC Press: Boca Raton, FL (2003).
- [285] A. E. Reed, F. Weinhold, L. A. Curtiss and D. J. Pochatko, *J. Chem. Phys.* **84**, 5687 (1986).
- [286] P. Treesukol, J. Limtrakul and T. N. Truong, *J. Phys. Chem. B* **105**, 2421 (2001).
- [287] J. Moc, D. G. Musaev and K. Morokuma, *J. Phys. Chem. A* **104**, 11606 (2000).
- [288] J. R. B. Gomes, Z. Lodziana and F. Illas, *J. Phys. Chem. B* **107**, 6411 (2003).
- [289] U. Eichler, M. Brändle and J. Sauer, *J. Phys. Chem. B* **101**, 10035 (1997).
- [290] J. O. Ehresmann, W. Wang, B. Herreros, D. -P. Luigi, T. N. Venkatraman, W. Song, J. B. Nicholas and J. F. Haw, *J. Am. Chem. Soc.* **124**, 10868 (2002).
- [291] R. W. Joyner, A. D. Smith, M. Stockenhuber and M. W. E. van den Berg, *Phys. Chem. Chem. Phys.* **6**, 5435 (2004).
- [292] V. A. Nasluzov, V. V. Rivanenkov, A. M. Shor, K. Neyman and N. Rösch, *Chem. Phys. Lett.* **374**, 487 (2003).
- [293] C. Bussai, S. Krüger, G. N. Vayssilov and N. Rösch, *Phys. Chem. Chem. Phys.* **7**, 2656 (2005).
- [294] K. M. Neyman, N. Rösch and G. Pacchioni, *Appl. Catal. A* **191**, 3 (2000).

APPENDIX

A

Low energy structural and spin isomers of Pd_n (n=2–13) clusters:

Table A1: Spin multiplicity (M), point group symmetry (PGS) and relative energy (ΔE) in eV of different structural isomers of neutral Pd₂–Pd₁₃ clusters.

Clusters	Structures ¹	M	PGS	ΔE
Pd ₂		1	D _{∞h}	0.0018
		3	D_{∞h}	0.0000
		5	D _{∞h}	2.0346
Pd ₃		1	D_{3h}	0.0000
			C _{2v}	0.0002
		3	D _{3h}	0.0463
			C _{2v}	0.0465
		5	D _{3h}	1.6843
	C _{2v}	1.6838		
Pd ₄	 4(a)	1	D _{4h}	0.6199
		3	D _{4h}	0.7144
		5	D _{4h}	1.6677
	 4(b)	1	C _s	0.0168
			T _d	0.0190
		3	C_s	0.0000
			T _d	0.0022
	5	C _s	1.1762	
	T _d	1.1785		

¹ Blue spheres throughout the whole chapter denote palladium atoms.

Table A1 (Continued)







Clusters	Structures	M	PGS	ΔE
Pd ₅	 5 (a)	1	D_{3h}	0.0000
		3	C ₁	0.0011
			D _{3h}	0.0235
		5	C ₁	0.0225
			D _{3h}	0.5610
	C ₁	0.5606		
	 5 (b)	1	C _{2v}	0.0017
		3	C _{4v}	0.0038
			C _{2v}	0.0280
		5	C _{4v}	0.0305
C _{2v}			0.6135	
Pd ₆	 6 (a)	1	C_{2h}	0.0000
		3	O _h	0.0037
			D _{2d}	0.0004
			C _{2h}	0.0670
		5	O _h	0.0706
			D _{2d}	0.0668
	C _{2h}		0.5188	
	 6 (b)	1	D _{2h}	1.4045
		3	D _{2h}	1.4592
		5	D _{2h}	1.7296
	 6 (c)	1	D _{3h}	0.4629
		3	D _{3h}	0.4746
		5	D _{3h}	0.7115
	 6 (d)	1	C ₂	0.3915
3		C ₂	0.4073	
5		C ₂	0.6600	

Table A1 (Continued)





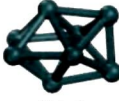



Clusters	Structures	M	PGS	ΔE
Pd ₇	 7(a)	1	D_{5h}	0.0000
		3	D _{5h}	0.0276
		5	D _{5h}	0.2097
	 7(b)	1	C _s	0.0130
		3	C _s	0.0404
		5	C _s	0.1600
	 7(c)	1	C _{2v}	0.0222
		3	C _{2v}	0.2293
		5	C _{2v}	0.3332
	 7(d)	1	C ₂	0.0699
		3	C ₂	0.0853
		5	C ₂	0.2255
Pd ₈	 8(a)	1	C _{2v}	0.2229
		3	C _{2v}	0.0000
		5	D _{2d}	0.2258
	 8(b)	1	C _{2v}	0.5195
		5	C _s	0.5895
	 8(c)	1	D _{3d}	0.3477
		3	D _{3d}	0.3416
		5	D _{3d}	0.4073
	 8(d)	1	C _s	0.2143
		3	C _s	0.2319
5		C _s	0.3456	

Table A1 (Continued)


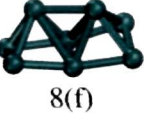





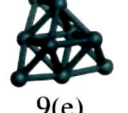

Clusters	Structures	M	PGS	ΔE	
Pd ₈	 8(e)	1	C _s	0.3371	
		3	C _{2v}	0.3587	
	 8(f)	5	C _{2v}	0.4607	
		1	C ₂	0.3828	
	 8(g)	3	C ₂	0.3904	
		5	C ₂	0.5131	
	Pd ₉	 9(a)	1	D_{3h}	0.0000
			3	D _{3h}	0.0224
		 9(b)	5	D _{3h}	0.1312
			1	D _{3h}	0.4332
 9(c)		3	D _{3h}	0.4423	
		5	D _{3h}	0.4861	
 9(d)		1	C ₂	0.4769	
		3	C ₂	0.4861	
 9(e)		5	C ₂	0.5454	
		1	C _{2v}	0.3187	
	3	C _{2v}	0.3302		
	5	C _{2v}	0.3928		
	1	C _{3v}	0.7075		
	3	C _{3v}	0.7118		
		5	C _{3v}	0.7476	

Table A1 (Continued)




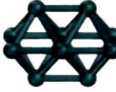




Clusters	Structures	M	PGS	ΔE	
Pd ₉	 9(f)	1	C _s	0.3729	
		3	C _s	0.3790	
		5	C _s	0.4483	
	 9(g)	1	C _s	0.4352	
		3	C _s	0.4457	
		5	C _s	0.5235	
	 9(h)	1	C _{4v}	0.6745	
		3	C _{4v}	0.6795	
		5	C _{4v}	0.7209	
	Pd ₁₀	 10(a)	1	D_{2h}	0.0000
			3	D _{2h}	0.0101
			5	D _{2h}	0.0681
 10(b)		1	D _{4h}	0.4117	
		3	D _{4h}	0.4266	
		5	D _{4h}	0.5040	
 10(c)		1	D _{4d}	0.2830	
		3	D _{4d}	0.2882	
		5	D _{4d}	0.3267	
 10(d)		1	C _{2h}	0.1682	
		3	C _{2h}	0.1804	
		5	C _{2h}	0.2446	
 10(e)		1	C _s	0.4292	
		3	C _s	0.4383	
		5	C _s	0.4967	

Table A1 (Continued)

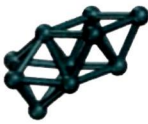

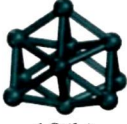
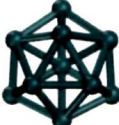



Clusters	Structures	M	PGS	ΔE
Pd ₁₀		1	C ₁	0.0588
	10(f)	3	C ₁	0.0795
		1	C _{2v}	0.2738
	10(g)	3	C _{2v}	0.2785
		5	C _{2v}	0.3135
		1	C _{2v}	0.0062
	10(h)	3	C _{2v}	0.0133
		1	C _{3v}	0.1313
	10(i)	3		0.1360
		5		0.1666
		1	C _{3v}	0.4180
	10(j)	3	C _{3v}	0.4224
	5	C _{3v}	0.4906	
Pd ₁₁		1	D_{3h}	0.0000
	11(a)	3	D _{3h}	0.0039
		5	D _{3h}	0.0317
		1	C _{2v}	0.2586
	11(b)	3	C _{2v}	0.2643
		5	C _{2v}	0.2952

Table A1 (Continued)

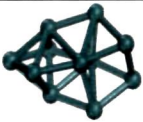
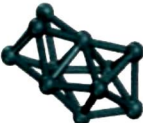
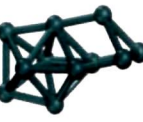

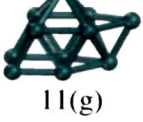
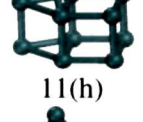
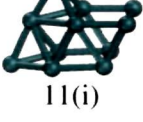
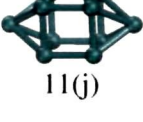
Clusters	Structures	M	PGS	ΔE
Pd ₁₁		1	C ₂	0.4125
	11(c)	3	C ₂	0.4239
		5	C ₂	0.4812
		1	C _s	0.1567
	11(d)	3	C _s	0.1765
		5	C _s	0.2575
		1	C _s	0.5173
	11(e)	3	C _s	0.5285
		5	C _s	0.6022
		1	C _{2v}	0.5514
	11(f)	3	C _{2v}	0.5604
		5	C _{2v}	0.6117
		1	C _s	0.4259
	11(g)	3	C _s	0.4303
	5	C _s	0.4625	
	1	C _s	0.6166	
11(h)				
	1	C _s	0.6689	
11(i)	2	C _s	0.6658	
	3	C _s	0.6826	
	1	C _{2v}	0.3650	
11(j)	3	C _{2v}	0.3777	
	5	C _{2v}	0.4430	

Table A1 (Continued)

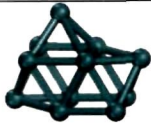

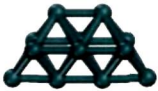

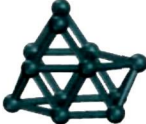
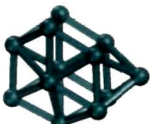
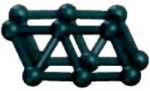

Clusters	Structures	M	PGS	ΔE
Pd ₁₁	 11(k)	1	C _s	0.1817
		3	C _s	0.1856
		5	C _s	0.2161
Pd ₁₂	 12(a)	1	C_s	0.0000
		3	C _s	0.0138
		5	C _s	0.0686
	 12(b)	1	C _{2v}	0.6629
		3	C _{2v}	0.6671
		5	C _{2v}	0.6993
	 12(c)	1	C _{2h}	0.6648
		3	C _{2h}	0.6701
		5	C _{2h}	0.7052
	 12(d)	1	C _s	0.2919
		3	C _s	0.2937
		5	C _s	0.3220
	 12(e)	1	C _s	0.2390
		3	C _s	0.2350
		5	C _s	0.2464
 12(f)	1	C _i	0.6040	
	3	C _i	0.6303	
	5	C _i	0.7140	
 12(g)	1	C _{2v}	0.1667	
	3	C _{2v}	0.1792	
	5	C _{2v}	0.2368	

Table A1 (Continued)

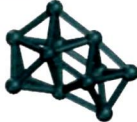
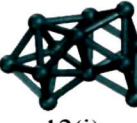

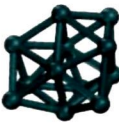

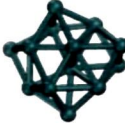
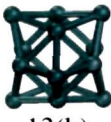
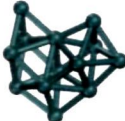
Clusters	Structures	M	PGS	ΔE
Pd ₁₂		1	C _s	0.2988
	12(h)	3	C _s	0.3078
		5	C _s	0.3517
		1	C _s	0.5471
	12(i)	3	C _s	0.5543
		5	C _s	0.5949
		1	C _{2v}	1.2045
	12(j)	3	C _{2v}	1.2119
		5	C _{2v}	1.2508
		1	C ₁	0.1739
	12(k)			
		1	I _h	0.6936
12(l)				
Pd ₁₃		1	C₁	0.0000
	13(a)	3		0.0143
		5		0.0726
		1	C _{4v}	0.3121
	13(b)	3	C _{4v}	0.3314
		5	C _{4v}	0.3992
		1	C _s	0.4107
	13(c)	3	C _s	0.4149
		5	C _s	0.4411

Table A1 (Continued)

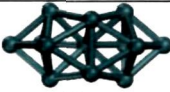

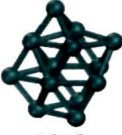


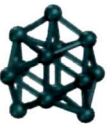
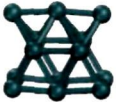

Clusters	Structures	M	PGS	ΔE
Pd ₁₃	 13(d)	1	C _{2v}	0.5070
		3	C _{2v}	0.5183
		5	C _{2v}	0.5571
	 13(e)	1	C _s	0.3496
		3	C _s	0.3540
		5	C _s	0.3877
	 13(f)	1	C _s	0.2356
		3	C _s	0.2353
		5	C _s	0.2540
	 13(g)	1	I _h	0.1240
		3	C _s	0.4816
		5	C _s	0.5195
	 13(h)	1	C _s	0.4816
		3	C _s	0.4861
		5	C _s	0.5195
	 13(i)	1	C _{2v}	0.0155
		3	C _{2v}	0.0143
		5	C _{2v}	0.0303
 13(j)	1	C _{2v}	0.5094	
	3	C _{2v}	0.5062	
	5	C _{2v}	0.5236	
 13(k)	1	C _{2v}	0.1497	
	3	C _{2v}	0.1617	
	5	C _{2v}	0.2108	

Table A1 (Continued)

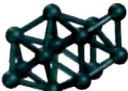




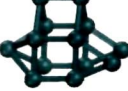
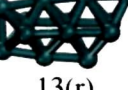
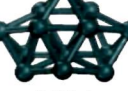
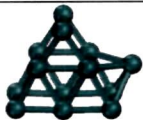
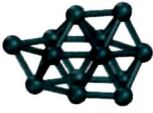
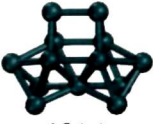
Clusters	Structures	M	PGS	ΔE
Pd ₁₃	 13(l)	1	C _s	0.5135
		3	C _s	0.5225
		5	C _s	0.5587
	 13(m)	1	C _{2v}	0.0197
		3	C _{2v}	0.0210
		5	C _{2v}	0.0425
	 13(n)	1	C _s	0.5691
		3	C _s	0.5724
		5	C _s	0.5984
	 13(o)	1	C _s	1.0640
		3	C _s	1.0792
		5	C _s	1.1364
	 13(p)	1	C _s	1.2601
		3	C _s	1.2652
		5	C _s	1.2975
 13(q)	1	C _s	0.5491	
	3	C _s	0.5631	
 13(r)	1	C _s	0.6398	
	3	C _s	0.6484	
	5	C _s	0.6898	
 13(s)	1	C ₁	0.0550	
	3	C _s	0.0609	
	5	C _s	0.0925	

Table A1 (Continued)



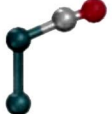

Clusters	Structures	M	PGS	ΔE
Pd ₁₃	 13(t)	1	C _s	0.2005
		3	C _s	0.2051
		5	C _s	0.2422
	 13(u)	1	C _s	0.4448
		3	C _s	0.4450
		5	C _s	0.4613
	 13(v)	1	C _{2v}	0.3179
		3	C _{2v}	0.3335
		5	C _{2v}	0.4009

APPENDIX

B

Low energy structural and spin isomers corresponding to the adsorption and co-adsorption of carbon monoxide and oxygen on Pd₄^{0,±} clusters:

Table B1: Relative energies of different structural and spin isomers of neutral Pd_nCO (n=1–7) complexes.

Pd _n CO	Multiplicity (M)	Structures ¹	Relative energy (eV)
Pd ₁ CO	1	 1a	0.0000
	3	 1b	2.0946
Pd ₂ CO	1	 2a	0.9937
		 2b	0.0000
	3	similar to 2a similar to 2b	1.3597 1.5896

¹ Blue, gray and red spheres throughout the whole document denote palladium, carbon and oxygen, respectively.

Table B1 (Continued)

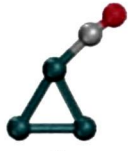

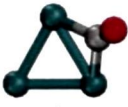
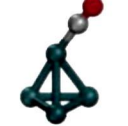
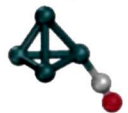


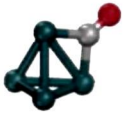
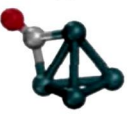

Pd_nCO	Multiplicity (M)	Structures	Relative energy (eV)	
Pd_3CO	1	 3a	0.7044	
		 3b	0.0000	
	3	similar to 3a	0.8234	
		 3c	0.9325	
		similar to 3b	1.1576	
	Pd_4CO	1	 4a	0.1321
			 4b	0.1298
 4c			0.1317	
 4d			0.1324	
 4e			0.2629	
 4f			0.2627	
 4g			0.2639	

Table B1 (Continued)


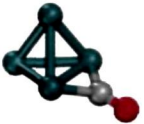
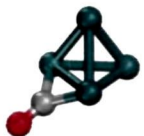

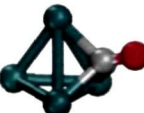
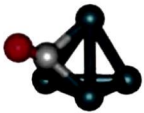

Pd_nCO	Multiplicity (M)	Structures	Relative energy (eV)
Pd_4CO	1		0.2619
		4h	
			0.2714
		4i	
			0.2611
		4j	
			0.0000
	4k		
		0.0000	
	4l		
		0.0000	
	4m		
		0.0000	
4n			
	3	similar to 4a	0.1386
		similar to 4b	0.1343
		similar to 4c	0.1383
		similar to 4d	0.1385
		similar to 4f	0.4340
		similar to 4g	0.4352

Table B1 (Continued)




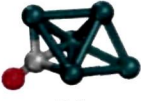
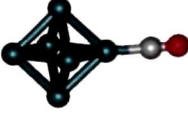
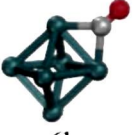
Pd_nCO	Multiplicity (M)	Structures	Relative energy (eV)	
Pd_4CO	3	similar to 4h	0.4328	
		similar to 4i	0.4352	
		similar to 4j	0.4331	
		similar to 4k	0.6109	
		similar to 4l	0.6107	
		similar to 4m	0.6109	
		similar to 4n	0.6107	
Pd_5CO	1	 5a	0.2395	
		 5b	0.0000	
		 5c	0.0932	
		 5d	0.1742	
	3	similar to 5a	0.2760	
		similar to 5b	0.0144	
		similar to 5c	0.1459	
		similar to 5d	0.3554	
	Pd_6CO	1	 6a	0.0000
			 6b	0.1957

Table B1 (Continued)

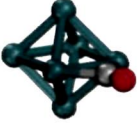
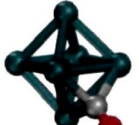
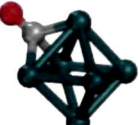
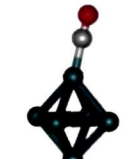
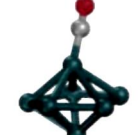
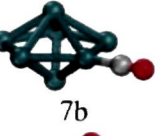
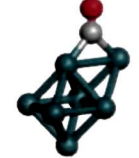
Pd_nCO	Multiplicity (M)	Structures	Relative energy (eV)
Pd_6CO	1		0.1902
		6c	
			0.2799
		6d	
			0.2799
	6e		
	3		0.0624
		similar to 6a	0.0615
		similar to 6b	0.2335
		similar to 6c	0.2293
similar to 6d		0.3774	
similar to 6e	0.3774		
Pd_7CO	1		0.5206
		7a	
			0.1561
7b			
	0.0000		
7c			

Table B1 (Continued)


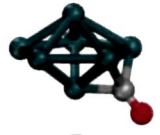
Pd_nCO	Multiplicity (M)	Structures	Relative energy (eV)
Pd_7CO	3		0.0287
		7d	
			0.2447
		7e	
		similar to 7a	0.5119
		similar to 7b	0.1876
		similar to 7c	0.0433
similar to 7d	0.0832		
similar to 7e	0.2963		

Table B2: Relative energies of different structural and spin isomers of cationic Pd_nCO ($n=1-7$) complexes.




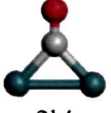
Pd_nCO^+	Multiplicity (M)	Structures	Relative energy (eV)
Pd_1CO^+	2		0.0000
	4	1a'	
Pd_2CO^+	4		3.7900
		1b'	
	2		0.8743
		2a'	
4		0.0000	
	2b'		
	4	Similar to 2a'	1.5839

Table B2 (Continued)


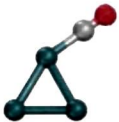

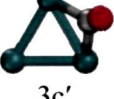
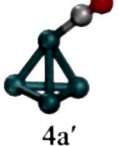
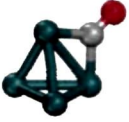
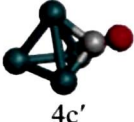
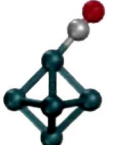

Pd_nCO^+	Multiplicity (M)	Structures	Relative energy (eV)
Pd_2CO^+	4	 2c'	2.3231
Pd_3CO^+	2	 3a'	1.0327
		 3b'	0.0000
	4	 3c'	1.4969
Pd_4CO^+	2	 4a'	0.3998
		 4b'	0.1485
		 4c'	0.0000
	4	Similar to 4a'	0.4327
		Similar to 4b'	0.7674
		Similar to 4c'	1.0838
Pd_5CO^+	2	 5a'	0.1249
		 5b'	0.1685

Table B2 (Continued)


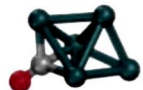
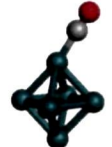

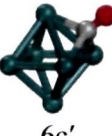


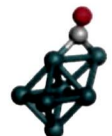
Pd_nCO^+	Multiplicity (M)	Structures	Relative energy (eV)
Pd_5CO^+	2	 5c'	0.1597
		 5d'	0.0000
	4	Similar to 5a'	0.1363
		Similar to 5b'	0.1987
		Similar to 5c'	0.3212
Similar to 5d'	0.5258		
Pd_6CO^+	2	 6a'	0.0000
		 6b'	0.1624
		 6c'	0.0893
	4	Similar to 6a'	0.0458
		Similar to 6b'	0.2053
		Similar to 6c'	0.3932
Pd_7CO^+	2	 7a'	0.4522
		 7b'	0.1892
	2	 7c'	0.0000

Table B2 (Continued)


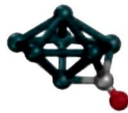
Pd_nCO^+	Multiplicity (M)	Structures	Relative energy (eV)
Pd_7CO^+	2		0.1120
			0.2610
	4	Similar to 7a'	0.4997
		Similar to 7b'	0.2455
		Similar to 7c'	0.0451
		Similar to 7d'	0.2135
		Similar to 7e'	0.4036

Table B3: Relative energies of different structural and spin isomers of anionic Pd_nCO ($n=1-7$) complexes.




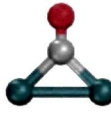
Pd_nCO^-	Multiplicity (M)	Structures	Relative energy (eV)
Pd_1CO^-	2		0.0000
	4		2.5590
Pd_2CO^-	2		0.0000
			0.2131

Table B3 (Continued)

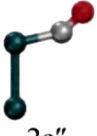


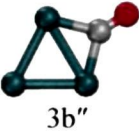


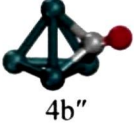
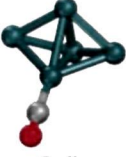
Pd_nCO^-	Multiplicity (M)	Structures	Relative energy (eV)
Pd_2CO^-	4		1.9238
		2c''	
Pd_3CO^-	2		1.8588
		2d''	
			0.0000
	4		0.3212
		3b''	
			0.4221
3c''			
Pd_4CO^-	2	Similar to 3a''	1.0344
		Similar to 3b''	1.0523
	4	Similar to 3c''	1.4003
			0.0000
2	4a''		
		0.5803	
4b''			
Pd_5CO^-	2	Similar to 4b''	1.1356
			0.2069
5a''			

Table B3 (Continued)


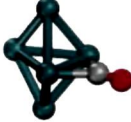

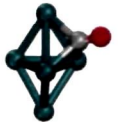

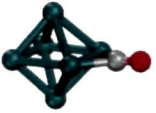
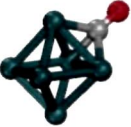
Pd_nCO^-	Multiplicity (M)	Structures	Relative energy (eV)
Pd_5CO^-	2		0.0000
		5b''	
			0.6906
		5c''	
		0.2118	
	5d''		
		0.4516	
	5e''		
	4	Similar to 5a''	0.5338
		Similar to 5b''	0.4491
Similar to 5c''		0.5732	
Similar to 5e''		0.8339	
Pd_6CO^-	2		0.0000
		6a''	
			0.2305
	6b''		
		0.3735	
	6c''		
	4	Similar to 6a''	0.2038
Similar to 6b''		0.4396	
Similar to 6c''		0.5669	

Table B3 (Continued)


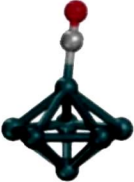
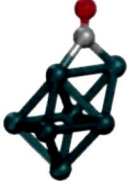

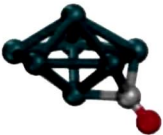
Pd_nCO^-	Multiplicity (M)	Structures	Relative energy (eV)
Pd_7CO^-	2		0.0828
		7a''	
			0.4211
		7b''	
			0.0977
	7c''		
		0.0000	
	7d''		
		0.2215	
	7d''		
4		Similar to 7a''	0.4644
		Similar to 7b''	0.2165
		Similar to 7c''	0.1683
		Similar to 7d''	0.2616
		Similar to 7e''	0.3658

Table B4: Relative stability of different structural isomers of molecular adsorption complexes of O₂ on neutral Pd₄ clusters.

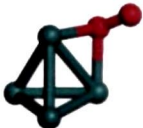
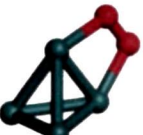

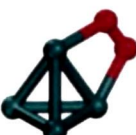



Relative energy (eV)							
M=1		M=3		M=5		M=7	
	0.5431						
	0.0075		0.0000		0.2914		1.7805
	0.2351						
	0.0914						

Table B5: Relative stability of different structural isomers of dissociative adsorption complexes of O₂ on neutral Pd₄ clusters.











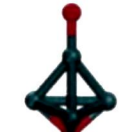






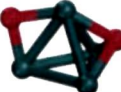
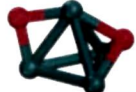
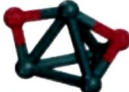
Relative energy (eV)							
M=1		M=3		M=5		M=7	
	0.0000		0.0149		0.3753		1.2851
	0.4358		0.5292		0.7909		
	1.7993						
	0.9717		0.8910		0.9453		1.7440
	0.9813		0.8715		0.9045		1.5770
	0.1473		0.1914		0.4625		1.3118

Table B6: Relative stability of different structural isomers of molecular adsorption complexes of O₂ on cationic Pd₄ clusters.


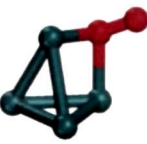
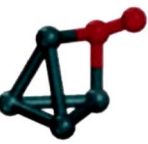


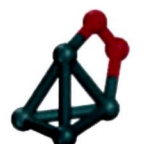
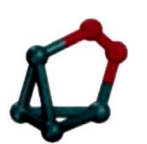

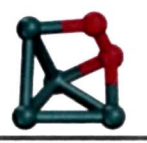
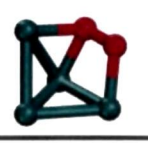
Relative energy (eV)							
M=2		M=4		M=6		M=8	
	0.0000						
	0.3493		0.4348		0.7618		
	0.1004		0.1239		0.3742		2.6787
	0.2983		0.4438				

Table B7: Relative stability of different structural isomers of dissociative adsorption complexes of O₂ on cationic Pd₄ clusters.




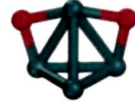









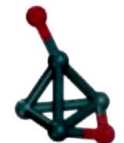
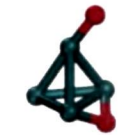



Relative energy (eV)							
M=2		M=4		M=6		M=8	
	0.0000		0.3267		0.8764		1.8368
	0.2312				0.9378		
	0.0818						
	2.2900		2.5226				2.9285
	0.9476						
	1.2682		1.1851		1.4021		2.3591
	0.0842		0.3014				1.8421

Table B8: Relative stability of different structural isomers of molecular adsorption complexes of O₂ on anionic Pd₄ clusters.

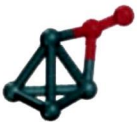



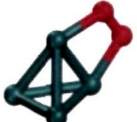
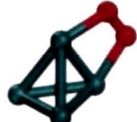
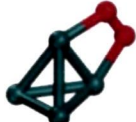
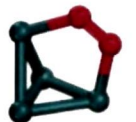
Relative energy (eV)							
M=2		M=4		M=6		M=8	
	0.2599		0.5510		0.8315		2.4028
	0.1880		0.0000		1.0476		2.4808

Table B9: Relative stability of different structural isomers of dissociative adsorption complexes of O₂ on anionic Pd₄ clusters.




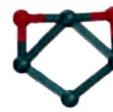

















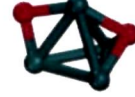

Relative energy (eV)							
M=2		M=4		M=6		M=8	
	0.0000		0.0809		0.2916		1.9070
	0.8887		1.0737		1.5122		
	0.9108		0.8898		0.9344		2.3213
	0.5459		0.5521		1.0054		2.4103
	0.6460		0.7840		1.3322		2.5925
	0.3871		0.4800		0.9193		2.4646

Table B10: Relative stability of different structural isomers of atomic adsorption of O on neutral, cationic and anionic Pd₄ clusters.



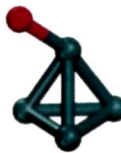

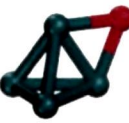


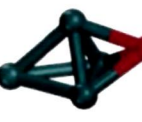

Pd ₄ O	Relative energy (eV)		Pd ₄ O ⁺	Relative energy (eV)		Pd ₄ O ⁻	Relative energy (eV)	
	M=1	M=3		M=2	M=4		M=2	M=4
	0.6749	0.5850		1.2966	1.2849		0.1356	0.1059
	0.0000	0.0254		0.1298	0.2627		0.0000	0.2276
	0.0751	0.0999		0.0000	0.1689		0.2792	0.4680

Table B11: Relative stability of different structural isomers of co-adsorption complexes of O₂ and CO on neutral, cationic and anionic Pd₄ clusters.

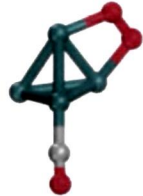
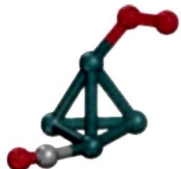
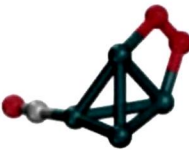
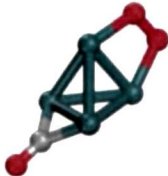
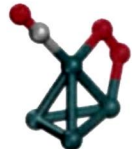
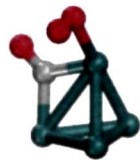

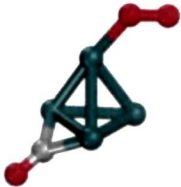
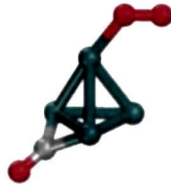

Structural isomers of Pd ₄ O ₂ CO	Relative energy (eV)	Structural isomers of Pd ₄ O ₂ CO ⁺	Relative energy (eV)	Structural isomers of Pd ₄ O ₂ CO ⁻	Relative energy (eV)
	0.3285		0.3359		0.0000
	0.0558		0.3056		0.4183
	0.0000		0.0000		0.3112
					0.2521

Table B12: Relative stability of different structural isomers of co-adsorption complexes of 2O and CO on neutral, cationic and anionic Pd₄ clusters.

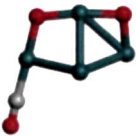




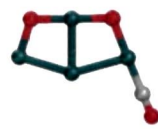
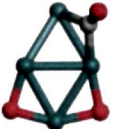



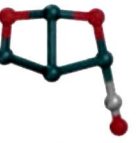
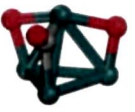


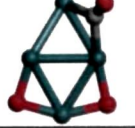
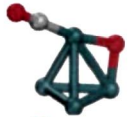

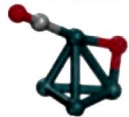



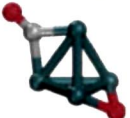

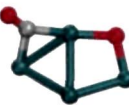


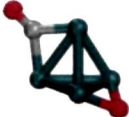



Structural isomers of Pd ₄ 2OCO	Relative energy (eV)	Structural isomers of Pd ₄ 2OCO ⁺	Relative energy (eV)	Structural isomers of Pd ₄ 2OCO ⁻	Relative energy (eV)
	0.0177		0.5259		1.3160
	0.4537		0.4754		0.0000
	0.0000		0.3529		0.3967
	1.1569		0.0000		1.5335
			1.0186		0.6994
			0.2376		

Table B13: Relative stability of different structural isomers of co-adsorption complexes of O and CO on neutral, cationic and anionic Pd₄ clusters.

Structural isomers of Pd ₄ OCO	Relative energy (eV)	Structural isomers of Pd ₄ OCO ⁺	Relative energy (eV)	Structural isomers of Pd ₄ OCO ⁻	Relative energy (eV)
	0.0000		0.4848		0.0000
	0.2911		0.5795		0.1072
	0.4077		0.8834		0.4621
	0.4904		0.0000		0.1265
	0.2662		0.5640		
			0.8813		

LIST OF PUBLICATIONS

In Journals

- 1) **B. Kalita** and R. C. Deka, *DFT study on structural and electronic properties of small neutral and charged Pd_n (n=8–13) clusters* (under preparation).
- 2) **B. Kalita** and R. C. Deka, *Nature of CO and NO interactions with Pd-HZSM-5 catalyst: A comparative study of DFT based cluster and ONIOM methods* (communicated).
- 3) **B. Kalita** and R. C. Deka, *Adsorption of CO on oxygen pre-adsorbed neutral and charged gas phase Pd₄ clusters: A density functional study*, **J. Comput. Chem.** (under revision).
- 4) **B. Kalita** and R. C. Deka, *Reaction intermediates of CO oxidation on gas phase Pd₄ clusters: A density functional study*, **J. Am. Chem. Soc.** 131 (2009) 13252.
- 5) **B. Kalita** and R. C. Deka, *Investigation of reverse-hydrogen spillover on zeolite-supported palladium tetramer by ONIOM method*, **J. Phys. Chem. C** 113 (2009) 16070.
- 6) R. C. Deka, P. Mondal and **B. Kalita**, *Adsorption of small molecules on Ti-Zeolites: An Embedded Cluster Approach*, **The Icfai University Journal of Chemistry** 2 (2009) 38.
- 7) **B. Kalita** and R. C. Deka, *DFT study of CO adsorption on neutral and charged Pd_n (n=1–7) clusters*, **Eur. Phys. J. D** 53 (2009) 51.

- 8) **B. Kalita** and R. C. Deka, *Stability of small Pd_n (n=1–7) clusters on the basis of structural and electronic properties: A Density Functional Approach*, **J. Chem. Phys.** 127 (2007) 244306.
- 9) **B. Kalita** and R. C. Deka, *Density Functional Studied on Structure and Reactivity of Pd_n Clusters for n=1–13*, **Bull. Catal. Soc. India** 5 (2006) 138.

In Conferences

- 1) **B. Kalita** and R. C. Deka, *DFT studies on CO oxidation and NO reduction by Pd₄ clusters*, **International Conference on Advanced Nanomaterials and Nanotechnology (ICANN-2009)**, Indian Institute of Technology Guwahati, December 9-11, 2009 (accepted).
- 2) **B. Kalita** and R. C. Deka, *Stability of Palladium Nanoclusters using Density Functional Theory*, **10th Anniversary of CRSI National Symposium in Chemistry (NSC-10)**, Indian Institute of Science, Bangalore, February 1-3, 2008.
- 3) **B. Kalita** and R. C. Deka, *Density Functional Study on Structure and Reactivity of Pd_n Clusters for n=1–13*, **National Symposium on Condensed Matter Days**, Tezpur University, August 29-31, 2006.